Enhanced Methods of Signal Decoding and Time of Arrival Estimation for SSR Signals

Dissertation

Stephan Bernhart

Institute for Microwave and Photonic Engineering
Graz University of Technology

in cooperation with

ADB Safegate Austria GmbH

Supervisor: Ao. Univ.-Prof. Dr. Erich Leitgeb

Graz, January 2019

Abstract

Multilateration (MLAT) and automatic dependent surveillance-broadcast (ADS-B) are state-of-the-art surveillance and identification technologies on the civil air traffic management (ATM) market. They are the complement to the conventional primary and secondary surveillance radars (PSR and SSR) for airport and wide area. ADS-B systems use only decoding and MLAT systems use decoding and time of arrival (ToA) estimation methods. International and European specifications require a high system reliability and a low bit error rate (BER) for the decoding methods, and as well as a high position accuracy for the ToA estimation techniques. Nowadays, most of the installed aircraft transponders are Mode S, although the older interrogation method Mode 3/A/C can occasionally be found. Transponder replies of both interrogation methods work on the SSR downlink using a center-frequency of 1,090 MHz and a narrowband bandwidth of 2.6 MHz. At airports the transponder replies are deteriorated mostly by radio wave propagation effects, fading, garbling and multipath. These phenomena lead to pulse distortions and inter-symbol interferences (ISI), both eventually resulting in decoding bit errors, inaccurate and missing ToA estimations. Furthermore, the implementation costs of the receiving stations should be as low as possible, i.e. using a simple dipole antenna with a single receiving stream.

In this thesis, low-cost methods for transponder reply decoding and ToA estimation were analyzed, developed, implemented and evaluated, especially those for multipath overlapping in airport applications. This thesis is focused on multipath for Mode S signals, which is a severe issue at airports with Mode S transponders. The multipath overlapping was simulated and validated in the first step of the algorithm development.

As an important milestone in the development of the algorithms, a transponder reply receiving and ToA estimation station (RX station) was developed, fully implemented and has still been used in the ADB Safegate MLAT system at the Salzburg airport W. A. Mozart in Austria. The RX station fulfills the specifications defined in ICAO Annex X Volume IV, ED-117, ED-117A, ED-129B and ED-142. The digital signal processing and the algorithms were low-cost implemented on the field programmable gate array (FPGA) of the RX station for their evaluation and validation. Furthermore, the stations were used for real-world data collection and the ToA estimation algorithms were evaluated with test drives according to European ED-117 specifications.

This work has shown that the results of multilevel threshold detection decoding algorithm were superior to the results of other compared decoding algorithms, including the multilevel threshold detection decoding with mean filtered input, the edge detection decoding and the state-of-the-art Mode S secondary radar decoding technique. All those algorithms were developed in this work, except the common-known SSR decoding technique.

In addition, this work has shown that the developed rising edge detection ToA estimation (REDTOE) algorithm delivers the best results in terms of position accuracy in case of multipath overlapping at airports. The REDTOE algorithm was evaluated and validated with real-world data and combined with the 50% threshold detection ToA estimation algorithm as fallback to achieve best results according ED-117 specifications. The algorithms developed in this work were compared with the matched filter with differentiator, the state-of-the-art algorithm. Furthermore, the correlation ToA estimation algorithm has been presented.

Kurzfassung

Multilateration (MLAT) und Automatic Dependent Surveillance-Broadcast (ADS-B) sind moderne Überwachungs- und Identifizierungstechniken im zivilen Flugverkehrsmanagement (ATM). Sie sind die Ergänzungen zu den konventionellen Primär- und Sekundärradaren (PSR und SSR) für Luft- und Flughafenbereiche. ADS-B Systeme verwenden nur Dekodierungsmethoden und MLAT Systeme Zeitstempelvergabe- (ToA) und Dekodierungsmethoden. Internationale und Europäische Regulierungen fordern Systeme mit hoher Zuverlässigkeit, Dekodierungsmethoden mit einer geringen Bitfehlerrate und Zeitstempelvergabemethoden mit einer hohen Genauigkeit. Heutzutage benutzen die am Flugzeug installierten Transponder meistens die Interrogationsmethode Mode S, wobei es auch immer noch die älteren Mode 3/A/C Transponder gibt. Die Transponderantworten der beiden Interrogationsmethoden arbeiten an der SSR Abwärtsstrecke mit einer Mittenfrequenz von 1.090 MHz und einer 2,6 MHz Bandbreite. Die Transpondersignale an Flughäfen werden hauptsächlich von Wellenausbreitungsphänomenen wie Fading, Garbling und Mehrwegausbreitung gestört. Diese Phänomene führen zu Pulsverzerrungen und Intersymbolinterferenzen (ISI), welche letztendlich in Bitfehlern beim Dekodieren und inakkuraten oder fehlenden Zeitstempeln resultieren können. Zusätzlich sollen die Implementierungskosten so niedrig wie möglich durch die Verwendung einer Dipolantenne und nur einem Empfangskanal gehalten werden.

In dieser Arbeit wurden low-cost Verfahren zur Transponder Signaldekodierung und Zeitstempelvergabe für Anwendungen mit Mehrwegausbreitungsüberlagerung an Flughäfen analysiert, entwickelt, implementiert und evaluiert. Der Schwerpunkt dieser Arbeit liegt bei Mehrwegausbreitungsphänomenen von Mode S Signalen, die das Hauptproblem an Flughäfen darstellen. Für die Entwicklung der Algorithmen wurde die Überlagerung von Mehrwegausbreitung simuliert und validiert.

Als wichtiger Meilenstein zur Entwicklung der Algorithmen wurde eine Transponderempfangsstation (RX) entwickelt, vollständig implementiert und im ADB Safegate MLAT-System am Salzburger Flughafen W. A. Mozart in Österreich eingesetzt. Die RX-Station erfüllt ICAO Annex X Volume IV, ED-117, ED-117A, ED-129B und ED-142 Spezifikationen. Die digitale Signalverarbeitung und die Algorithmen wurden kostengünstig auf dem Field Programmable Gate Array (FPGA) der RX-Station implementiert, evaluiert und validiert. Darüber hinaus wurde die Station für die Datenerfassung verwendet und die Zeitstempelvergabe-Algorithmen wurden mit Testfahrten gemäß den europäischen Spezifikationen ED-117 ausgewertet.

In dieser Arbeit wurde gezeigt, dass der Multilevel Threshold Detection Decoding Algorithmus zu besseren Ergebnissen als die anderen verglichenen Dekodierungsalgorithmen führt, dies sind der Multilevel Threshold Detection Dekodierer mit gemitteltem Input, der Edge Detection Dekodierer und der State-of-the-art Mode S Sekundärradar Dekodierer. Mit Ausnahme der allgemein bekannten SSR Dekodierung wurden alle Algorithmen in dieser Arbeit entwickelt.

In dieser Arbeit wurde gezeigt, dass der entwickelte Algorithmus zur Zeitstempelvergabe Rising Edge Detection ToA Estimation (REDTOE) die besten Ergebnisse in Bezug auf die Positionsgenauigkeit bei Mehrwegausbreitungsüberlagerung an Flughäfen liefert. Der REDTOE Algorithmus wurde mit realen Daten evaluiert und validiert und mit dem 50% Threshold Detection ToA Estimation Algorithmus kombiniert, um beste Ergebnisse gemäß den ED-117 Spezifikationen zu erzielen. Die in dieser Arbeit entwickelten Algorithmen wurden mit dem Matched Filter mit Differenzierer, der State-of-the-art Algorithmus, verglichen.

Deutsche Fassung:
Beschluss der Curricula-Kommission für Bachelor-, Master- und Diplomstudien vom 10.11.2008
Genehmigung des Senates am 1.12.2008

EIDESSTATTLICHE ERKLÄRUNG

Ich erkläre an Eides statt, dass ich die vorliegende Arbeit selbstständig verfasst, andere als die angegebenen Quellen/Hilfsmittel nicht benutzt, und die den benutzten Quellen wörtlich und inhaltlich entnommene Stellen als solche kenntlich gemacht habe.

Graz, am …… ……..
(Unterschrift)

Englische Fassung:

STATUTORY DECLARATION

I declare that I have authored this thesis independently, that I have not used other than the declared sources / resources, and that I have explicitly marked all material which has been quoted either literally or by content from the used sources.

…… ……..
date (signature)

Acknowledgments

First of all, I would like to thank the colleagues of the RADAR department and Helmut P. from ADB Safegate Austria GmbH, especially Uli and Gerhard, which supported me during the thesis. They gave me inspiration and helped me in many interesting discussions to get new ideas and keep my motivation high. I also want to gratefully acknowledge my CEO Dr. Konrad Köck, which made the thesis possible and gave me the opportunity to work in such an interesting field. Special thanks also for my superior R&D director Dr. Arnold Maier, who supported me through all lows and highs at the end of my work.
Further, I would like to thank my supervisor Prof. Erich Leitgeb, who always provided me the necessary guidance and support.
Special thanks to the Austro Control, the Salzburg Airport W. A. Mozart and the Institute of Microwave and Photonic Engineering at the University of Technology in Graz, for their encouragement and support throughout this work.
Special thanks also to the Austrian Research Promotion Agency (FFG), which funded this thesis with the project name EMEMU and number 843411.

Graz, January 2019 Stephan Bernhart

Contents

List of Figures

List of Tables

1 Introduction

This thesis presents investigations in design, simulation, implementation and evaluations with real-world data of secondary surveillance radar (SSR) signal processing. It is a multidisciplinary work involving radio-frequency (RF) engineering, radar engineering, telecommunications engineering, digital chip design and digital signal processing. The main emphasis of the thesis is the low-cost decoding and the time of arrival (ToA) estimation of transponder replies at airports. Multipath propagation overlapping happening due to reflecting surfaces nearby, deteriorates the signals and leads possibly to higher bit error rates (BER) and low accurate or missing ToA estimations. Furthermore, the thesis concerns the implementation costs and so all analyzed algorithms are low-cost and easy implementable on a field programmable gate array (FPGA) or digital signal processing (DSP).

1.1 Overview

For decades primary surveillance radar (PSR) and SSR were the main surveillance technologies in the civil air traffic control (ATC). Both technologies are used for air or ground situation and are sometimes obligatory depending on the situation. The PSR detects and localizes non-cooperative targets by delivering a video of the reflected electromagnetic waves. This video targets can be extracted and combined with other radar technologies. The SSR instead is not only able to localize the target, but also to identify and to communicate with it via the internationally defined interrogation methods Mode 3/A/C and Mode S. The Mode 3/A/C interrogation method is the older method and the Mode A code is used for identification and Mode C is the barometric measured altitude. The newer interrogation method Mode S instead delivers the registration address for identification and many more aircraft data like the GPS position, when applicable. The ATC uses as complement the PSR for detecting non-cooperative targets and the SSR for detecting cooperative ones [28]. The enhancements of SSR and the introduction of Mode S lead to newer technologies like automatic dependent surveillance-broadcast (ADS-B) and multilateration (MLAT). MLAT can provide much lower hardware installation costs, higher position accuracy, less maintenance costs, higher reliability and both have an easier scalable architecture [8].
Nowadays, ADS-B and MLAT are the state-of-the-art technologies for surveillance and identification in civil aviation. Both technologies are key enablers for the Single European Sky ATM Research (SESAR) infrastructure modernization program [17]. The MLAT technology typically fulfills specifications defined by the European organization for civil aviation equipment (EUROCAE) in the Minimum Operational Performance Specification for Mode S Multilateration Systems for use in Advanced Surface Movement Guidance and Control Systems (A-SMGCS) ED-117A [13] at the ground and the Technical Specification for Wide Area Multilateration (WAM) Systems ED-142 [15] document for wide area. ADS-B specifications are defined in the Technical Specification for a 1,090 MHz Extended Squitter ADS-B Ground

System ED-129B [14].
Transponder replies received at airports suffer from radio wave propagation effects like fading, garbling and multipath. The multipath overlapping for transponder replies at airports is analyzed in a first step to gain knowledge of the behavior and to develop algorithms partly resistant against the high multipath occurrence. To fulfill European regulations MLAT systems need to accurately estimate the ToA and to have a low BER when decoding. Decoders for ADS-B and MLAT systems typically are distributed over the area of interest and should not be expensive installations. Therefore, in this thesis low-cost implementations for decoding are analyzed. The concerned ToA estimation algorithms are low-cost too and aim to achieve a high position accuracy. Especially the rising edge detection ToA estimation algorithm (REDTOE) works at the first rising edge, on which the multipath overlapping occurrence at airports is the lowest. Using this property, the algorithm achieves the best results in terms of position accuracy.
For evaluating and validating the algorithms, a transponder reply receiving and ToA estimation station is implemented. The station is installed fourteen times at the Salzburg airport W. A. Mozart in Austria in the ADB Safegate MLAT system. With the installed receivers (RX), all developed and analyzed algorithms can be evaluated according to the European MLAT standard ED-117A. The performance measurements are analyzed and listed in this thesis.

1.2 State-of-the-Art Literature Review

The SSR field for ground radars and transponders is already well investigated. The list of books and publications is extensive [26, 31, 39], as is the list of manufacturers. The digital signal processing for narrowband communication is also a well investigated field [1, 9, 10, 30, 35, 38].
In the research area of MLAT there exist already several algorithms and signal investigations, i.e. decoding algorithms for the separation of Mode S replies using spectral analysis [20, 22]. The work uses super resolution based on Tufts-Kumaresan, Music, Esprit and Unitary Esprit algorithms to discriminate signals in the frequency domain and to decode Mode S replies and squitters with sensible improvements [20]. Furthermore, there is an implementation of an experimental transponder data recorder using a wideband linear array antenna [23]. The RX stations deployment strategies based on metaheuristic optimization techniques, like Genetic Algorithm [32], and the regularized location estimator, based on Tikhonov regularization and on maximum-likelihood estimation, for time difference of arrival (TDOA) estimation MLAT systems [33] are also published.
The decoding method of conventional Mode S secondary radars, like it used in the SIR-S, marks each decoded bit as low or high confidence [20]. The bit decoding compares the signal amplitude with a pulse threshold at the time interval of the payload where the pulse transition is expected. Additionally, it compares the signal with a ± 1.5 dB threshold centered on the preamble pulse level. The data part is pulse position modulated (PPM) and each pulse transition is according the ICAO Annex X Volume IV regulations [27] at a certain time in the payload. The pulse threshold is typically set to the half of the pulse peak. The corresponding bit gets marked as high confidence, if the both samples before and after the expected time interval cross the threshold by rising or descending and the pulse level correlates with the ± 1.5 dB threshold. Otherwise the corresponding bit is marked as low confidence, i.e. both samples are higher or lower the pulse threshold.

The most common ToA estimation technique is the threshold detection ToA estimation, as described in Section 5.1. Typically, it compares the first rising or falling edge with a certain threshold and sets there the ToA [21]. The state-of-the-art ToA estimation algorithm consists of a signal filter, a zero-crossing detection and an interpolation step [21]. The signal filter is a combination of a matched filter (MF), which matches to the pulse waveform of the transponder replies, and a differentiator. This digital filter is applied to the input stream and from the output stream a zero-crossing can be detected to set the interpolated ToA. Both algorithms are compared in this work with the developed algorithms.

1.3 Thesis Structure and Contributions

This thesis is structured as follows: in Chapter 2 the ATC fundamentals for decoding and ToA estimating of transponder replies are described in detail. In Chapter 3 multipath overlapping is simulated and analyzed as base for the decoding and ToA estimation chapters. In Chapter 4 low-cost decoding methods and in Chapter 5 ToA estimation algorithms are described, analyzed and compared. Chapter 6 contains the implementation of a transponder reply receiving and precision ToA estimation station, on which all mentioned algorithms are evaluated and validated. In Chapter 7 the test setup at the Salzburg airport is described, where the ToA estimation are evaluated according European Specifications ED-117 [12]. The main contributions of this work are:

- **Multipath overlapping simulation:** The simulations of overlapping are the base to understand the influence of multipath and to develop decoding and ToA estimation algorithms. Furthermore, they supported significantly the development of the digital signal processing and the multipath detectors for the algorithms.
- **Decoding algorithms:** There are three low-cost decoding algorithms developed in this work and compared with each other and with the Mode S secondary radar decoding technique using real-world data. These are the multilevel threshold detection decoding with standard and mean filtered input and the edge detection decoding. Especially the multilevel threshold detection decoding leads to better results, also in case of multipath overlapping.
- **ToA estimation algorithms:** There are two low-cost ToA estimation algorithms with combination developed in this work, the correlation ToA estimation, the REDTOE algorithm and the hybrid using the REDTOE as primary algorithm and the 50% threshold detection ToA estimation as fallback. The REDTOE and the hybrid algorithm are compared with real-world data from Salzburg airport according European specification ED-117. Especially the evaluations of the hybrid algorithm have shown that the algorithm leads to the best performance in terms of position accuracy and probability of detection, in case of multipath overlapping at airports. Additionally, variations of the common known threshold detection ToA estimation are presented.
- **Receiving and ToA estimation station:** The design and implementation of the RX station is developed in this work and used for evaluation and validation purposes at the Salzburg test airport as part of the ADB Safegate MLAT system. The station fulfills

the specifications defined in ICAO Annex X Volume IV [27], ED-117 [12], ED-117A [13], ED-129B [14] and ED-142 [15]. Furthermore, it was used to analyze the algorithms and determine the implementation costs on the FPGA.

- **ToA estimation algorithms evaluations at the Salzburg airport:** The full evaluation analysis according to European specifications ED-117 in terms of position accuracy, probability of detection, probability of false detection and probability of update is presented. For the ToA estimation four algorithms are evaluated and validated, three out of four are presented in this work.

2 Fundamentals

In this chapter, the fundamentals for the decoding and ToA estimation methods are described. The fundamentals contain the basic of ATC, surveillance radar knowledge of PSR, SSR, MLAT and ADS-B. Furthermore, the ATC frequency band with Mode A/C and Mode S interrogation methods, for which the developed algorithms are designed and also the radio wave propagation effects, especially for airports applications, are described as well.

2.1 Air Traffic Control

The aim of ATC is to control and order safely and efficiently the traffic on air and ground. The ATC supervises flights according to instrument flight rules (IFR) and visual flight rules (VFR). The service of ATC is to deliver flight data information, flight traffic, weather information, aeronautical telecommunications and the responsibility of ATC infrastructure. The world-wide regulation is done by the international civil aviation organization (ICAO), which is a suborganization of the united nations (UN). In Europe the highest aviation organization is the Eurocontrol, in the United States of America it is the federal aviation administration (FAA). Typically, every nation has a local air navigation service provider (ANSP) which is responsible for a safe and economic air traffic management. In Austria it is the Austro Control for the Austrian airspace.

2.2 MSPSR, PSR, SSR

The PSR used by the ATC, is a radar sensor which sends pulsed electromagnetic waves and receives the echoes reflected from the target. It has typically a rotating antenna with narrow beam width and high transmitting power. The PSR knows the angle by the antenna's position and the distance by the elapsed time when receiving the reflected waves from the aircraft body. The output of the PSR is a video of the ground or air situation, from which plots can be extracted and used for aircraft detection.
The SSR used by the ATC, communicates over the downlink and uplink with the vehicle and aircraft transponder. The downlink is 1,090 MHz with a 3 dB-bandwidth of 2.6 MHz and the uplink at 1,030 MHz with a 3 dB-bandwidth of 8 MHz [27]. The interrogation methods are Mode A/C and Mode S. A transmission of the ground station to the target is called interrogation and the transmission of the target is called reply. Originally, the SSR was used for identification of friend or foe (IFF), it enabled the ATC to identify aircraft as friendly with bearing and range information. One of the issues with secondary radars is the transponder signal overlapping of different transponders and is called garbling.
The newest radar technology is the multi-static PSR (MSPSR), which calculates the position of non-cooperative targets by using a network of distributed transmitting and receiving

stations. There is no fixed frequency, but ultra-high frequency (UHF), L and S band are typically used [16].

2.3 Transponder Reply Signal Properties

Mode A/C and Mode S are interrogation methods defined for ATC. They define the interrogation of the ground station to the transponder and the transponder replies. The transponder can be installed on aircraft or vehicles. Mode A/C is the old interrogation method and Mode S the newer one. The main issues of Mode A/C are the limited size of the 4,096 possible identification codes, the limited data information and communication, the missing checksum and the Mode A/C interrogation. The Mode A/C interrogation has the drawback, that all reachable transponder are replying to a single call, which leads to an overlapping of the signals and therefore to a low decoding probability. Mode S was introduced after Mode A/C and solves some of these issues by introducing longer payload and addressed interrogation. Furthermore, Mode S can contain a global navigation satellite system (GNSS) position of the aircraft, which is the key element for surveillance technologies.

2.3.1 Mode A/C Reply

The downlink signal of Mode A/C is pulse position modulated (PPM) and contains 12 data bits. The reply signal has two framing pulses, one at the beginning and one at the end. The transponder reply is identified as Mode A/C by detecting the framing pulses. They are separated by 20.3 microseconds and have a pulse duration of 0.45 microseconds. The other twelve payload pulses are spaced by 1.45 microseconds within the framing pair. There exists an additional pulse spaced 4.35 microseconds after the framing pulse at the end, the special purpose identification (SPI) pulse. The pulse at the center of the reply is always missing. A logical '1' is detected, when the pulse is present and a logical '0' if not [27]. Depending on the interrogation mode the extracted data represents a four-digit octal code and is the Mode A code or is the barometric measured height for Mode C. The Mode A code, also called squawk, is used for identification and the height is the Gillham coded flight level with a resolution of 30.48 m or 100 ft.

2.3.2 Mode S Reply

The downlink signal of Mode S consists of a preamble and a data part. The transponder reply is identified as Mode S by detecting the preamble. The data block can contain either 56 or 112 bits. The preamble consists of four pulses, which are spaced at 0.0, 1.0, 3.5 and 4.5 microseconds, having a pulse duration of 0.5 microseconds. The data segment is coded using unipolar Manchester codes [38], in this case with an offset of half amplitude level. A logical '1' is detected, when the pulse amplitude descends from pulse to pause level and a bit is logical '0', when the amplitude rises from the pause to pulse level. There are 25 downlink formats (DF) defined for Mode S, each format has its own particular purpose. Relevant Mode S squitter formats for ADS-B and MLAT are DF11, DF17, also known as the extended squitter (ES) and DF18 [27]. From the ES signal the GNSS position can be extracted and be used in ADS-B, MLAT or traffic information service-broadcast (TIS-B) systems.

2.4 Radio Wave Propagation Effects

The radio wave propagation effects concerned in this thesis for transponder replies at airports are fading, garbling and multipath. Fading is the overlapping of the line-of-sight (LOS) signal with its own ground reflection. Garbling is the overlapping from different transponder signals at the receiver antenna. Whereas fading is the overlapping of the LOS signals with the reflected wave on ground at the receiver antenna from one transponder. Multipath is the overlapping of the LOS signal with the reflected signal at physical objects, e.g. aircraft components or masts. All types of overlapping are in frequency and time domain [39].

2.4.1 Fading and Garbling

Fading is the overlapping of the LOS signal with the ground wave. The received power and phase shift can be described by a path-loss model. Fading with a LOS component stronger than the other components is described by the Rician fading [1].
Garbling is the overlapping of different transponder replies. It occurs frequently for targets which are close to each other in range, as measured from the secondary radar. In Mode A/C interrogation, garbled replies can often not be resolved and can lead to a loss of detection/information. While the same issue can exist with Mode S interrogations, several technical options exist which can mitigate the issue, or at least correctly detect garbling with a higher probability. Algorithms for separating the transponder replies, are typically named as degarbling. Garbling is divided in asynchronous and synchronous garbling. Asynchronous garbling is when the transponder reply pulses of the different transponders are not overlapping each other, which is easier to separate. Synchronous garbling is happening when the pulses overlap each other, so that only the signal pulses with higher power are visible on the time diagram.

2.4.2 Multipath Propagation

Transponder replies can be affected by multipath and therefore the receiver antenna receives the superposition of multiple signal copies. The copies may differ in attenuation, phase shift and reception time and lead to a constructive or destructive interference [1]. When signal duplicates are delayed too long, this can cause inter-symbol interferences (ISI) at the communication channel. The delay spread is a measurement ratio to express the number of containing signal copies and it shows if ISI is happening [38].
The example of a baseband Mode S signal with overlapping multipath distortion is shown in Figure 2.1. The multipath signal is received, compared to the LOS signal, approx. 800 nanoseconds later and the amplitude is damped by 3 dB. Here, the delay spread is higher than the symbol duration and therefore the communication channel is not free from ISI. Another recorded baseband Mode S signal without any propagation effects is shown in Figure 2.2.

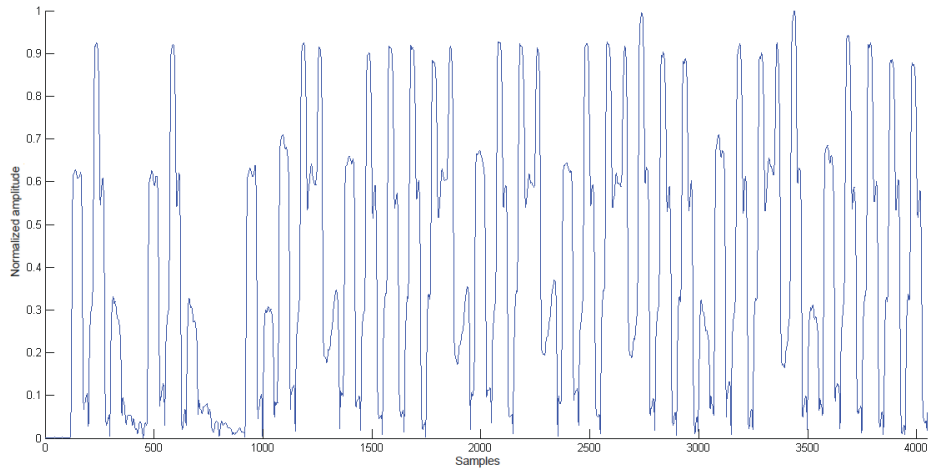

Figure 2.1: Baseband Mode S signal corrupted by multipath propagation [7]

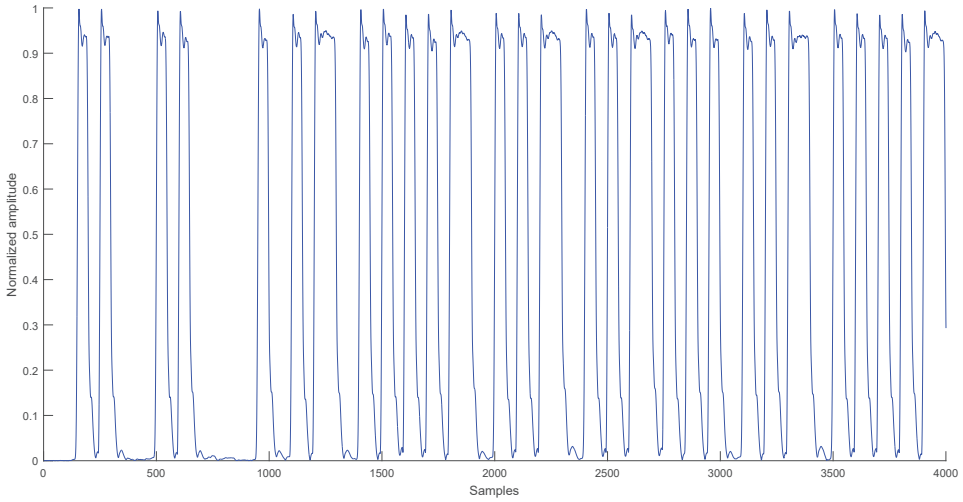

Figure 2.2: Recorded baseband Mode S signal

2.5 ADS-B

ADS-B is a technology for communications, navigation and surveillance in ATC. It operates without human intervention and depends on the position determined by GNSS. It broadcasts automatically Mode S data, containing information as its own position, identification and more to other aircraft or ground stations [29]. The advantages of ADS-B are to be a cheap solution and allowing the exchange of traffic and weather information with ADS-B in and out. ADS-B uses Mode S ES as physical layer for relaying position reports [37]. It is a series of Mode S signals broad-casted by the aircraft and containing identification, position and

status data to enable position tracking. One important security criterion is that ADS-B is vulnerable to spoofing. ADS-B is depending on the information of the aircraft's aeronautical equipment. For an ADS-B system the low-cost decoding methods, as described in Chapter 4, are of importance.

2.6 Multilateration

A typical MLAT system consists of RX, transmitting (TX), reference transponder (RT) stations, central processing station (CPS) and control and monitoring system (CMS), as shown in Figure 2.3. Typically, the TX stations are receiving stations too (RXTX). At least the RX and TX stations are connected to the CPS via communication links. The main aim of the RT station is to continuously validate the calculated position with the measured one and determine the accuracy deviation of the MLAT system. MLAT systems are also categorized in active and passive systems. A passive system is when no transmitting of the system itself is happening (without TX component) and an active system is when its transmitting to interrogate the transponders. MLAT systems installed at European airports should fulfill surveillance specifications, which are defined by the EUROCAE in the ED-117A document, which is the minimum operational performance specification (MOPS) for Mode S multilateration systems for use in A-SMGCS [13]. The ED-117A document contains information how the factory acceptance tests (FAT) and the site acceptance tests (SAT) need to be done. Furthermore, it contains directives for environmental and electromagnetic compatibility (EMC) tests, requirements for monitoring, control, reporting, logging, recording, redundancy, reliability, maintainability, availability of service, recovery after failure, lightning protection, obstruction lights, etc. Some of the MOPS regarding position tracking are target report update rate, probability of target report, probability of identification, position accuracy, maximum gap time of the position output and target initiating time. The MOPS are defined for different areas at the airport the maneuvering area (runway, taxiway, apron centerlines), apron taxiways and taxi lanes, and stands. The performance of a MLAT systems, in terms of position accuracy, probability of (false) detection, probability of (false) identification and gaps, depend mostly on the signal processing of the RX, decoding and ToA estimation, and on the number and position of the RX stations [13].

2.6.1 Receiving Station

The RX station consists typically of an antenna, a RF receiver and a digital processing part. The RX station can be mounted on masts, pedestals or buildings with an outdoor housing. It can also be mounted indoor, e.g. in a server rack. The antenna is typically realized as a half-wave dipole, used on top or with a reflector e.g. on the wall of a building. The antenna has a center frequency of 1,090 MHz and a half-bandwidth of 30 MHz, it is simple to realize, affordable and has an omnidirectional radiation pattern. There exist also RX stations with other antenna types, like phased arrays [23], which are, due to its complexity, more used in scientific test systems. The receiver consists of the down-conversion of the received transponder reply to the intermediate frequency (IF). The signals are further demodulated, digital signal processed, ToA estimated and decoded in the digital processing part, which is typically implemented on FPGA or microcontroller. Eventually, the ToA estimated and

decoded transponder replies are send to the CPS for further processing.

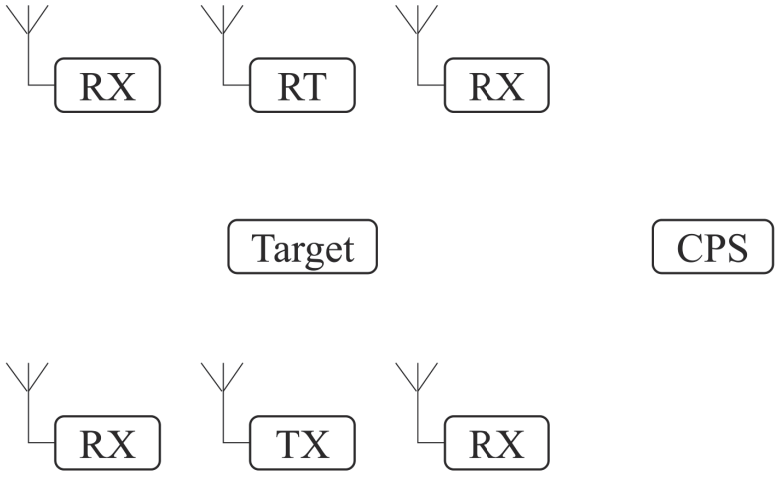

Figure 2.3: Typical MLAT system at airports

2.6.2 Time-Synchronization

Each MLAT system must be time-synchronized to achieve an accurate ToA estimation, so there are two types of time-synchronization systems, centralized and decentralized. Centralized schemes set the ToA for each received transponder reply at the CPS by using only one single time source. They correct the ToA of the received signals with the known measured fixed delay to each RX station. To assure an accurate ToA, each RX station must be connected to the CPS via data lines which have a fixed transmission delay like fiber optics. Decentralized schemes instead set the ToA of the transponder replies at the RX stations itself. To do so each RX stations must be time-synchronized. Typical methods are to use the pulse per second (PPS) of GNSS receivers like GPS [24] or to use reference transponder or transmitter. Furthermore, the RX stations must have an accurate time source with a high short-term stability. A ToA precision of at least 1 nanoseconds leads to a maximal position accuracy of 0.3 m. Commonly an oven-controlled crystal oscillator (OCXO) is used as time source, because they are enough accurate and affordable.

2.6.3 Central Processing Station

The CPS stations calculate the 2D or 3D position of the transponder with the given RX station signals. The calculation is done with the time difference of arrival (TDOA) or the time sum of arrival (TSOA) principle. The CPS receives the ToA and the signal content from all receiving station and with this data the CPS is able to calculate the intersections of the hyperboloids and can estimate the transponder position. Typically, the calculated position is tracked with a Kalman filter [44].

The TSOA principle also includes the interrogation time in the position calculation. The knowledge of the sending time, the transponder delay and the receiving time enables the CPS to furthermore intersect an ellipsoid with the hyperboloids. Due to the unknown or only estimated transponder response time, the computed distance is not that accurate and the TSOA is typically used for wide area, outside of the area surrounded by the RX stations.
A typical CPS consists of the following main tasks: data collection, synchronization, measurement correlation, calculation and result emission, as shown in Figure 2.4. The data collection receives the decoded and ToA estimated signal data from the RU stations, the synchronization does the time-synchronization for each RX, the measurement correlation identifies the signals and tags them as tuples, the calculation does the position computation and the result emission, emits the position information in the corresponding format [18].

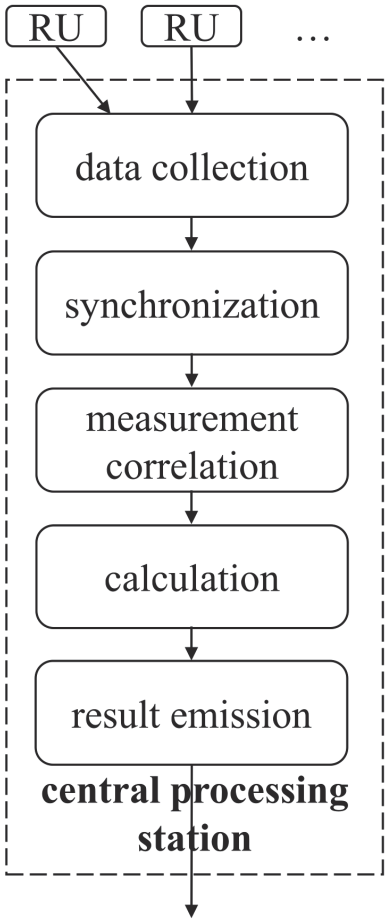

Figure 2.4: Block diagram of the central processing station

2.6.4 Station Deployment Determination

Important for the performance of the MLAT system is the determination of the location of RX, TX and RT stations. After the CPS tuning the system must fulfill all ED-117A performance specifications, which involves also the $N + 1$ redundancy [13]. The main criteria for the RX locations is that at least three sensors are needed for the 2D and four for the 3D position calculation. Considering the redundancy there must be at least five RX sensors having LOS to each point in the area of interest. At airports, typically many kinds of buildings block the LOS to the stations and so the number of needed RX stations increases. Furthermore, each RX station must have LOS to at least one RT stations and there must be at least two RT stations, due to the redundancy reason. There must be also at least two TX stations for redundancy reasons and they must be reach the point at the area of interest, in order to be able to reliably interrogate the transponders. Additionally, if they are used for time-synchronization, each RX stations must have LOS to at least two TX stations.
As a first step, the deployment of the different type of stations at the airports can be done with a simulation software. Depending on the simulation software, it computes the LOS visibility, Fresnel zones or electromagnetic fields and gives an estimate for the possible positions. The simulations are also depending on the quality of the available technical drawings of the airport to create a 2.5D or 3D model. There exist also strategies for the stations deployment based on metaheuristic optimization techniques [32] and, especially for ToA estimation MLAT systems, the regularized location estimator [33].

3 Multipath Overlapping Analysis

In this chapter, inference caused by multipath overlapping is simulated and analyzed. The simulations are used for the development of signal processing, decoding and ToA estimation algorithms of transponder replies. The simulations are done with the program MATLAB and include the most common cases of multipath overlapping with only one dominant multipath component. Empirically, it has been shown that multipath overlapping at airports mostly contains only one multipath component. These parts lead to constructive and destructive interferences. In case of a LOS signal with multipath components, the channels behave like the Rician fading channel [1].

3.1 Simulation Model

The simulation model for the MATLAB script generates an PPM 1,090 MHz Mode S signal with a tolerance of ±1 MHz and a half-bandwidth of 2.6 MHz [27]. Additionally, it generates one additive multipath component and white Gaussian noise. The simulation model considers for the sake of simplicity only the first dominant overlapping multipath component. The model generates the modulated signal $y(t)$ with the configured carrier frequency f_C, the amplitude A and the baseband signal $m(t)$, as shown in Equation 3.1. The normalized baseband signal contains the defined timing and pulse properties by ICAO Annex X Volume IV [27]. The data format is configurable as the containing 24 bit Mode S address.

$$y(t) = Asin(2\pi f_C t)[1 + m(t)] \tag{3.1}$$

The multipath component $y(t - \tau)$ has some additional parameters than the LOS component $y(t)$. These are the damping factor DF, the phase shift ϕ_{MP} and the time delay τ. The damping factor is the transmission power reduction of the multipath component and is due to the additional radio wave propagation distance in relation to the LOS signal amplitude. The phase shift is due to surface reflection. Eventually, the LOS and multipath component are summed together with an additional additive white Gaussian noise $n(t)$ and create the received signal $r(t)$, as shown in Equation 3.2. The white noise is uniformly distributed and the time t of the received signal starts with zero.

$$r(t) = y(t) + y(t - \tau)DF \exp(j\phi_{MP}) + n(t) \tag{3.2}$$

The normalized baseband signal of Mode S preamble with an SNR of 35 dB is shown in Figure 3.1 and the corresponding modulated preamble in Figure 3.2.

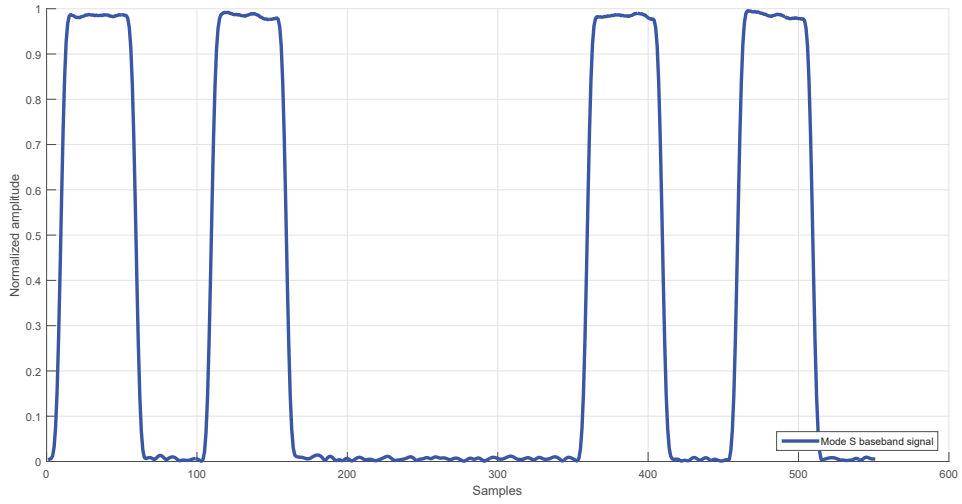

Figure 3.1: Mode S baseband signal

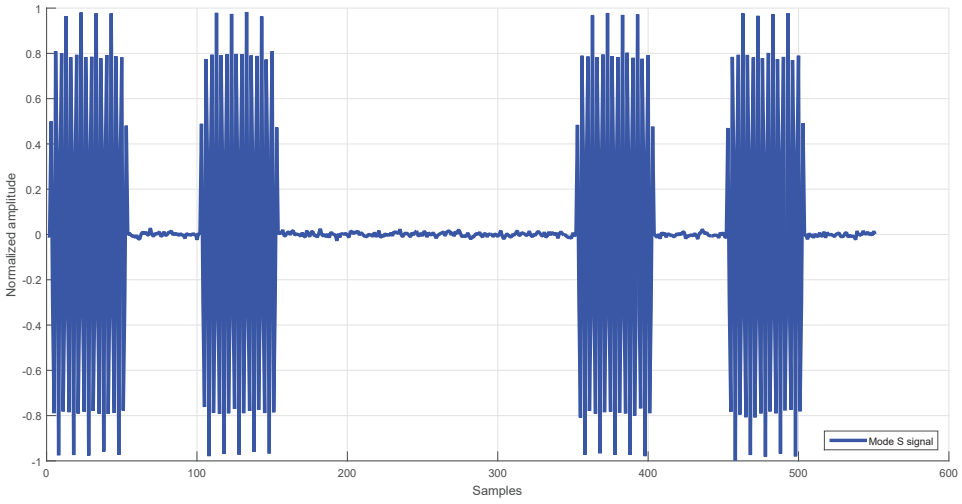

Figure 3.2: Mode S signal

3.2 Simulations

The Mode S signals, simulated according to the data model, are demodulated and have a SNR of 35 dB, no smoothing filter, a phase shift of $-\pi$ radians, an attenuation of the overlapped signal DF of -6 dB and the time delay τ varies from 0, 25, 50, 75, 100, 125 and 150 m, as shown in Equation 3.2. The simulation results are shown in Figure 3.3, 3.4, 3.5 and 3.6.

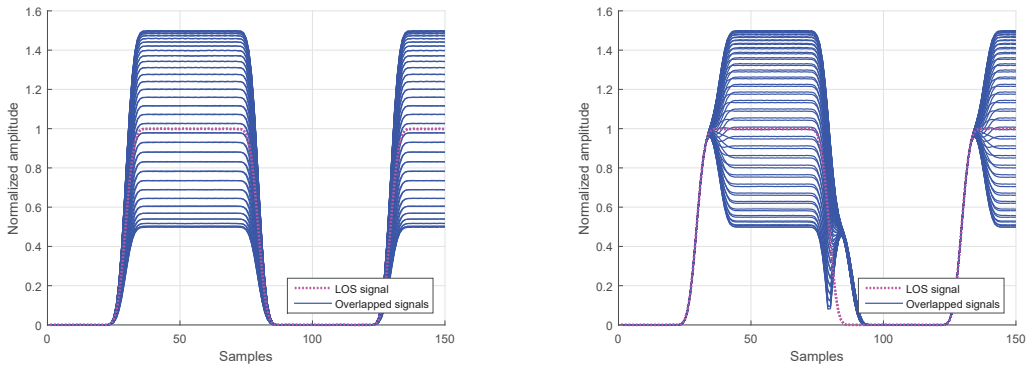

Figure 3.3: Multipath simulation - time delay of 0 (left) and 83.33 nanoseconds (right)

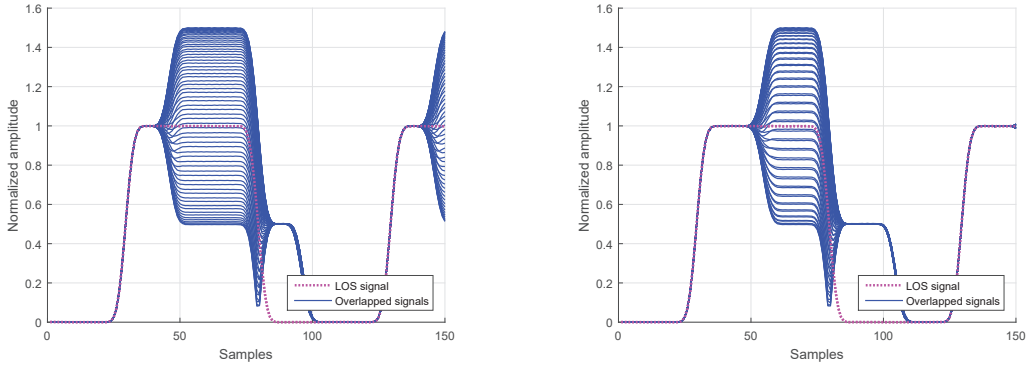

Figure 3.4: Multipath simulation - time delay of 166.67 (left) and 250 nanoseconds (right)

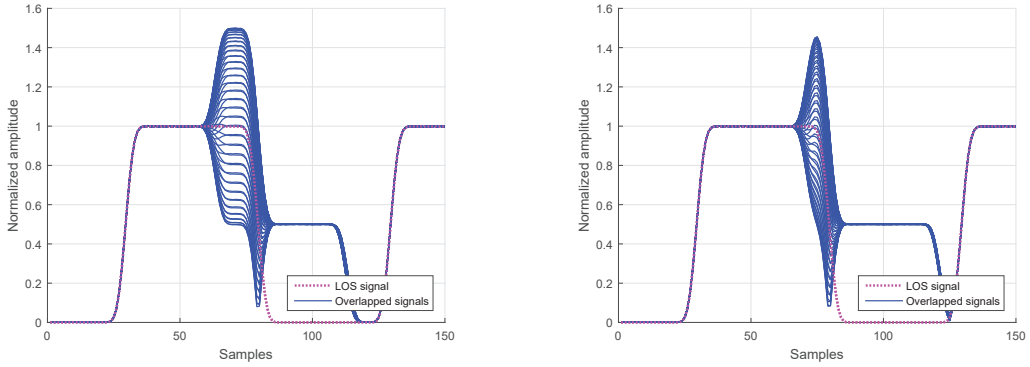

Figure 3.5: Multipath simulation - time delay of 333.33 (left) and 416.67 nanoseconds (right)

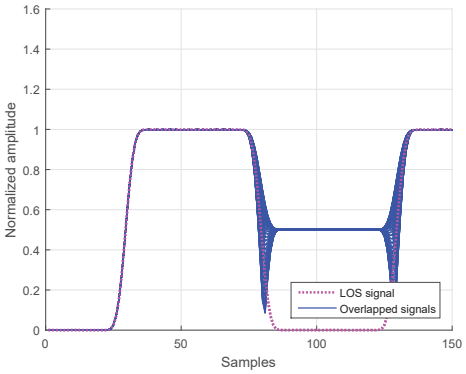

Figure 3.6: Multipath simulation - time delay of 500 nanoseconds

3.2.1 High-Amplitude Multipath Component

In recordings the overlapping with a high-amplitude multipath component can be seen very often. In this example, as shown in Figure 3.7, the multipath component is damped by 0 dB and the time delay is 60 m.

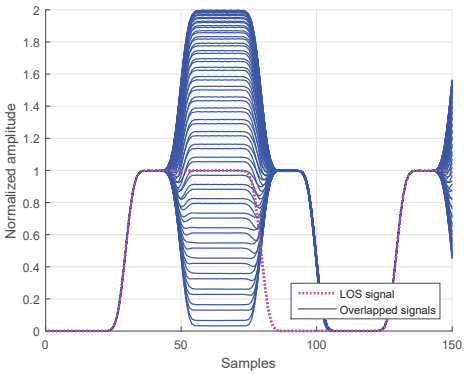

Figure 3.7: Multipath simulation - high-amplitude multipath component

3.2.2 No and very Low-Amplitude LOS Component

There is also the case of receiving non-LOS (NLOS) signals which only consists of multipath components. Typically, this is happening if another object, e.g. aircraft, is located in the first Fresnel zone between transponder and RX antenna [9, 38]. When concerning the ToA estimation, NLOS signals with only multipath components from a RX station are very difficult to detect and can easier identified by the CPS. The outlier detection of the CPS can detect signals with a bad ToA when calculating the position. They lead to a position with a high error or to no position. Having an overdetermined MLAT system helps the CPS to detect the RX station with the bad ToA and to exclude it from the computation, as described in

Section 3.3.5.
There exists also the case that the amplitude of the LOS signal is much lower than the multipath component. For this case it can be checked whether the first pulse of the signal a low-amplitude pulse is located. This pre-pulse can then be detected and ToA estimated. The CPS receives both ToAs, from the pre-pulse and the first pulse, and estimates by calculating the position using an outlier detection, which ToA of the LOS signal is.

3.3 Results of Multipath Overlapping Analysis

The conclusions of the multipath overlapping analysis contain the multipath influence on the transponder reply edges, as shown in Section 3.3.1, the digital signal filter, as shown in Section 3.3.2, conclusions for the threshold detection ToA estimation algorithm and the REDTOE, as shown in Sections 3.3.3 and 3.3.4, the overlapping detection and the pulse width, as shown in Section 3.3.5.

3.3.1 Multipath Overlapping - Signal Edges Influence

Overlapping multipath at Mode S signals with a time delay τ of less than 50 nanoseconds or 15 m in distance, influence both edges very similar, rising and falling of the first pulse. With a higher time delay than 50 nanoseconds or 15 m in distance, the falling edge is more influenced than the rising. With a time delay of 450 nanoseconds or 135 m in distance, the first rising edge is not overlapped anymore, but the falling edge and rising edge of the second pulse is strongly overlapped, as shown in Table 3.1.

Time delay τ (nanoseconds)	Corresponding distance x (m)	Multipath overlapping MPO on rising (RE) and falling (FE) edges
$0 < \tau \leq 50$	$0 < x \leq 15$	$MPO_{RE} \sim MPO_{FE}$
$50 < \tau \leq 450$	$15 < x \leq 135$	$MPO_{RE} < MPO_{FE}$
$450 < \tau < \infty$	$135 < x < \infty$	$MPO_{RE} \ll MPO_{FE}$

Table 3.1: Multipath Overlapping on the First Pulse's Edges

3.3.2 Digital Filtering

For the ToA estimation, the digital signal filtering smooths the input baseband signal to reduce the additive white Gaussian noise. This is implemented on digital designs with a cascaded integrated comb (CIC) using 2 taps [7] at 70 MHz IF.
For the decoding, the digital signal filtering smooths the input baseband signal very strongly to reduce the white noise and overlapped signals by a CIC using 32 taps. The digital filter has 32 coefficients, so that the filter length corresponds to the whole baseband signal's pulse duration at 70 MHz IF. Furthermore, it is a multiple of two, that it can be easily implemented in digital designs [4].

3.3.3 Threshold Detection ToA Estimation Algorithm

In case of multipath overlapping, the pulse peak varies the most by increasing or decreasing the peak power, as it is shown in Section 3.2. This happens even when the peak power is averaged. So, algorithms depending on the peak power, like the threshold detection ToA estimation algorithm, lead to higher ToA estimation deviations in case of multipath overlapping. The algorithm, which works on the rising edge of the first pulse, is affected in case of a multipath time delay from 0 to over 450 nanoseconds or 135 m in distance, as it is shown in Table 3.1. In case of a higher time delay, the algorithm is not disturbed anymore by multipath, simply because the overlapping wave starts after the first pulse.
Furthermore, knowing that the estimated ToA deviation for the threshold detection ToA estimation algorithm relates to the pulse variation caused by multipath propagation, the conventional 50% threshold could be improved by setting it lower, i.e. to 25%. The same threshold is applied on the rising edge of the first preamble pulse. The lower 25% threshold has a theoretical improvement of factor two in terms of the ToA estimation deviation. The improvement is based on the fact that the 25% threshold has a similar slope than the 50% threshold.

3.3.4 Rising Edge Detection ToA Estimation Algorithm

The multipath overlapping parts are always delayed compared to the LOS wave. This means, that the first rising edge is the less influenced signal part by multipath overlapping. The REDTOE uses this property for its advantage by only applying the method on the first rising edge, as described more in detail in Chapter 5.

3.3.5 Overlapping Detection

A very simple signal overlapping detector is that the RX station calculates not only the peak power of the pulses, but also the signal level in the pulse pause. The ratio of pulse peak to pulse pause level is similar to the SNR. This is easy to implement and provides a good indicator for overlapped signals when the ratio gets significantly lower than the SNR.
Another method is to calculate the target position at the CPS with different RX stations and according to the computation's error, the CPS is able to decide which position output to take for further processing. This is only possible with an overdetermined RX system. If more RX stations combinations deliver the same position, the calculated position with higher error can be identified and excluded as outlier. Also tracking algorithms are able to exclude computed outlier positions.
In terms of multipath overlapping detection, the falling edge of the baseband signal could be used as indicator. The reason is that the falling edge is mostly strongly influenced by the overlapping.
The pulse width, computed by subtracting the falling edge ToA from the rising edge ToA, can be used as an indicator to detect multipath overlapping and estimate the rising edge ToA deviation. But it cannot be used to correct this error. Observations have shown that, if the pulse width differs from its typical width, there must be an error on the estimated ToA due to distortions, like multipath overlapping. There are cases where the pulse width of a signal with destructive multipath has the same width as the LOS signal. Due to destructive

multipath overlapping the peak amplitude decreases. But when calculating the pulse width, it seems that there is no overlapping influence. This means that not every type of multipath overlapping can be detected as multipath by only observing the pulse width. Since multipath varies the peak power, the pulses shape and the pulse width, it seems to be difficult to find a way to correct the estimated ToA in a general approach.

3.4 Fading Propagation

Fading is the overlapping of the ground wave with the LOS wave from the same transponder at the RX antenna. It is deteriorating the transponder replies and therefore an issue at airports. At the ground areas of an airport, the aircraft equipped with transponders are in range of several kilometers, typically up to 5 km. The installed RX antennas of the MLAT system are mostly at a height of 6 to 10 m mounted on masts. On other mounting points, like buildings, lightning masts, hangar, they can be even mounted higher. The additional distance delays of the fading ground waves are listed from 50 to 5,000 m of distance between the RX and TX antenna in Table 3.2 [9]. The minimum distance delay of an aircraft is 50 m, because they typically cannot come closer to RX antennas. Higher values than 5,000 m are also not shown, because they have a distance delay lower than 0.014 m, which is already negligible.

Distance delay (m)	RX/TX antenna height (m)	Distance between RX to TX antennas (m)
0.014	6	5,000
0.072	6	1,000
0.144	6	500
0.72	6	100
1.44	6	50

Table 3.2: Fading Path Loss

According to Table 3.2, fading with an RX antenna height higher than 6 m results in a maximal fading distance delay of 1.44 m. The fading distance delay is very small compared to the 150 m pulse width. Having only such small values, the overloaded signal part increases and decreases the pulse shape symmetrically. This means that the rising and falling edges of the reply pulses are influenced equally.

3.5 Multipath Overlapping Analysis Summary

In this chapter, a MATLAB simulation model for multipath overlapping of Mode S signals is presented. The simulations show graphically the multipath influence, by varying the time delay and the amplitude of the multipath part. Special cases, like no and low-amplitude of the LOS signal are also considered. Furthermore, it has been shown, how multipath propagation relates to the threshold detection ToA estimation algorithm and the rising edge detection ToA estimation algorithm and how the signal processing could be done for ToA estimation and decoding algorithms. Additionally, the pulse width is analyzed as indicator for multipath propagation and eventually the fading influence on Mode S signal is summarized.

4 Decoding Algorithms

In this chapter, the decoding methods are described, which are designed for transponder replies and are low-cost implementations for FPGA and DSP. They are the multilevel threshold detection with standard, as described in Section 4.3.1, and with mean input, as described in Section 4.3.2, and the edge detection, as described in Section 4.3.3. The methods need corresponding digital signal preprocessing and signal detection, as described in Section 4.1, and the payload timing pattern for bit detection, as described in Section 4.2. The methods are implemented on the FPGA, as described in Section 4.4, and are evaluated and validated with real-world data, as described in Section 4.5.

4.1 Signal Detection and Digital Filtering

The transponder reply detection uses the technique MF. The digital filter contains as coefficients the ideal reply pulse samples. For Mode A/C the two framing pulses are used and for Mode S the four pulses of the preamble [20].
The input of the digital signal filtering is given by the received transponder replies, already down-converted and demodulated to the baseband signal. This signal is further smoothed, by a CIC structure using 32 taps, as described in Section 3.3.2. The filter reduces transient signal overlaps and noise. The digital filter is used for all analyzed methods and the evaluations have been shown that it improves the decoding significantly.

4.2 Payload Timing Pattern

To decode the payload a time pattern with fixed pulse timing is used. The pattern is laid over the signal and contains the timing for the expected pulses, as shown in Figure 4.1. Since Mode A/C has data bits which are modulated according to the PPM, the aim of the decoding algorithm is to detect if a pulse is present or not. The time pattern (red dotdash lines) is oriented to the framing pulses, which are also used for the signal detection. The framing pulses for Mode A/C are the first and the last pulse. The pulse detection is done using the pulse threshold (green dotted line), which is taken from the first pulse. Empirically it has been shown that the first pulse is the less influenced part of the signal in case of multipath overlapping [7]. Mode A/C replies are PPM coded, each bit is represented by a pulse or no pulse at a certain time, as described in Section 2.3.1.
To decode the Mode S data bits, the time frame is laid over the signal by starting with the preambles four pulses, which are also used for the signal detection. The pattern starts with the first payload pulse and ends with the 112^{th} bit. A short Mode S signal is if the payload only contains 56 bits. When decoding short Mode S signals, the algorithm stops after a configured number of not decoded bits, because there are no pulses available anymore. The method uses the timing (red dotdash lines) to detect the rising and falling edges, as shown

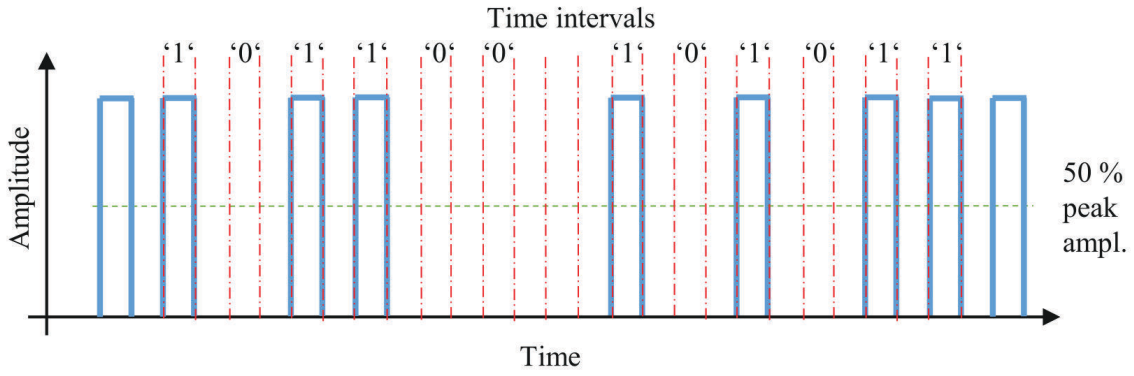

Figure 4.1: Time frame with intervals for Mode A/C pulses

in the pattern in Figure 4.2. The pulse detection is done using the pulse threshold (green dotted line), which is taken for Mode S from the first payload pulse. The first payload pulse is not the first pulse of the signal, but it has a pulse pause of more than 2.5 microseconds before and therefore it is also less influenced than the other bits afterwards in the payload. Mode S replies consist of a preamble and a payload part. The preamble consists of pulses with fixed timing and the data part is coded using unipolar Manchester codes, each bit is represented by a transition of pulse to pulse pause or vice versa at a certain time, as described in Section 2.3.2.

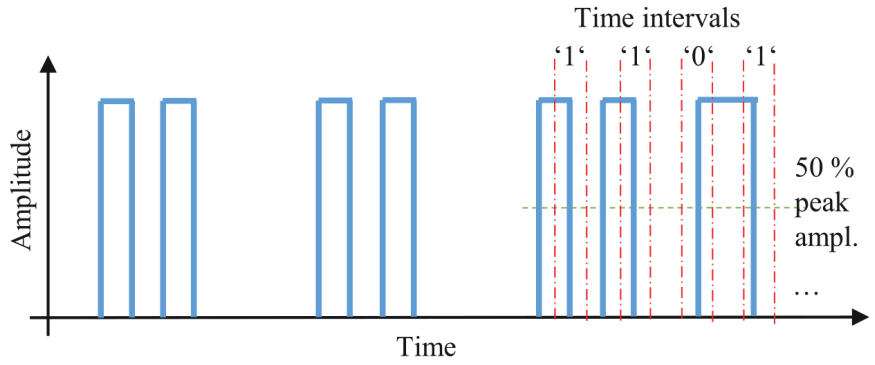

Figure 4.2: Time frame with intervals for Mode S data pulses [4]

The frequency drift of the transponder is unknown and therefore the time pattern gets a tolerance of ±15 samples for each timing interval. The frequency shift of the center frequency is allowed internationally up to ±1 MHz [27].

4.3 Decoding Techniques

The presented and analyzed decoding techniques are the multilevel threshold detection with standard and mean input and the edge detection decoding. The decoding bit errors of the presented decoding algorithms are marked, which is the same method as the confidence bit principle presented in [20]. The bit error marking principle improves the further processing of the signals at the CPS.

4.3.1 Multilevel Threshold Detection Decoding

The multilevel threshold detection decoding is based on the commonly known threshold detection principle. It compares the input signal with the threshold for detection. The threshold is set to 50% of the pulse peak of the first data pulse. The detection of a rising edge is when the sample before the expected time interval of the pattern is lower than the defined threshold and the sample after is higher. The detection of a falling edge is, when the sample before the expected time interval is higher and the sample after is lower than the threshold. The detected rising edge is decoded as logical '0' and the falling edge as logical '1'. A bit is marked as error when the samples before and after the expected time interval are both lower or higher than the threshold. The bit error marking principle is the same as the confidence bit principle [20]. Additionally, to the 50% threshold also a 40% and a 60% threshold are used for the detection, as shown in Figure 4.3. When the signal has overlapping in the pulse pause, like it has with asynchronous garbling or multipath, then the 60% threshold helps to detect the edge anyway. When the signal has a destructive interference, which causes mostly a decrease of the amplitude of the signal, the 40% threshold helps to detect the edge anyway.

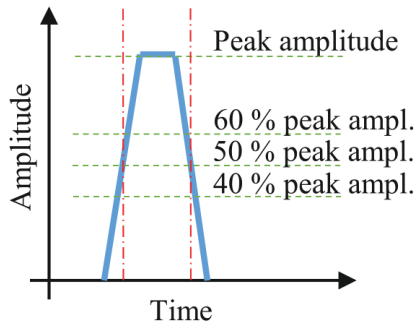

Figure 4.3: Multilevel threshold detection decoding [4]

4.3.2 Multilevel Threshold Detection Decoding with Mean Input

The multilevel threshold detection decoding with mean input uses the decoding technique, as described in Section 4.3.1, but with timely averaged values for threshold comparison. The method computes the average for the sample window before (mean1) and after (mean2) the

time interval (red dotdash line), as shown as example with the rising edge in Figure 4.4. The mean values are then compared with the threshold, in the Figure example mean1 must be lower and mean2 higher than the 50% threshold to decode the detected rising edge as logical '0'. When the mean1 value is higher and the mean2 is lower than the detection threshold, the detected falling edge is decoded as logical '1'. The configured averaging window is set to 15 samples, which results in 38.57% of the Mode A/C pulse duration and 42.85% of the Mode S pulse duration. The used detection thresholds are at 40%, 50% and 60% of the pulse peak. The average window with 15 samples (Δt) showed the best results with the given real-world data set.

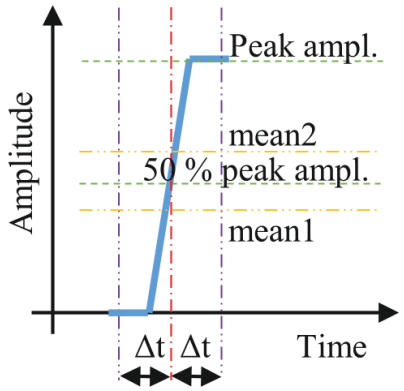

Figure 4.4: Multilevel threshold detection decoding with mean input [4]

4.3.3 Edge Detection Decoding

The edge detection decoding is based on edge detection [25]. The input signal (blue line) is derived (yellow dotted line) and results in a positive pulse for the rising edge and in a negative pulse for the falling edge, as shown in Figure 4.5. The peaks of the derived signal are then detected by a detection threshold and decoded to bits. The positive peak is decoded to a logical '1' and the negative peak to a logical '0'. The threshold for the peak detection is $\frac{1}{32}$ of the pulse peak. This threshold is defined to improve the robustness against noise pulses in case of low SNR signals. The pulse peak is derived from the first payload pulse when it is Mode S and from the first signal pulse when it is Mode A/C.

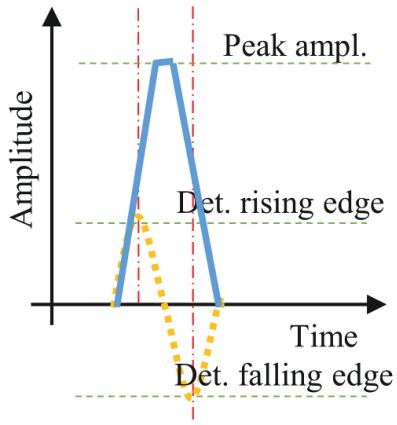

Figure 4.5: Edge detection decoding [4]

4.4 Implementation

The multilevel threshold detection decoding algorithm is implemented for Mode A/C and Mode S on the FPGA of the transponder reply receiving and ToA estimation station, as described in Section 6.4. With the implementation the algorithm can be evaluated and validated with a real-world data set, as described in Section 4.5. The decoding method is high-level behavioral implemented using a finite state machine and can be easily integrated in any other design. The state machine contains modules for the computation of the peak amplitude, the threshold calculation and eventually the decoding. The implementation costs for the Mode S multilevel threshold detection decoding algorithm are 4,957 FPGA logic cells and for the Mode A/C decoding method 3,713 logic cells. The implementation costs show that the implementation is low-cost. The implementation costs for Mode S are slightly higher, because the Mode S signal is longer and more complex to decode.

4.5 Real-World Data

The decoding algorithms are analyzed, developed and evaluated using the program MATLAB with two data sets and are compared against the decoding technique of conventional Mode S secondary radars [20]. The first is described in Section 4.5.1 and contains mostly multipath data. The second contains mixed input data, as described in Section 4.5.2. The recorded datasets contain Mode S vehicle transponder signals from the ground of the Salzburg airport only. They do not contain any aircraft signals. According ICAO Annex X Volume IV specifications [27] both must fulfill the standards of Mode S and therefore there is no difference in the signal. But there is a difference in the data format of the signal and in the mounting, height and type of the antenna. The recorded signals are probably more similar to signals from small aircraft on the ground. Aircraft which are airborne typically do not have much multipath or fading issues, but they have a high number of garbling. Furthermore, it

should be considered that the propagation effects will differ with the airport site, antenna types and transponder manufacturers.
The decoding technique of conventional Mode S secondary radars is used for comparison to the designed algorithms in this work. Like for all other algorithms the signal amplitude is taken from the preamble to be compared with the pulses of the payload. In addition, for all methods the Mode S signal detection is done with a preamble MF. It detects the signal and identifies it as Mode S. Furthermore, for each algorithm the signal is compared with a noise threshold and Mode S is only detected if they are higher than this threshold. The threshold helps that the decoders are not triggered by noise. The pulse threshold of the conventional method is set to 50% of the preamble signal amplitude.
The BER in relation to SNR illustrated in the diagrams is computed by bit errors ($\#_{bit\ errors}$) divided with number of bits ($\#_{bits}$), as shown in Equation 4.1. A BER of 0 signifies that no BER occurred and 1 that there are only errors.

$$BER = \frac{\#_{bit\ errors}}{\#_{bits}} \tag{4.1}$$

4.5.1 Test Drive for Multipath Recording

The algorithm evaluations are done with transponder replies recorded at the Salzburg airport W. A. Mozart in Austria on Monday 2016-12-07. ADB Safegate installed at the Salzburg airport a MLAT system with 14 RX stations, which was used for the recording of the test drive. The used vehicle transponder was the Squid of the Czech company ERA a.s. It sends short Mode S replies, also named as squitters, for identification and position acquisition twice per second as downlink format 18. The test drive started at 12:33 a.m. UTC for ten minutes and the car speed was about 30 $\frac{km}{h}$. The transponder was mounted on the roof of the 2 m height car and powered with the car battery.
The test route (blue line) for multipath overlapping was on a part of the taxiway of the Salzburg airport, as shown in Figure 4.6. The 3 m height wire-netting fence (green line) near the taxiway causes a high number of multipath overlapping at the antennas of the four RX stations (RX1, RX2, RX3 and RX4), therefore the route was chosen. The distance from the fence to the taxiway centerline is about 40 m. The fence causes multipath reflections depending on the angles between RX antennas, car and fence itself. It results in a different reception time, damping and phase of the multipath component. The antenna is omnidirectional and the height over ground of RX1 is 10 m, of RX2 12 m, of RX3 7.6 m and of RX4 5 m. The RX1 station is about 550 m away from exit B on the taxiway, RX2 320 m from the taxiway centerline, RX3 700 m to the exit 1 of the general aviation center and RX4 is about 500 m away from exit B on the taxiway. The recording contains 4,278 Mode S signals and the algorithms are evaluated and validated with the recorded data using the program MATLAB.

4.5.2 Test Data for Mixed Input Recording

The recording was done for a whole day at the Salzburg airport W. A. Mozart in Austria on Monday 2017-02-20. There were recorded five Mode S vehicle transponder by three RX stations. The Squid vehicle transponders is from the Czech company ERA a.s and the vehicles

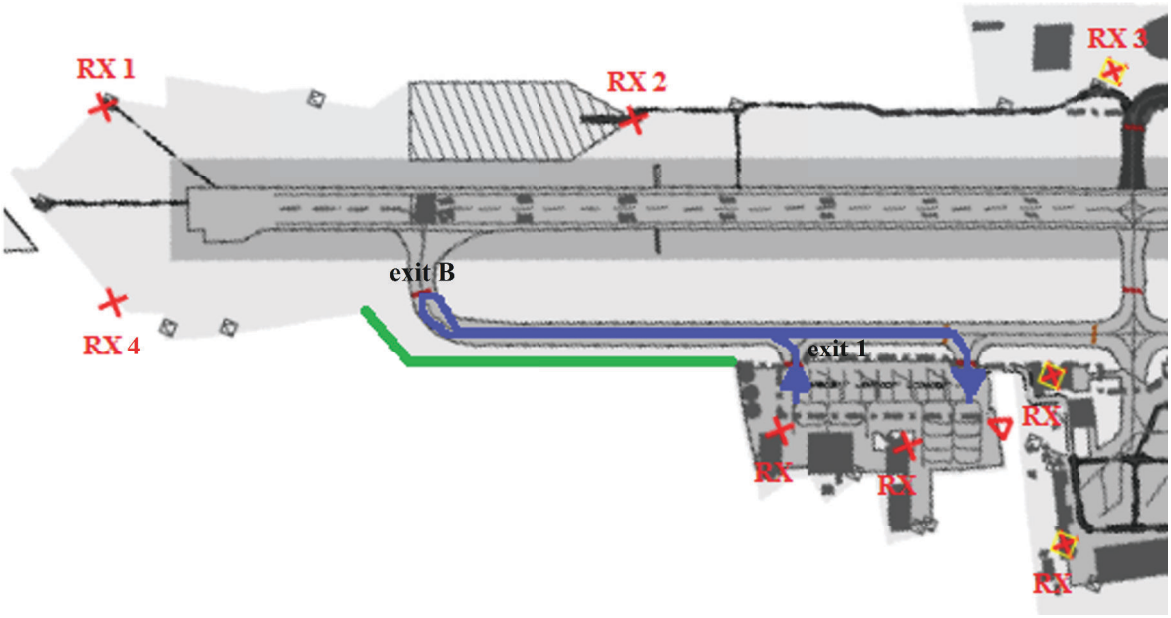

Figure 4.6: Test route at the Salzburg airport [7]

were driving around on the whole airport, near buildings, on taxiway, runway, apron, parking positions, etc. So, the recording contains 416,325 short Mode S signals having different types of propagation effects, like fading, garbling, multipath overlapping and NLOS signals. Due to lack of time it was not possible to classify the dataset. They can only be classified by visual inspection and are then counted. Sometimes it is not even possible to classify them and with this high amount of dataset it would take months. Furthermore, the recording is only a cutout of a certain day and it is unfortunately unknown how representative the numbers of the propagation effects are.

4.5.3 Results

The evaluation diagrams show the BER on the y-axis with the SNR in dB on the x-axis. The SNR is categorized from 4.4 dB to 52.8 dB in steps of 4.4 dB. The evaluation results diagram of the multipath input dataset is shown in Figure 4.7 and the diagram of the mixed input dataset in Figure 4.8.
The diagram in Figure 4.7 shows that the multilevel threshold detection decoding algorithm with standard input has mostly the lowest BER. The method is followed by the threshold detection decoding algorithm with mean input. Last but not least, the edge detection decoding and the conventional Mode S radar method follow with similar results. It can be observed for all four algorithms, that lower SNR values have higher BER than higher SNR values. At most it can be seen with the multilevel threshold detection decoding algorithm. The BER at higher SNR values differ more between the presented methods.

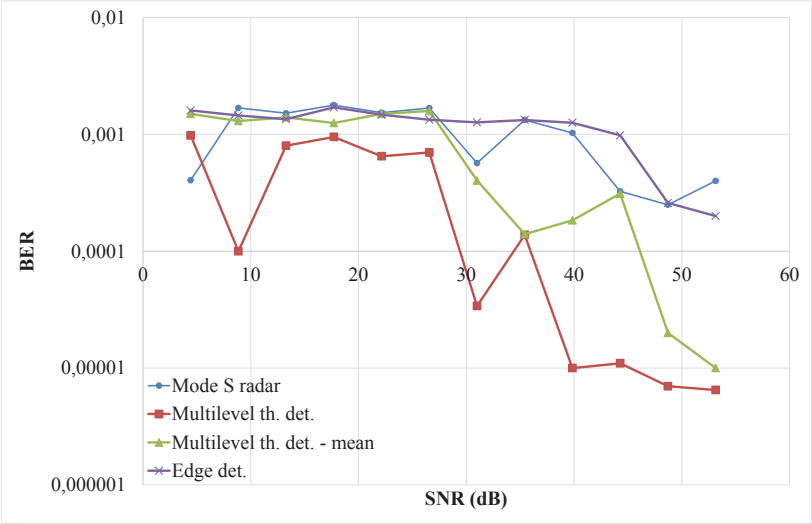

Figure 4.7: BER comparison with multipath input [4]

Figure 4.8: BER comparison with mixed input [4]

The diagram shows that the multilevel threshold detection decoding method with standard input has the lowest BER, as shown in Figure 4.8. It is again followed by the threshold detection decoding algorithm with mean input and lastly by the edge detection decoding method and the conventional secondary radar, which have both similar BER. But in this case, it is conspicuous that the BER does not depend significantly on the SNR, like it is shown in the latter with multipath input. The BER is similar to low and high SNR values.
When comparing the diagrams of the multipath input dataset with the mixed input, it shows that the analyzed algorithms seem to be more resistant against multipath overlapping. The results of the mixed input dataset are not like expected. Probably this is the case due to the high number of garbling. This means that signal overlapping from different transponders is an issue and it is also not covered by the presented decoding algorithms. More advanced algorithms using spectral analysis are able to cope with this issue [22].

4.6 Limitations

The decoding algorithms are only limited evaluated and validated with Mode A/C, because there is not enough test data available and because Mode S is the newer interrogation method. The edge detection decoding method has a disadvantage with transponder replies, which have low-power. This is because the method contains a derivation, which drops the SNR.

4.7 Decoding Algorithms Summary

In this chapter, the multilevel threshold detection decoding with standard and mean input, the edge detection decoding and the Mode S secondary radar decoding technique [20] are compared in the time-domain. The input data is taken from the Salzburg airport, one dataset containing mostly multipath overlapping and one dataset with mixed input signals. The evaluations showed, that the multilevel threshold detection decoding algorithm with standard input has the lowest BER compared to the others. Furthermore, this algorithm is implemented on the FPGA two times, for Mode A/C and for Mode S. The implementation costs for Mode A/C are 3,713 FPGA logic cells and for Mode S 4,957 logic cells. The edge detection decoding algorithm instead has the highest BER, irrespective of the dataset, what is probably due to SNR drop when calculating the derivation. The presented algorithms work well with multipath overlapping, but they can still be improved for garbling, as shown by the evaluation results of the dataset with mixed input.

5 ToA Estimation Algorithms

In this chapter, ToA estimation algorithms working in the time-domain are presented. The algorithms are the threshold detection ToA estimation algorithm in Section 5.1, the correlation ToA estimation algorithm in Section 5.2 and the REDTOE algorithm in Section 5.3.
The ToA estimation algorithms are analyzed and evaluated with only one dominant multipath component, which is typically the case at airports, as described in Section 5.3.1. If there are more multipath components, the algorithms reach their limits. Furthermore, the ToA estimation algorithms depend on the quality of the decoding algorithms. Only if the signal can be partly decoded, as described in Chapter 4, the ToA can be used. Furthermore, the described ToA estimation algorithms also do not contain any method against garbling (the signal overlapping of different transponders) as described in Section 2.4.1.

5.1 Threshold Detection ToA Estimation Algorithm

The most common known ToA estimation technique is the threshold detection ToA estimation [21], it compares the signal amplitude with a threshold to set the ToA. In this section some variations of the method are shown and the 50% threshold detection ToA estimation with interpolation of the first rising edge is used for comparison to the other ToA algorithms in Chapter 7.
To estimate the ToA, the threshold detection ToA estimation algorithm first calculates the peak power of the pulse and then the detection threshold. Typically, the threshold is set to 50% of the peak power. The threshold is further used to find the intersection with the rising edge, as shown in the left part of Figure 5.1. To improve the accuracy by a factor of ten, the intersection is interpolated. In the RX implementation of Chapter 6, the oversampling has resolution of 10 ns and is improved with interpolation to 1 ns, which corresponds to a distance accuracy of 0.3 m.
It is also possible to use the threshold detection ToA estimation algorithm to estimate the ToA for the pulse center. To achieve a pulse center ToA, the ToA of the rising and for the falling edge are averaged. In Figure 5.1, the threshold detection ToA estimation algorithm for the rising edge (left) and for the pulse center (right) is shown.

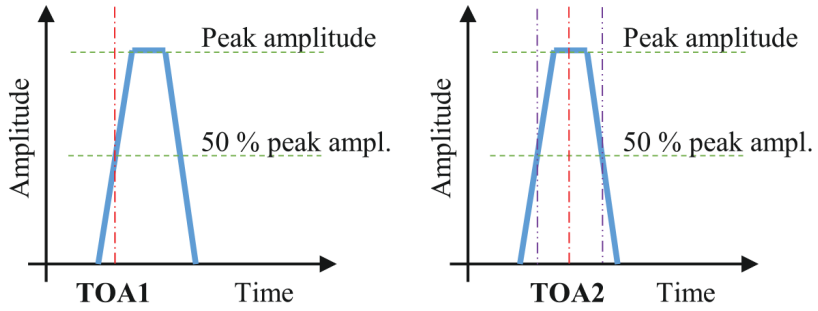

Figure 5.1: Threshold detection ToA estimation for rising edge (left) and pulse center (right)

The threshold detection ToA estimation algorithm determines an estimated ToA at the same position in the time-domain for every peak power, assuming to have an ideal pulse shape, as shown in Figure 5.2. Therefore, the algorithm estimates the ToA for the ideal signal correctly. In the Figure this is shown, for the 50% threshold detection ToA estimation algorithm for the rising edge (left) and for the pulse center (right).

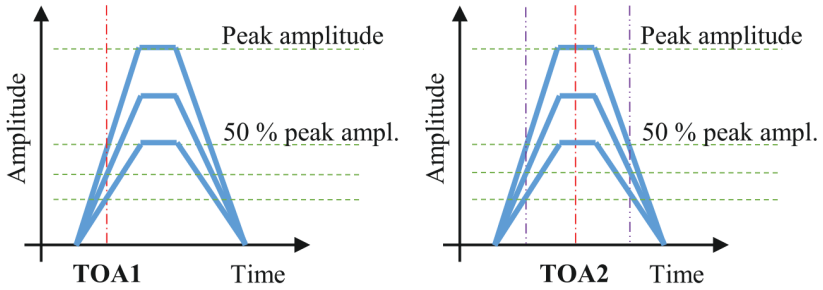

Figure 5.2: 50% threshold comparison for rising edge (left) and pulse center (right)

5.2 Correlation ToA Estimation Algorithm

The input of the correlation ToA estimation algorithm is the demodulated baseband stream $s[n]$ and delivers as output the ToA. The method splits up the processing chain into two branches, one for determining the filter coefficients of the pulse matched filter (MF) and the other one for determining the ToA, as shown in Figure 5.3. The branch for determining the sample coefficients of the 2nd pulse uses the preamble MF and the pulse cutter. The preamble filter detects the incoming Mode S signals by the preamble and delivers as output the start point of the signal respectively. The filter coefficients are determined by using the ICAO Annex X Volume IV specifications of a Mode S preamble [27]. Using the output of the preamble filter the pulse cutter is able to copy the preamble's 2nd pulse samples from the delayed signal stream. The pulse's samples are then the new coefficients for the pulse MF FIR filter. The delay line delays the input stream with approx. 800 clock cycles. It is the delay of the preamble MF, which needs the filter to detect the preamble itself, as it is described in the implementation of the RX station Chapter 6. The input is then used by the pulse cutter for the detection of the preamble pulse. The accuracy of the sample cutout by the pulse cutter is not that much relevant. It is more important that the whole pulse is covered and that the filter contains enough pulse coefficients.
The branch for the ToA determination contains the delay line, the low-pass (LP) filter, the pulse MF and the ToA estimation algorithm. The delay line has almost the same delay as the delay line of the coefficients determination part has. It assures that the pulse MF gets the coefficients in time. The LP FIR pulse shaper filters the input stream to avoid as much noise as possible. Afterwards the pulse MF filters the stream with the pulse coefficients provided by the pulse cutter and outputs the convolution output to the ToA estimation algorithm.

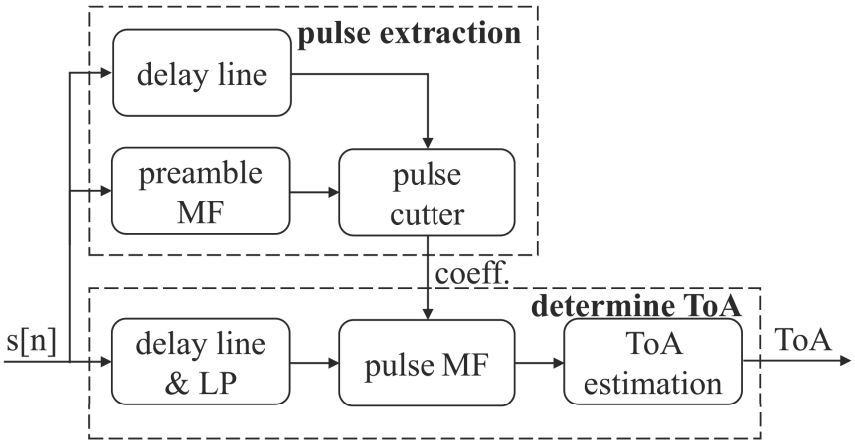

Figure 5.3: Correlation ToA estimation algorithm

5.2.1 Low-Pass Filter – Pulse Shaper

The LP pulse shaper filter is a simple moving average filter and has 45 taps with the cut-off frequency at 2.25 MHz. The coefficient's values are $\frac{1}{45}$ for each. The reason for the coefficients is that the filter should cover the whole pulse without reducing the outputted peak amplitude compared to the filter's input. According to the Mode S specifications and the given 100 MHz sampling frequency at the RX station, the pulse width has $50 \pm 5 \frac{samples}{microsecond}$. This leads to the amount of 45 coefficients; it is the lower bound of the ICAO Annex X Volume IV regulation for the Mode S pulse. The LP filter also ensures that the additive white Gaussian noise on the channel is smoothed as much as possible.

5.2.2 Pulse Matched Filter

The aim of the pulse MF is to calculate the convolution of the Mode S input stream with the filter coefficients taken from the 2nd preamble pulse. The pulse MF computes the convolution sum for the samples of the 2nd and the 3rd pulse and in addition the convolution sum for the 2nd and the 4th pulse. The resulting signals are then the input of the ToA estimation algorithm. The preamble, according to the ICAO Annex X Volume IV specifications [27], with overlapping multipath is shown in the first row's diagram of Figure 5.4. The second row's diagram shows the preamble filtered by the pulse shaper and the third row the convolution sums of the 2nd with the 3rd and 4th pulse. From this output the ToA estimation algorithm determines the ToA for the 3rd and 4th pulses only. For the given testbed, as described in Section 5.2.5, the ToA of the 4th pulse is used for comparison.

5.2.3 ToA Estimation

The purpose of the ToA estimation algorithm is to estimate the ToA for the filtered Mode S preamble's pulses. The chosen algorithm is the 50% threshold detection ToA estimation algorithm to estimate the ToA for the pulse center, as described in Section 5.1. The algorithm is the simplest approach for the given correlated input signal [30]. It calculates first the pulse's peak amplitude and sets the threshold at 50%. The crossing point is afterwards interpolated for the rising and the falling edge respectively. With the interpolated points the middle point of the pulse can be computed and its ToA can be set. The ToA estimation is done with an accuracy of $\frac{1}{4}$ of the 100 MHz sampling frequency, which is 2.5 nanoseconds and corresponds to a distance accuracy of 0.75 m. The accuracy can be even improved with an additional interpolation step of 8 bit fractional value. The advantage of the estimation algorithm is that multipath influence on just one edge, rising or falling, has less influence on the ToA. Once the ToA is estimated for the 3rd and 4th pulse, it can be easily moved to the 1st and 2nd pulse or for the whole preamble by adding the ICAO Annex X Volume IV specified time differences. The calculated ToA can then be used for comparison. The error between the 1st and 4th pulse is due to the frequency drift about ±1 sample.

5.2.4 Implementation

The correlation ToA estimation algorithm is implemented for Mode S on the FPGA of the transponder reply receiving and ToA estimation station, as described in Section 6.4. The algorithm's implementation is low-cost and can be easily realized on a FPGA or a DSP. The

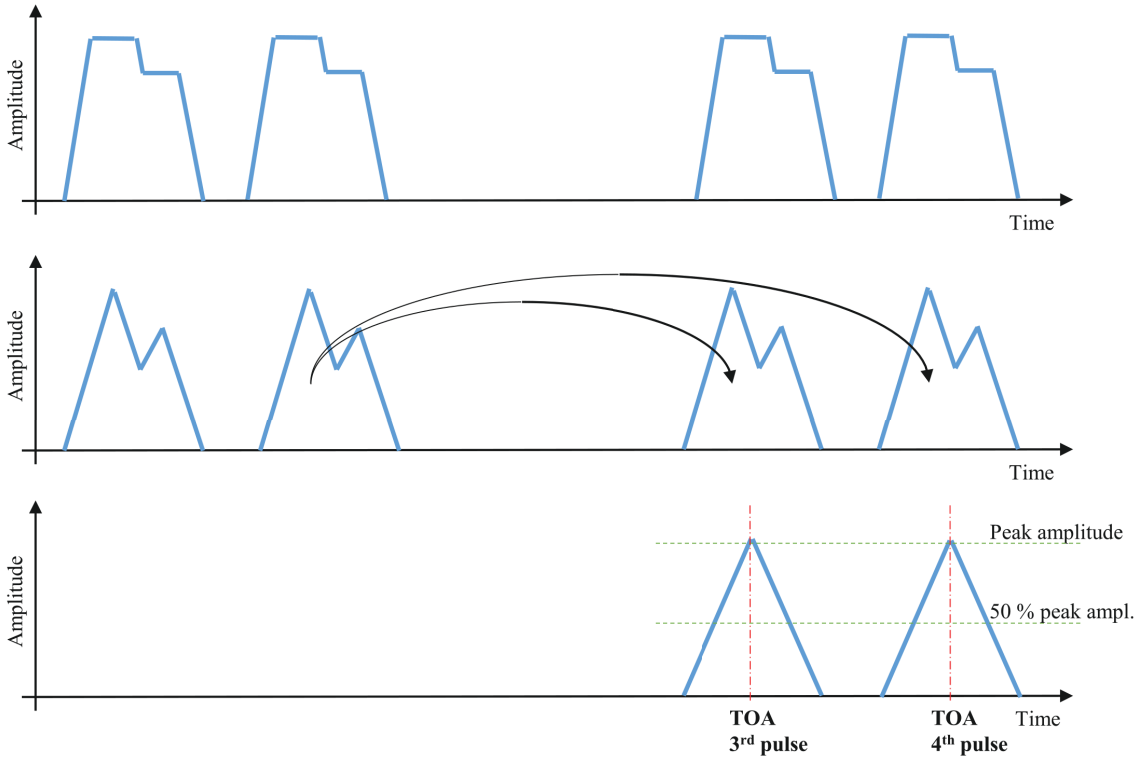

Figure 5.4: Mode S preamble filtering

algorithm's coefficients determination part consists of a delay line, a FIR and some small logic for the pulse cutter. The delay line can be implemented by using latches and the FIR by using some adders and multipliers. The ToA estimation part consists of a delay line, two FIR filters and the estimation logic. The algorithm's implementation at a FPGA needs about 1,500 multiply-accumulate operations (MAC) and 1,800 logic cells.

5.2.5 Simulation Testbed

The simulations for the ToA comparison of the proposed algorithms are done with the simulation program MATLAB. The script uses the simulation model of Section 3.1 generating a LOS signal, add one additive multipath signal some white Gaussian noise resulting in a 1,090 MHz Mode S signal with multipath overlapping. There is only one dominant overlapping considered, because it is statistically the main issue at airports. Furthermore, the generated signals are ToA estimated for each algorithm, compared to the optimal ToA of the LOS signals and the ToA RMS errors (RMSE) are shown in the diagrams for each algorithm separately.
The received signal $r(t)$ is used for comparison in the simulations, as shown in Equation 3.2. The phase shift ϕ_{MP} of the multipath component happens because of the reflection on the surface and the damping factor, which is a transmission power reduction due to additional

radio wave propagation distance. The phase shift is varied from 0 to π in 16 steps and the damping value from 0 to -16 dB by steps of 1 dB. The time t of the received signal starts with zero and the LOS signal SNR is 25 dB. The damping factor is the amplitude attenuation of the additional multipath overlapping component in relation to the LOS signal amplitude.
The simulation results show the ToA RMSE of the generated signal $r(t)$ compared to the LOS signal ToA. The runs, MP1 to MP5, were repeated 5,000 times for each multipath overlapping case. Each multipath case has different noise, a different time delay and varied phase shift of the multipath component. Table 5.1 shows the time delay and the corresponding distance of the multipath component. The time delay relates to the additional radio wave travel time in relation to the LOS signal and so the corresponding distance relates to the additional radio wave distance in relation to the LOS signal. For the sake of simplicity, the ToA RMSE is averaged over the phase shifts for each attenuation simulation.

Name	**Time delay (nanoseconds)**	**Corresponding distance (m)**
MP1	10	3
MP2	50	15
MP3	166.67	50
MP4	250	75
MP5	333.33	100

Table 5.1: Simulated Time Delays [7]

5.2.6 Simulation Results

The simulation testbed for the correlation ToA estimation algorithm and the 50% threshold detection ToA estimation algorithm for the pulse center is described in Section 5.2.5. The simulation results show the ToA RMSE related to the transmission power reduction of the multipath component for each simulated multipath case. Figure 5.5 shows the performance of the 50% threshold detection ToA estimation algorithm for the pulse center and Figure 5.6 the performance of the correlation ToA estimation algorithm. The five multipath cases, which are listed in Table 5.1, differ in propagation delay of the multipath component, i.e. additional travel time compared to the LOS signal.
Comparing the RMSE diagrams of the correlation ToA estimation algorithm (Figure 5.6) with the 50% threshold detection ToA estimation algorithm for the pulse center (Figure 5.5) shows notable differences in the curve forms and values. The RMSE curve of the correlation ToA estimation algorithm is not that smooth, but more linear over the damping factor range than the threshold detection ToA estimation algorithm. At high damping factor values, DF between 10 to 16 dB, the RMSE values of the correlation ToA estimation algorithm are in average higher and for low damping factor values, between 1 to 6 dB, they are lower than the RMSE values of the threshold detection ToA estimation algorithm for the pulse center. In the diagram middle section both algorithms achieve similar results. An exception is the MP1 of the threshold detection, which has in any case a lower RMSE. Unfortunately, the correlation ToA estimation algorithm does not show over all damping factors extraordinary results, but it can be used in case of multipath overlapping with low damping factors, i.e. below 6 or 7 dB.

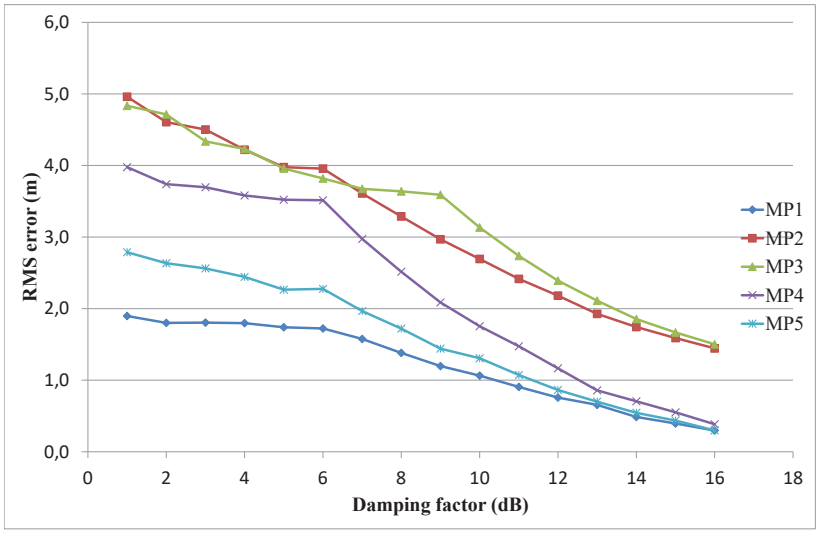

Figure 5.5: ToA RMSE diagram of the threshold detection ToA estimation algorithm for the pulse center

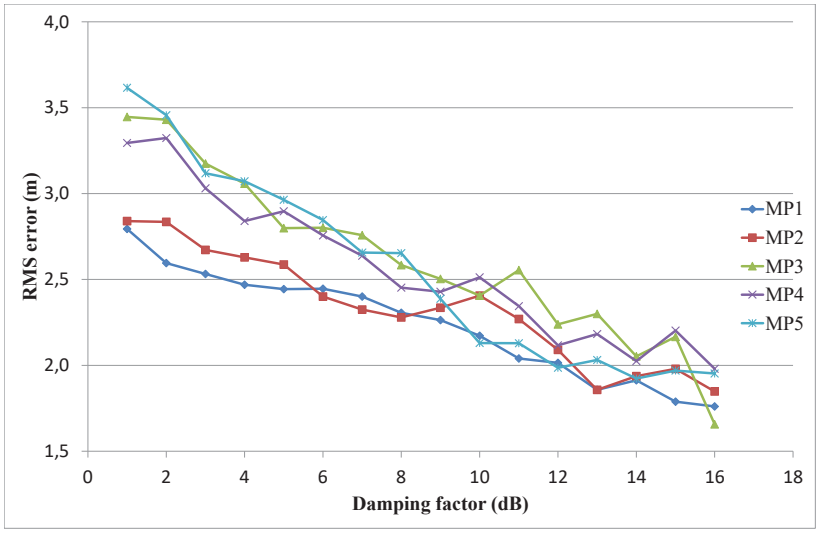

Figure 5.6: ToA RMSE diagram of the correlation ToA estimation algorithm

5.2.7 Limitations

The correlation ToA estimation algorithm achieves in same cases a lower TOA RMSE than the 50% threshold detection ToA estimation algorithm for the pulse center, when the multipath overlapping has one dominant component with high power, i.e. not less than 6 dB damping compared to the LOS signal. An exception is in case of multipath overlapping with a lower time delay, like the MP1 case, when the threshold detection achieves for all cases better results. Unfortunately, the algorithm does not have such a high ToA estimation accuracy than the others in case of Mode S signals with no disturbance. The outcome of this work is to use the correlation ToA estimation algorithm not as main algorithm, but as fallback with a multipath detector. Should the algorithm be used in addition to other algorithms, a decision logic is needed, which determines the output of the algorithms with less position error. For this issue two possible methods are proposed. The first is to use a multipath detector at the RX station, as described in Section 3.3.5. Another method is to exclude ToA of outlier stations for the computed position with the CPS software, as described in Section 3.3.5.
The algorithm is designed for Mode S and would have to be extended for Mode A/C.

5.3 Rising Edge Detection ToA Estimation Algorithm (REDTOE)

The REDTOE algorithm is based on the edge detection principle and estimates the ToA on the first rising edge of the transponder reply. The edge detection is well known from image processing [25] and detects the zero-crossing of the signal's second derivation. Because of the safety distance of the aircraft wings to other objects at airports, overlapping has typically a higher time delay of the multipath component, as described in Section 5.3.1. Combined with this property the REDTOE algorithm achieves as single algorithm the best results at airports.

5.3.1 Multipath Propagation Delay Occurrence at Airports

Typically at airports, aircraft only drive on centerlines of the runways, taxiways, aprons and at stands. This is due to the safety distances of the aircraft's wings to fences, hangars or other obstacles installed at the airport. For radio wave propagation this means that the occurring timing delays of the multipath component are typically higher than 133 nanoseconds, which corresponds to 40 m of additional traveled distance compared to the LOS signal. Exceptions are vehicles, which are allowed to pass by buildings and parking aircraft more closely. The REDTOE algorithm benefits from this property, because the timing delay of the multipath component higher than 50 nanoseconds or 15 m in distance, does not influence its estimated ToA performance. This means that multipath occurring at airports typically does not influence the REDTOE algorithm, because of the safety distances for aircraft. An exception of course are vehicles, i.e. ground support equipment (GSE), like refuelers, tractors, ground power unit, buses, container loader, transporter, air start unit, lavatory service vehicle, catering vehicle, belt loaders, pushback tugs, firefighters, police, security, etc.

5.3.2 Algorithm Design

The REDTOE uses the property that the first pulse is the less influenced by multipath overlapping than the rest of the signal, as described in Section 3.3.4. The algorithm estimates the ToA for the interpolated zero-crossing of the second derivation of the filtered baseband signal at the time of the rising edge in the baseband signal. The first derivation of the rising edge is a positive pulse and the second derivation results in a positive followed by a negative pulse with zero-crossing, as shown in Figure 5.7. The first derivation of the falling edge is a negative pulse and the second derivation a negative pulse followed by a positive pulse.

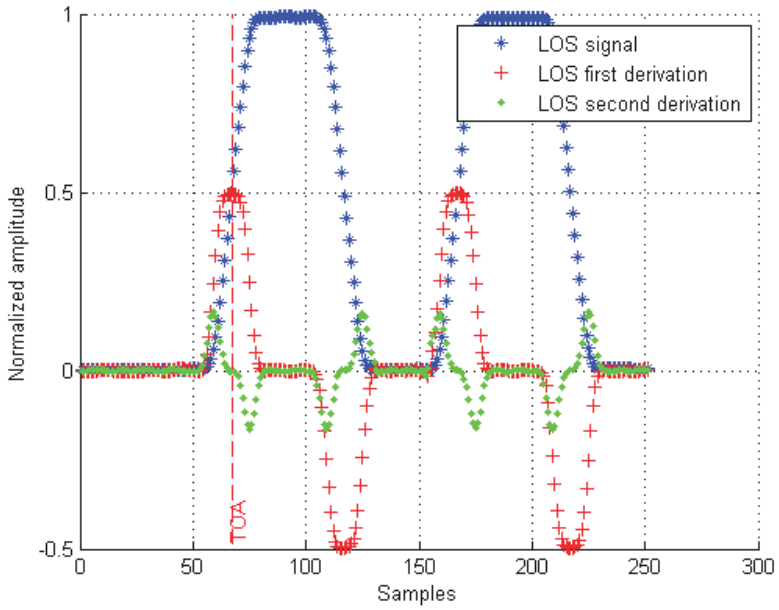

Figure 5.7: Derivations of an ideal baseband signal [7]

5.3.3 Algorithm States

The REDTOE algorithm has a finite state machine, which describes how the ToA is estimated, as shown in Figure 5.8. The algorithm calculates the ToA for the rising edge of the first pulse using the second deviation of the baseband signal. The ToA is estimated at the rising edge by detecting it with the zero-crossing detection of the Laplacian signal.

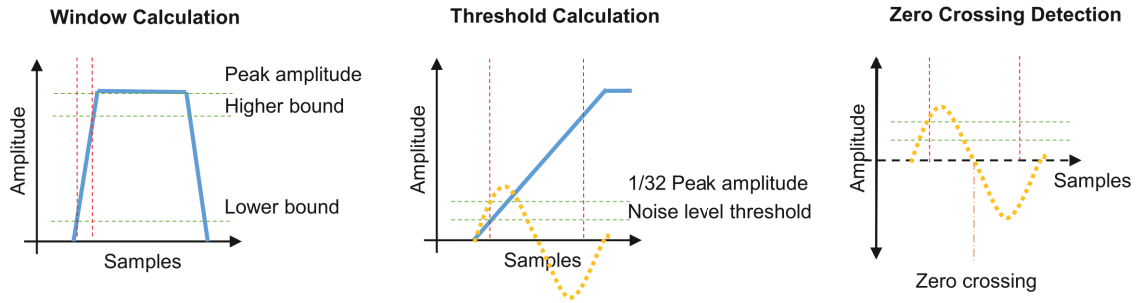

Figure 5.8: REDTOE state machine phases [7]

- **Detection window for the rising edge:** First of all, the peak amplitude of the first pulse is calculated, then the lower and higher bound thresholds are set, i.e. at 10% and 90% of the previously computed peak amplitude. These bound thresholds form the window for the zero-crossing, as shown as red dotted lines in Figure 5.8.

- **Threshold determination:** The detection threshold is set to $\frac{1}{32}$ of the previously calculated peak amplitude. It is used to improve the results in case of low SNR signals as input by avoiding the influence of noise pulses. Furthermore, a noise level threshold is statically configured for the pulse detection to avoid the detection to reduce the disturbance from the noise on the Laplacian signal.

- **Zero-crossing:** The baseband stream is compared with the detection threshold and the noise level threshold in the window with the bounding thresholds. If at least one sample of the input stream exceeds both thresholds, the state machine goes to the next state and looks for the zero-crossing. The zero-crossing in the Laplacian signal is detected if the samples change from positive and zero to negative values, to detect only rising edges. The algorithm stops after having detected the first zero-crossing, to assure that no other zero-crossing possibly caused by multipath overlapping are captured.

- **Interpolation:** An interpolation is computed at the detected zero-crossing samples to improve the ToA accuracy with an 8 bit fractional value. The ToA is interpolated between the two samples, above and below the zero point, to achieve an accuracy resolution of 39 picoseconds.

5.3.4 Multipath Overlapping

The estimated ToA of the REDTOE and of the 50% threshold detection ToA estimation algorithms are equal in case of a simulated ideal signal pulse as input, i.e. both algorithms work optimal in this case, as shown in Figure 5.9. The input signal (blue line) is the ideal LOS signal and the REDTOE computes the second derivation of it (green line).

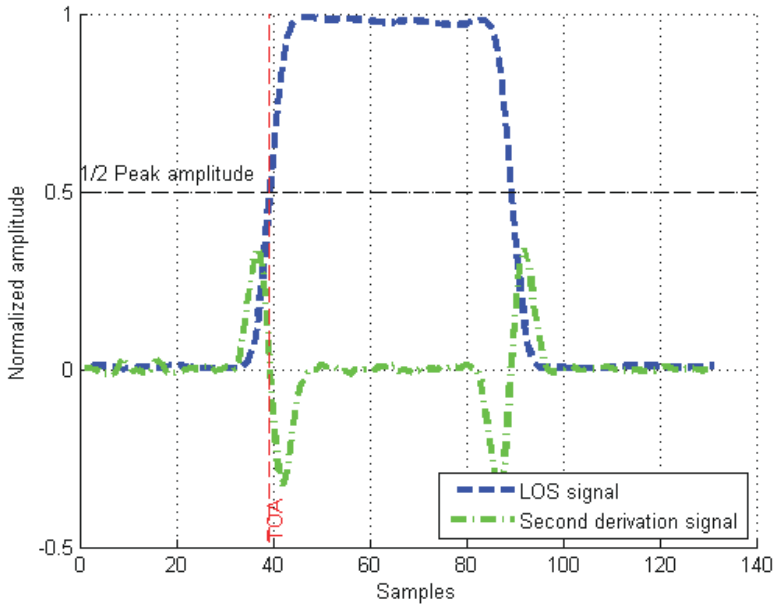

Figure 5.9: Baseband first preamble pulse with edge and threshold detection ToA [7]

Multipath overlapping may result in different signal shapes depending on the amplitude, phase, additional traveled distance and number of overlapping signals. As an example, a constructive interference of the real-world dataset, with the LOS signal (magenta signal) and multipath signal (yellow signal) are overlapped (blue signal), as shown in Figure 5.10. The resulting signal has only one additional multipath signal, both have a zero phase, the same SNR of 35 dB and the multipath component has a propagation time delay of 500 nanoseconds compared to the LOS signal.
The presented multipath overlapping example (Figure 5.10) is used as input for the REDTOE and the 50% threshold detection ToA estimation algorithm (Figure 5.11). The REDTOE ToA1 is here different to threshold detection ToA2. ToA1 remains at the same time as in the example with the optimal signal input, as shown in Figure 5.9. ToA2 instead has a right shift of 12 samples due to the peak power distortion by the multipath overlapping. The shift corresponds to a distance of 36 m, which is a tremendous deviation for the ToA estimation. The example shows that for this case, the ToA estimation differs significantly between the two algorithms and that the ToA of the REDTOE does handle this overlapping without disturbance in the resulting ToA.
The REDTOE algorithm is influenced by multipath overlapping until a timing delay of 50

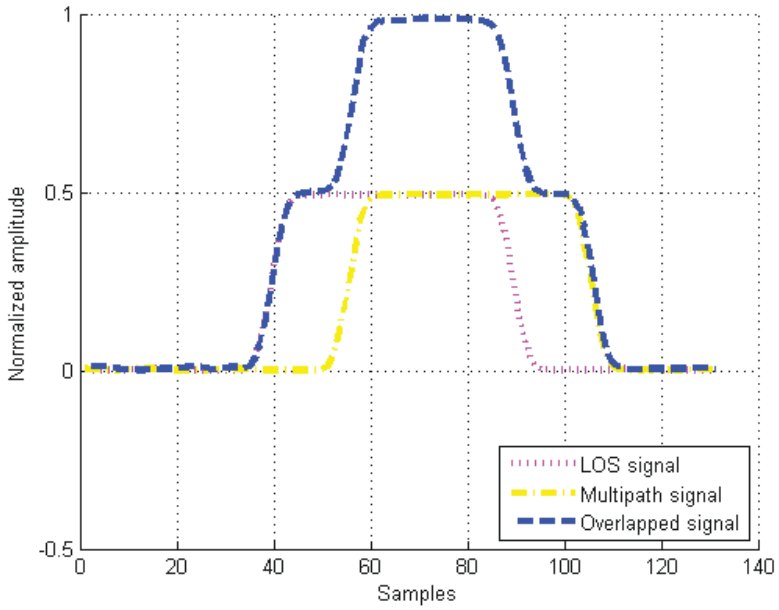

Figure 5.10: Baseband first preamble pulse with overlapping multipath [7]

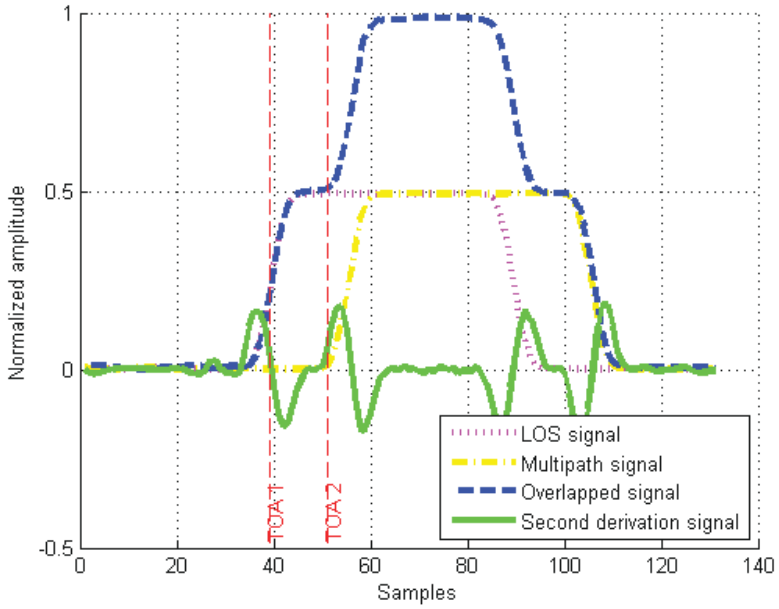

Figure 5.11: Baseband first preamble pulse with threshold detection ToA and REDTOE ToA [7]

nanoseconds, which are 5 samples at 100 MHz sampling frequency. Overlapping with more than 50 nanoseconds, which correspond to 15 m of additional traveled distance compared to the LOS signal, does not influence the REDTOE, because it is already after the rising edge. Timing delays of less than 50 nanoseconds are a rare case, as described in Section 5.3.1 overlapping occurrence at airports.

5.3.5 Implementation

The REDTOE is implemented for Mode S on the FPGA of the transponder reply receiving and ToA estimation station, as described in Section 6.4. The algorithm's implementation is validated and evaluated with a real-world data set, as described in Section 4.5. The ToA estimation algorithm is high-level behavioral implemented using a finite state machine and can be easily integrated in any other design. The implementation contains a module for the peak amplitude computation, for the threshold determination, a delay line for the input, the zero-crossing detection and the interpolation. The implementation costs for the REDTOE algorithm are about 3,000 FPGA logic cells, containing the LUT and the latches for the delay line. The number of implementation costs show that it is low-cost. The Laplacian signal is computed by the five-point stencil function with grid h set to 1, as shown in Equation 5.1, which is an approximation from the numerical analysis. It can be implemented with 5 additions and subtractions, 7 multiplications and 1 division.

$$f''(x) \approx \frac{-f(x+2h) + 16f(x+h) - 30f(x) + 16f(x-h) - f(x-2h)}{12h^2} \tag{5.1}$$

5.3.6 Simulation Results

The used simulation testbed for the REDTOE algorithm and the 50% threshold detection ToA estimation algorithm is described in Section 5.2.5, which is based on the simulation model described in Section 3.1. The simulation results show the ToA RMSE related to the damping factor of the multipath component, which is in relation to the LOS component, for each simulated multipath case in Figure 5.12 for the 50% threshold detection ToA estimation algorithm and in Figure 5.13 for the REDTOE algorithm. The five multipath cases, which are listed in Table 5.1, differ in propagation delay of the multipath component, i.e. additional travel time compared to the LOS signal.
Comparing the diagrams of the 50% threshold detection ToA estimation algorithm in Figure 5.12 and the REDTOE in Figure 5.13, shows a visible difference. Starting with the MP1 simulations, they deliver similar errors for both algorithms. The MP2 simulations already differ slightly, because the ToA RMSE of the threshold detection is higher. The MP3, MP4 and MP5 simulations differ significantly, because the ToA RMS errors of the threshold detection ToA estimation algorithm increase rapidly. For these simulated multipath cases the ToA RMS errors of the REDTOE algorithm shows improved performance. The errors are only influenced by the noise for these simulations and not by multipath. Since it is known that the REDTOE algorithm is only influenced by multipath overlapping when the time delay of the multipath component is below nanoseconds, which is the case with MP2, the simulations behave according to the theory. With the MP1 and MP2 simulations, the ToA RMSE is below 2 m and with the other simulations, it is below 0.5 m. In summary it is

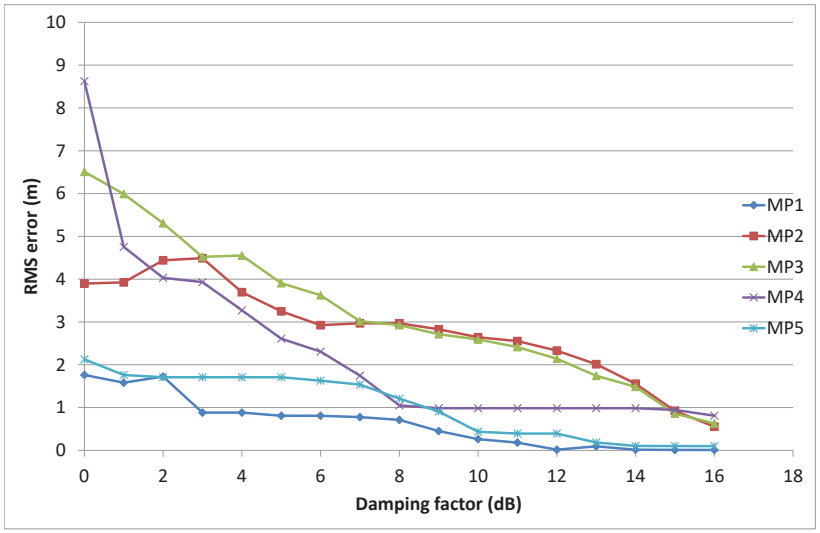

Figure 5.12: ToA RMSE diagram of the threshold detection ToA estimation algorithm [7]

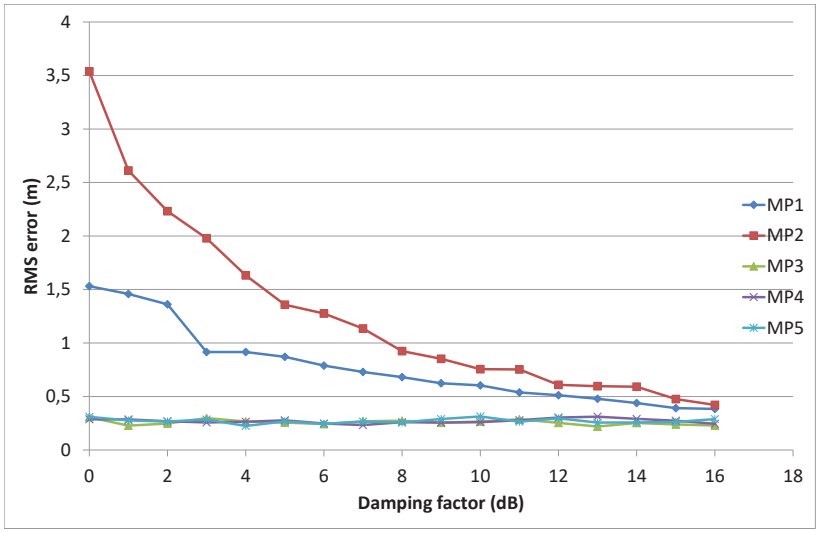

Figure 5.13: ToA RMSE diagram of the REDTOE algorithm [7]

shown, that the REDTOE has less ToA error than the threshold detection ToA estimation algorithm in case of multipath overlapping with a time delay of more than 50 nanoseconds and similar performance otherwise.

5.3.7 Real-World Test Drive

The real-world test drive dataset is the same as used for decoding algorithms, as described in Section 4.5.1. The test drive evaluation uses all RX stations recordings, as described in Section 7.1. Especially the stations RX1, RX2 and RX3 stations have a high number of multipath overlapping due to the fence near the taxiway.

5.3.8 Real-World Test Drive Results

The tracks with the calculated positions of the REDTOE algorithm (green line) and of the threshold detection ToA estimation algorithm (red line) are shown in Figure 5.14. The tracks are not smoothed, so that the algorithms can be better compared. The diagram shows that the REDTOE is more stable, has less spikes than the threshold detection and also less error. Furthermore, the REDTOE has more estimated positions than the threshold detection and enhances also the probability of detection. This is this case, because the positions have less error, are not filtered out by the outlier detection and lead to a higher number of estimated positions.

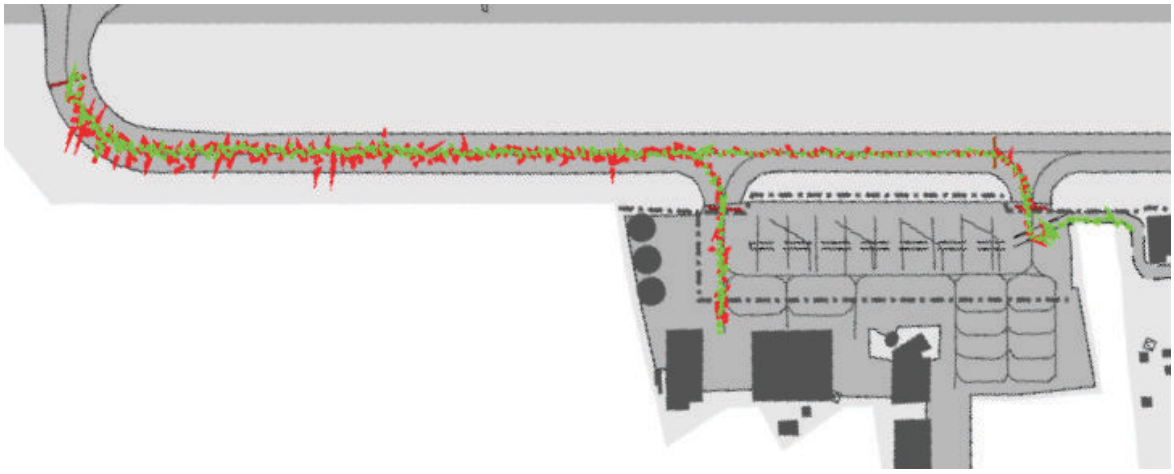

Figure 5.14: Overlaying tracks of positions calculated with the REDTOE algorithm (green line) and with the threshold detection ToA estimation algorithm (red line) [7]

5.3.9 Limitations

The REDTOE algorithm delivers better results than the 50% threshold detection ToA estimation algorithm when the multipath overlapping occurs with a time delay of at least 50 nanoseconds, i.e. the multipath component has an additional distance of 15 m compared to the LOS signal. In this period the REDTOE is not influenced by multipath overlapping

anymore. Its limit is reached when reception time of the multipath component is below 15 m. Another algorithm limit is that the derivations decrease the SNR, i.e. that the amplitude drops significantly so that the algorithm does not always work with low-power signals.
The REDTOE is only evaluated with Mode S signals. It is expected that it also works well with Mode A/C as the differences between Mode S and Mode A/C are not relevant for the algorithm. These differences are the pulse duration, which is 0.45 microseconds for Mode A/C and 0.5 microseconds for Mode S, and the rising and falling edge timing [27].

5.4 ToA Estimation Algorithms Summary

The ToA estimation algorithms are low-cost and reach their limits in case of multiple dominant multipath components, which is not the typical case at airports. Furthermore, they have no mechanisms against signal overlapping from different transponders, i.e. garbling.
In this chapter the well-known threshold detection ToA estimation algorithm is presented [21]. It is analyzed how it works and shown that is has the optimal ToA estimation for the ideal signal. It is further used for comparing with the REDTOE and the correlation ToA estimation algorithm.
Furthermore, the correlation ToA estimation algorithm is presented. The correlation ToA estimation algorithm delivers for some cases better results than the 50% threshold detection ToA estimation algorithm for the pulse center, in case of multipath overlapping with one high power component, i.e. not less than 6 dB damping compared to the LOS signal. Furthermore, the algorithm does not have such a high ToA estimation accuracy than the others when an ideal signal. The algorithm can be used as fallback algorithm, steered by a multipath detector. Another algorithm limitation is, that it only works with Mode S.
Additionally, the REDTOE algorithm is presented. The algorithm is compared with the 50% threshold detection ToA estimation algorithm with simulations and with a test drive on the Salzburg airport. In summary, the REDTOE achieves less ToA error in case of multipath overlapping of at least 50 nanoseconds, which corresponds to an additional travel distance of 15 m of the multipath component. Multipath is typically happening at the airports, due to reflecting objects like hangars, buildings, masts or other aircraft. It is also the area where the algorithm has its most benefits. The algorithm works with centralized and decentralized time-synchronization MLAT systems. The implementation is low-cost 3,000 FPGA logic cells and can be easily integrated in any design of an FPGA or DSP.

6 Receiving and ToA Estimation Station

In this chapter, a full implementation of a transponder reply receiving and ToA estimation station is presented. The station is designed to be used as RX station for a MLAT system or as ground station for an ADS-B system [3]. Actually, the RX station is used in the ADB Safegate MLAT system at the Salzburg airport. The system design of the whole RX station is presented in Section 6.1. The implementation on the FPGA and the simulation with results are described in Section 6.2 and 6.3.

6.1 System Design

The system design of the RX station consists mainly of the analog RF part and the digital part, as shown in Figure 6.1. The RF input of the RX PCB is connected to the antenna and to the CPS. The analog part front-end receives the 1,090 MHz transponder replies from the antenna and splits them up with a 10 dB directional coupler to two branches. In each branch, the signal is down-converted and digitized with the analog-to-digital converters (ADC). The ADC has 14 bit channels with a 100 mega samples per second (MSPS) sampling rate. In the digital part, the XC6SLX150 FPGA performs the digital signal processing, demodulation, decoding and ToA estimation for the RF signal. The processed data is transferred over an AMBA bus architecture to the Atmel ARM-9 based 400 MHz system-on-chip (SoC) AT91SAM9M10. The microcontroller communicates also with the CPS for delivering the processed reply data and for monitoring and control functionalities. The monitoring values are send in the simple network management protocol (SNMP) and are read from the build in test-equipment (BITE). The BITE measures voltages, currents, temperatures and states. The PCB also contains the power supply (P/S) components for several different supply voltages of the analog and digital circuits.

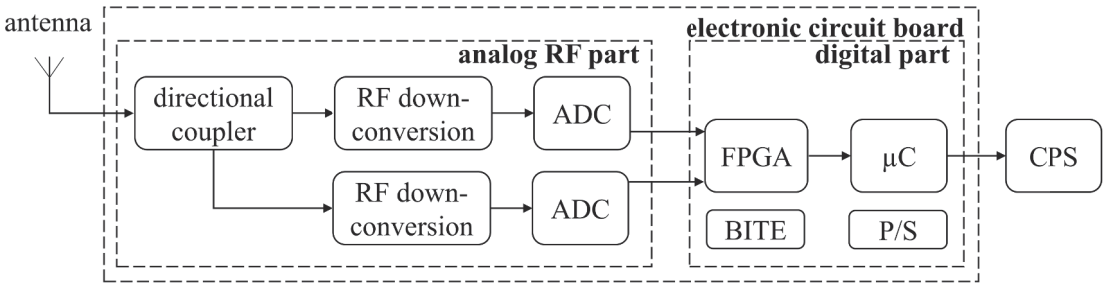

Figure 6.1: RX system overview [6]

The FPGA is programmed with the very high speed integrated circuit hardware description language (VHDL) [2] and the microcontroller runs C++ software on an embedded operating system.

6.1.1 Antenna

For the RX station a simple dipole antenna was chosen to keep the hardware costs as low as possible. The antenna of the RX station is a $\frac{\lambda}{2}$ dipole, as shown in Figure 6.2. It is vertically polarized and has an azimuthal omnidirectional radiation gain pattern 6.3. The antenna can also be installed with a reflector to achieve an azimuthal view of 180°. The antenna has a maximal allowed power of 1 kW, 1.1 dBi gain at a center frequency of 1,060 MHz and half-bandwidth of 30 MHz. The antenna is intended to be mounted on top, i.e. on top of masts, shelters, etc. The antenna with reflector is intended to be mounted in front of objects, i.e. walls of buildings, etc.

Figure 6.2: Half-wave dipole antenna

6.1.2 Analog Front-end

The aim of the analog front-end is to down-convert the 1,090 MHz transponder replies to the IF. To achieve the receiving dynamic range of 100 dB, the front-end uses two channels, the high- and low-power branch. The separated channels are independent and each one is connected to an ADC and then to the FPGA. The sum of the amplification for the high-power branch is 33 dB and for the low-power 10 dB. The dynamic range enables it to receive 250 W transponder replies from a distance of 10 m up to 300 km. The RX stations cannot only be used for airport areas, but also for wide-area applications. The analog front-end PCB is realized with the RO4003CTM microwave laminate from Rogers Corporation and the block diagram of the electronic circuit is shown in Figure 6.4. The input sensitivity of the linear receiver is -89 dBm with a 20 MHz bandwidth at the center frequency of 1,090 ± 1 MHz.
The RF down-conversion consists mainly of low-noise amplifiers (LNA), mixers, band pass (BP) filters, amplifiers, attenuators, a directional coupler and a phased locked loop (PLL). The received transponder replies are split into two branches, the high-power (RF_H) and low-power (RF_L). The coupler has a coupling factor of 13.15 dB, as shown in Figure 6.4. These branches are the same electronic circuit, with the difference of an additional digitally programmable step-attenuator after the directional coupler at the low-power branch. This attenuator balances the input range by adjusting the power level. For the testbed, as described in Section 6.3, this attenuator is set to 10 dB.
Each branch contains a LNA with 16 dB gain and noise figure of 0.5 dB. After the LNA

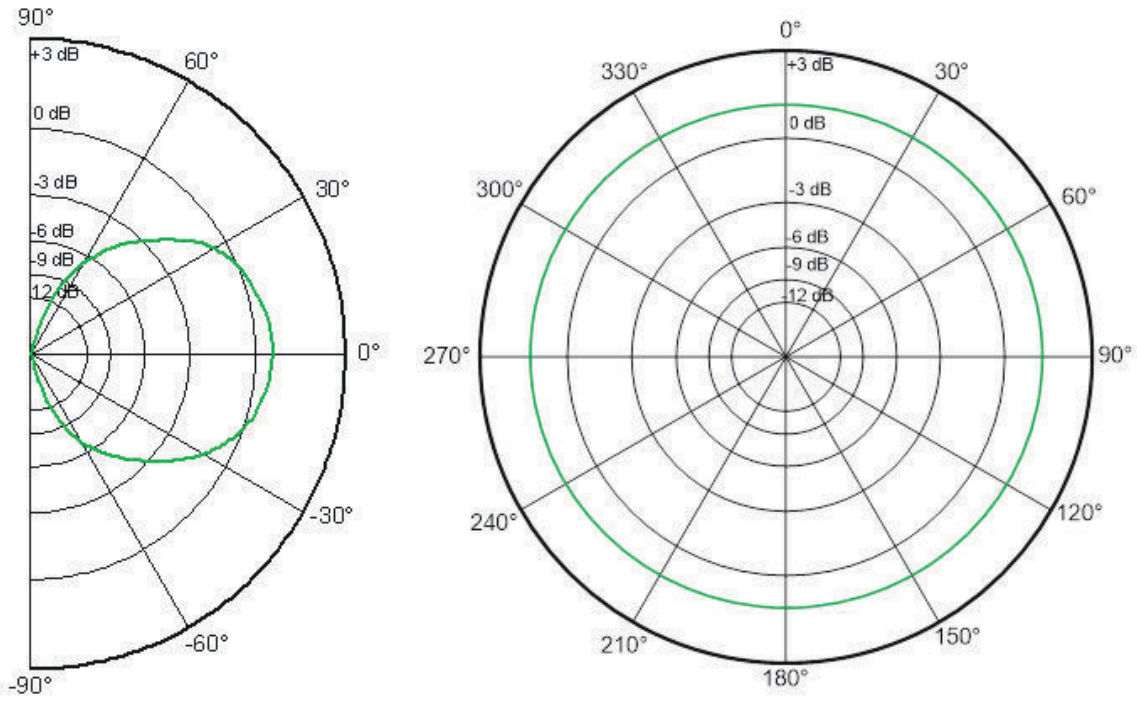

Figure 6.3: Vertical dipole elevation (left) and azimuth (right) gain pattern

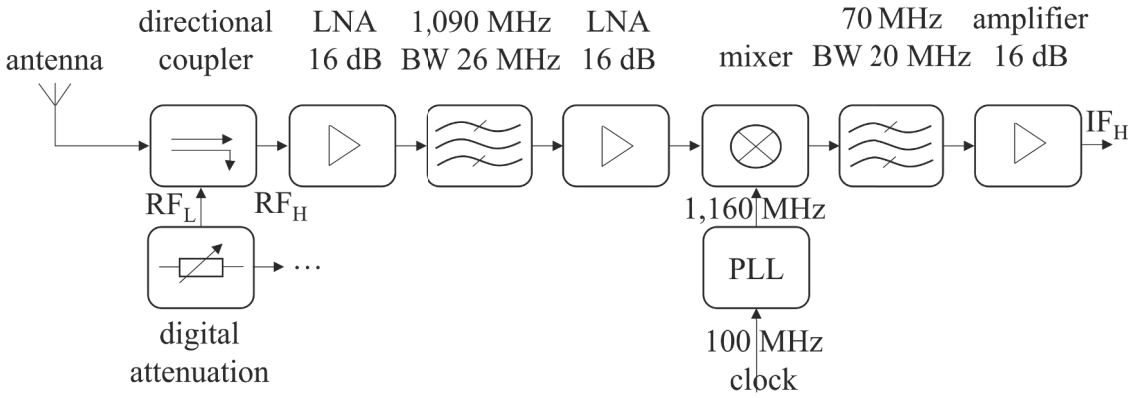

Figure 6.4: RF down-conversion circuit

follows the BP filter with 26 MHz bandwidth and 1.6 dB insertion loss, which can be realized with as a ceramic or surface acoustic wave (SAW) filter. The BP filter is used to reduce sidebands and unwanted signals. After the BP filter there is again a 16 dB LNA and a high IP3 mixer from Hittite Microwave. The mixer mixes the received signal with the local 1,160 MHz clock. This clock is generated from the local 100 MHz FPGA clock with the PLL, which

has 100 kHz loop bandwidth and 10 MHz phase comparator frequency [34] [40]. After the mixer there is the 70 MHz filter with 20 MHz bandwidth to filter the IF from the mixed signal. This signal is then again amplified by a 16 dB LNA (IF_H). This amplified signal is then digitized by the ADC and read from the FPGA, where also the further signal processing is done. The center frequencies of all filters are designed for the 1,090 MHz SSR downlink frequency.

6.2 FPGA Implementation

The FPGA implementation of the RX station down-converts the transponder replies from the IF to the baseband, does the demodulation, the digital signal processing, the decoding, the ToA estimation and the communication with the microcontroller. The implementation is the same for Mode A/C and Mode S, with the difference of the decoder. The main implemented modules of the FPGA are the ToA generation module, the ADC interfaces, the modulation and filtering modules, the ToA estimation algorithms, the Mode A/C and Mode S decoders, the buffers, the decision logic and the bus interface, as shown in Figure 6.5.

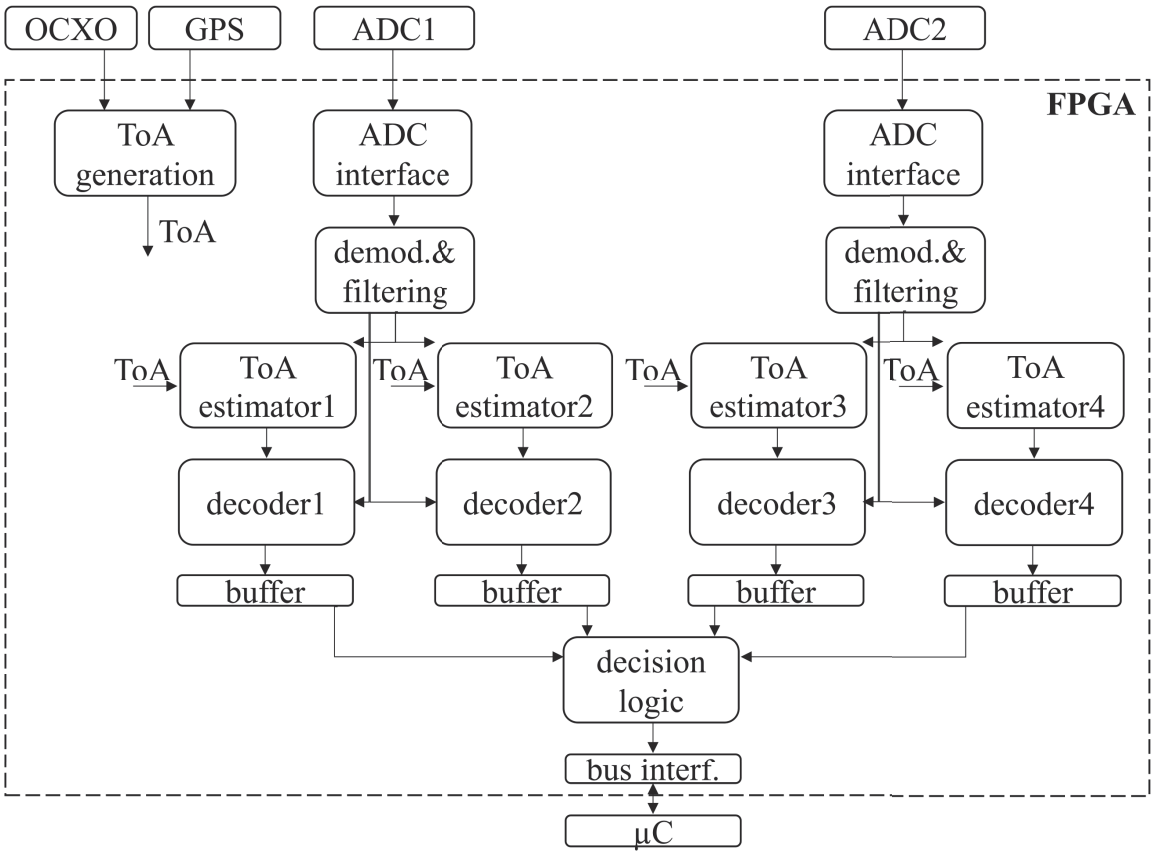

Figure 6.5: RX station FPGA modules

The local oscillator (LO) frequency of the FPGA is 100 MHz, which is also the ADC sampling frequency. The ADC clock is connected to the same clock source as the FPGA. ADC1 receives the RF signal from the high-power branch and ADC2 from the low-power. The received digitized IF samples are demodulated in the demodulation and digital filtering module, which is based on the quadrature-demodulation, and outputs filtered input streams for the ToA estimators and the decoders. The output differs in the digital filtering, since ToA estimation and decoding algorithms are based on different signal processing principles. ToA estimator1 and estimator2 get the same filtered stream from the high-power branch and ToA estimator3 and estimator4 the same from the low-power branch. Decoder1 and decoder2 get the same filtered stream from the high-power branch and decoder3 and decoder4 the same from the low-power branch. The reason to split up each power branch again in two branches, is to use different detection thresholds for the ToA estimation and the decoding. The detection threshold for ToA estimator1 and estimator3 are equal and the one of ToA estimator2 and estimator4. The detection threshold for decoder1 and decoder3 are equal and the one of decoder2 and decoder4. The two detection thresholds for each branch increase the detection probability in case of heavily distorted signals, because they are statically configured. A dynamic noise floor threshold calculation would solve this problem and reduce the complexity. The ToA estimation and the decoding processing is done simultaneously and eventually stored in the circular buffers. The decision logic recognizes when decoded data is stored in a circular buffer and decides which path is written to the bus interface. The bus interface uses an AMBA high-performance bus (AHB) for communicating with the microcontroller.

6.2.1 Demodulation and Digital Filtering

The demodulation and digital filtering module consists mainly of an quadrature-demodulation, as shown in Figure 6.6. The system is incoherent, i.e. that the exact transmitting frequency and phase of the transponder are unknown. The transmitting frequency is defined to 1,090 $\pm$ 3 MHz according ICAO Annex X Volume IV regulations [27]. Due to the incoherent system and of the easiness to compute the momentary signal power, the quadrature-demodulation was considered. The LO frequency is 100 MHz and used for the ADC and the FPGA. The digitized IF signal is filtered by a FIR BP filter using 64 taps. The filter has a 10 MHz bandwidth at 1,090 MHz and removes the direct current (DC) component [41]. The filtered IF signal is split up into two branches and multiplied by the sinus signal in one branch in the other with the cosine signal. The sinus and cosine signals are generated by the DDS and are steered by the same clock source. The DDS sources a 30 MHz numerically controlled oscillator (NCO) signal for the first branch and a 90° phase shifted cosine signal for the second branch. The first branch is the I- and the second branch the Q-path. The I- and Q-paths represent the real- and the imaginary-part of the input. The sampling with a frequency of 100 MHz is the sub-Nyquist sampling, fulfilling the Nyquist–Shannon sampling theorem with not overrunning the maximal frequency sum of the 70 MHz IF signal having a 20 MHz bandwidth. The I and Q branches have the same FPGA components, first the LP FIR filter as anti-aliasing filter with a 10 MHz cutoff frequency. Then the CIC FIR filter, which is a smoothing filter to reduce the white Gaussian noise. Eventually, each path is squared and summed up for the root extraction. The advantage of the CIC filters in the IF paths of the demodulator, I and Q, is that noise is averaged to the zero line, instead of correcting it to an

unknown signal amplitude. It enhances the SNR by about 3 dB. Typically, the smoothing filtering is done after the demodulation [11, 42].
The demodulated raw signal is split up in two streams, one for the decoding algorithms and for the ToA estimation algorithms. The decoding FIR filter filters the stream for the decoding algorithms and is a 32 tap CIC, as described in Section 4.1. The ToA estimation FIR filter filters the stream for the ToA estimation algorithms and is a 2 tap CIC, as described in Section 3.3.2. The filters can be adapted as needed for the corresponding algorithms.

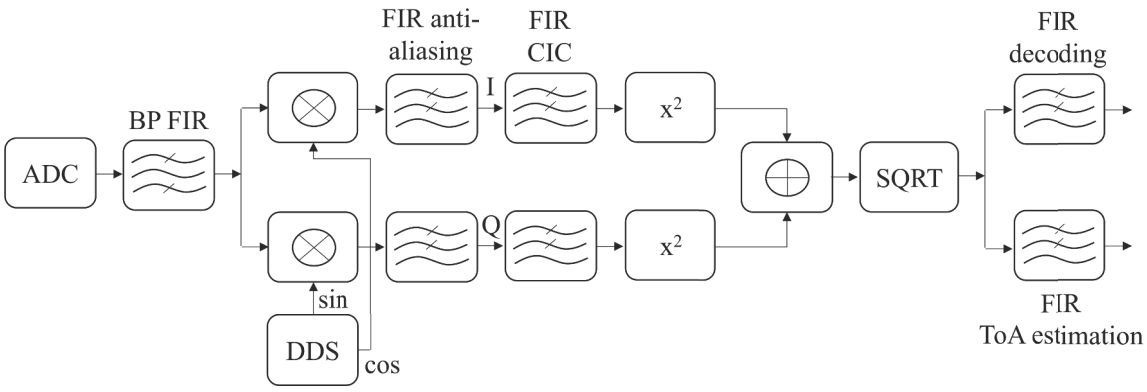

Figure 6.6: Demodulation

6.2.2 ToA Estimation

The ToA estimation algorithms are listed in Chapter 5. These algorithms are implemented in the ToA estimator modules, with the restriction that only one algorithm type at the time can be synthesized within the design. For Mode A/C there must be used a Mode A/C ToA estimator and for Mode S a Mode S ToA estimator, because of the different pulse specifications. The input of the ToA estimator is the demodulated and filtered reply baseband signal. The filter is a 2 tap CIC, as described in Section 3.3.2. The resulting ToA is stored in a circular buffer for the decision logic, when the decoding was successful.
The ToA estimation algorithms detect the pulses of the baseband transponder reply with a detection threshold. This threshold is statically configured and therefore not always right above the noise level. The detection threshold must always be set close to the noise floor, so that the algorithms can react in time using their timing windows. The noise floor can change and sometimes it increases shortly before the transponder reply, because the transmitters switch on the carrier signal before. This carrier leakage can disturb the ToA estimators to wrongly estimate the ToA for the first pulse of the transponder reply. When the transponder power level is low, i.e. the aircraft is far away, the carrier leakage is below the noise level and not visible. This means that the carrier leakage must be concerned with very high-power transponder replies. To solve this issue, the high- and low-power branches are split up. The ToA estimation algorithm 1 and 3 have a lower and the estimation algorithm 2 and 4 a higher threshold value, as shown in Figure 6.5, and all thresholds are above the noise floor. When a high-power transponder reply triggers the ToA estimation algorithm with a low detection

threshold, the algorithm will estimate the ToA of the first pulse wrongly, the ToA estimation algorithm with the higher detection algorithm instead will not. Another solution would be to dynamically calculate the average of the noise level and set the corresponding detection threshold.

6.2.3 Decoding

The low-cost decoding algorithms are listed in Chapter 4. These algorithms are implemented in the decoding module, with the restriction that only one algorithm type can be synthesized with the design. For Mode A/C there must be used a Mode A/C decoder and for Mode S a Mode S decoder, because of the different pulse specifications, different modulation and different framing. The input of the decoder is demodulated and filtered reply baseband signal. The filter is a 32 tap CIC, as described in Section 4.1. The decoded bits are also error marked, as described in Section 4.3. The resulting data is stored in a circular buffer for the decision logic.

6.2.4 Decision Logic

The decision logic decides which of the four branches, as shown in Figure 6.5, is selected to be written to the bus interface [36]. The decision logic takes the signal with the lower count of the decoding bit error masks. If the counts are equal, the decision logic compares the signal power in second step. The high-power signal is always preferred. The logic always takes the decoded bits and the estimated ToA from the same branch for further processing.

6.2.5 ToA Generation

The input of the ToA generation module is a clock source and generates a 64 bit time counter. The time counter value is used by the ToA estimation algorithms to set the ToA. In this implementation the clock source is an OCXO with a 1 second Allan deviation of maximal 10^{10}. The RX PCB also has the option to enable the GNSS receiver and source the FPGA with the PPS of the GPS corrected oscillator.

6.3 Testbed and Results

The RX station uses for the testbed the 50% multilevel threshold detection decoding algorithm with standard input as decoding algorithm, as it is described in Section 4.3.1, and as ToA estimation algorithm the 50% threshold detection ToA estimation algorithm, as described in Section 5.1. The decoding and ToA estimation functionality of the RX station is evaluated and validated with the testbed. In the testbed, the TT22 transponder of the company Trig Avionics Limited is connected to attenuators and to a 6 dB power splitter with RX1 and RX2 station, as shown in Figure 6.7. The RX stations are connected to a PC for the data recording. Both stations have the same clock source, an OCXO. The PC receives the transponder data and compares the estimated ToAs and the bit errors. The difference of the ToAs is computed to determine the RMSE. The attenuator changes from 30 dB to 80 dB to test the different power levels.

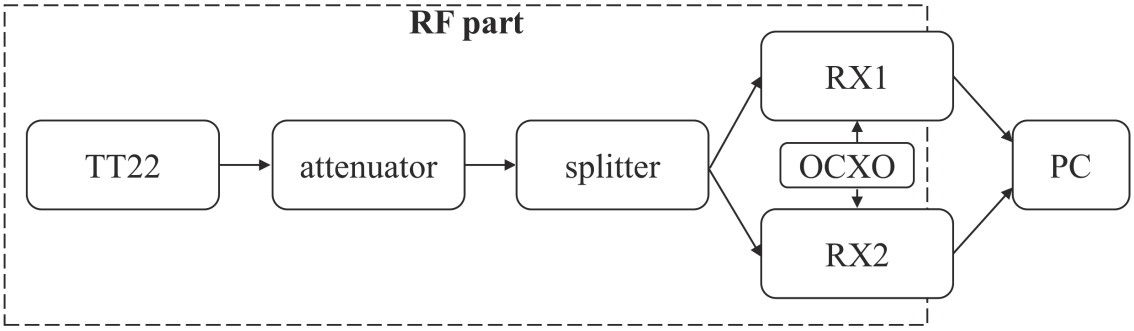

Figure 6.7: Testbed

The low-power branch ToA RMSE of the RX stations is evaluated and validated with different power levels, -30 to -78 dBm, as shown in Figure 6.8. The high-power branch has the same electronic-circuit and digital signal processing, so the results are the same and only shifted to higher power levels. The diagram shows that the ToA RMSE depends on the SNR. At a range of -30 to -60 dBm, the error increases slowly and is below 0.5 m, i.e. it rises almost linearly. At a range of -60 dBm to -78 dBm, the error increases rapidly, i.e. it rises almost exponentially. The test results above -30 dBm are not shown, because they do not lead to acceptable RMSE values. This is due to the input amplifier saturation. Combining the high- and low-power branch, the RX station gets at least a 60 dB input power level range in which the RMSE is below 0.5 m. The RX stations should be only used in the linear part of the high- and low-power branch.

6.4 FPGA Performance

The FPGA of the RX station PCB is from the Spartan 6 series of the company XILINX. It is the XC6SLX150 FPGA with the package FGG484. The FPGA has 23,038 slices, 147,443 logic cells, 184,304 flip flops and 268 random access memory (RAM) blocks with a size of 18 KB [43]. The presented design contains intellectual property (IP) cores from Xilinx, like the FIR filters, DDS, dividers, multipliers and RAM blocks. The rest of the FPGA design is dedicated.
The implementation for the testbed contains for the decoding algorithm, the 50% multilevel threshold detection decoding algorithm, as described in Section 4.1. And uses for the ToA estimation algorithm the 50% threshold detection ToA estimation algorithm, as described in Section 3.3.2. The design for the testbed needs 16,279 slices, resulting in a chip usage of 70.66%. The maximal allowed frequency is 150.37 MHz, corresponding to a minimum clock period of 6.65 ns.

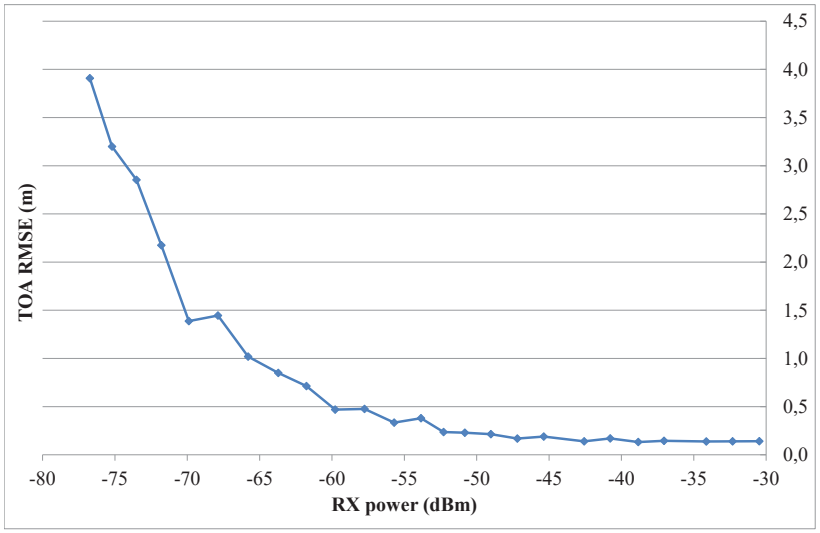

Figure 6.8: ToA RMSE diagram of the RX station [6]

6.5 Receiving and ToA Estimation Station Summary

In this chapter, the FPGA implementation and part of the PCB implementation are presented. The RX station is used to test and evaluate the decoding algorithms, as described in Chapter 4 and the ToA estimation algorithms, as described in Chapter 5. Furthermore, the station is installed at the Salzburg airport, as described in Chapter 7, and fulfills the specifications defined in ICAO Annex X Volume IV [27], ED-117 [12], ED-117A [13], ED-129B [14] and ED-142 [15]. The advantages of the RX station are the linear RX channels, the high 100 dB dynamic range and the design flexibility at the FPGA. The station can be installed for any kind of active or passive, centralized or de-centralized time-synchronization MLAT, WAM or ADS-B system. The RX housing box is shown in Figure 6.9 and the RX PCB in Figure 6.10.

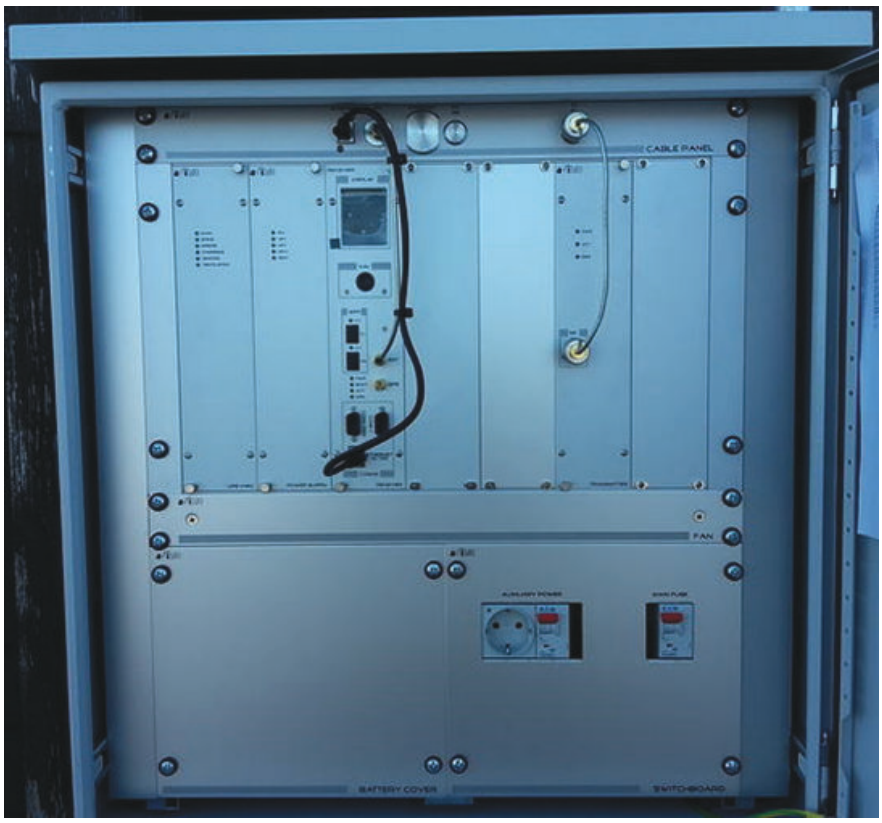

Figure 6.9: RX station

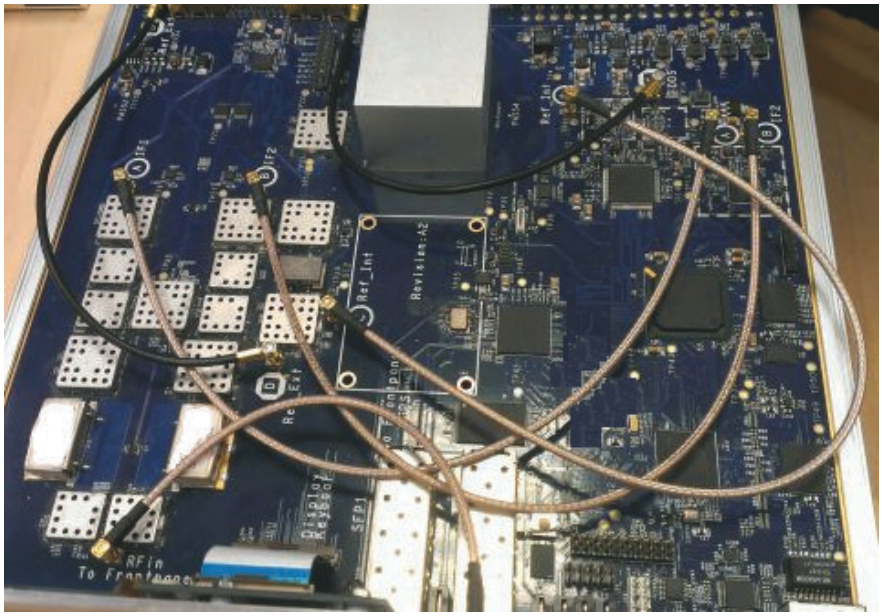

Figure 6.10: RX PCB [6]

7 ToA Estimation Algorithms Evaluations at the Salzburg Airport

In this chapter, the threshold detection ToA estimation algorithm, as described in Section 5.1, the REDTOE algorithm, as described in Section 5.3, the hybrid algorithm and the MF with differentiator algorithm [21], as described in Section 1.2, are evaluated with the MLAT system at the Salzburg airport according the most important ED-117 specification parameters [12]. The MF with differentiator algorithm is a FIR filter containing the differentiated ideal Mode S samples, followed by a zero-crossing detection and interpolation [21]. The hybrid algorithm uses the REDTOE algorithm and the threshold detection ToA estimation algorithm as fallback when the REDTOE ToA is not available.

7.1 MLAT Test System at the Salzburg Airport

The ADB Safegate MLAT system at the Salzburg airport W. A. Mozart in Austria consists of 14 sensors, as shown in Figure 7.1 and is operational since October 2017. The system consists of 11 RX stations (green cross), three RXTX stations (green square), two RT stations (green triangle) and the CPS in the tower. The system is time-synchronized with the TX stations and the RT stations are used as static ground targets to continuously validate the system accuracy by comparing the computed target position with the DGPS measured one. The CPS consists of two servers, due to the redundancy requirement, one is in exec mode and the other one in standby. The CPS software contains a tracker containing a Kalman filter [44] and an outlier detection. The Kalman filter configuration is for all methods the same and leads to a very basic smoothing. The outlier detection dismisses calculated plots which exceed a configurable threshold, i.e. 50 m.

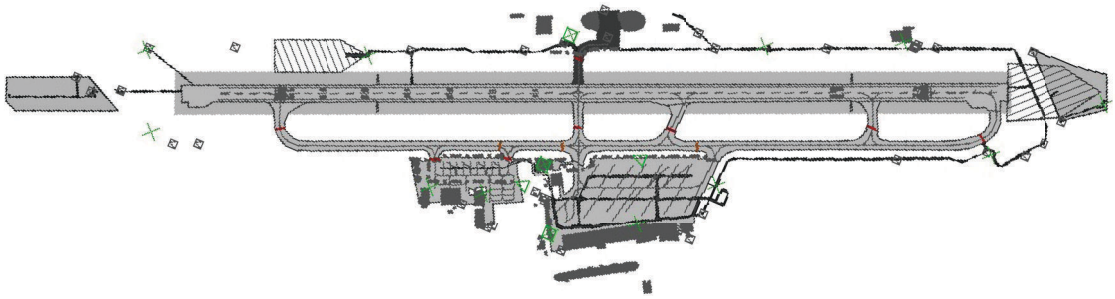

Figure 7.1: MLAT system at the Salzburg airport [5]

7.2 Real-World Test Drive

The real-world test drive at the Salzburg airport is described with the test setup, as described in Section 7.2.1, the driven route, as described in Section 7.2.2, and the performance evaluations, as described in Section 7.2.3.

7.2.1 Test Setup

The setup for the test drive was a vehicle equipped with an aircraft transponder and a DGPS on the rooftop. The transponder is the Trig Avionics TT22 class 1 transponder with 250 W nominal output power, certified for IFR and VFR and mounted with a dipole antenna, as described in Section 6.1.1. The antenna height was 3.3 m measured from ground to the antenna center. The aircraft transponder sends out Mode S replies with a transmit frequency of 2 Hz, which is equal to the recording rate of the DGPS equipment. The DGPS was the SPECTRA Precision ProMark 200, using the real time kinematic (RTK) technology with a virtual reference station (VRS). The DGPS contains a mobile phone to receive the VRS via GSM from the reference station network Austrian positioning service (APOS). The horizontal RMS (HRMS) of the DGPS equipment was 10.001 mm and the vertical RMS (VRMS) was the double of the HRMS. The antennas on the rooftop of the car with the measured distances are shown in Figure 7.2. The aircraft transponder is the test target for the position computation and the DGPS the reference for the evaluations.

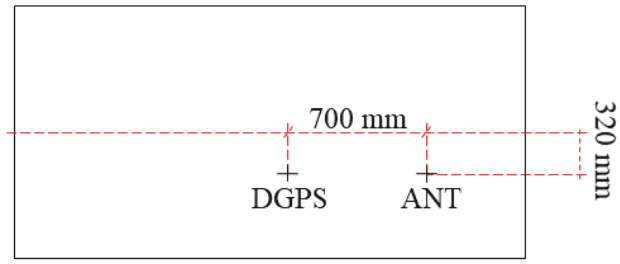

Figure 7.2: Top view of test drive vehicle with transponder and DGPS antenna [5]

7.2.2 Route

The test route (blue lines) covers all areas an aircraft is allowed to drive at the airport, as shown in Figure 7.3 and Figure 7.4. Due to operational traffic and already parking aircraft, the test route was driven slightly different than planned. The test drive was on the Tuesday 2017-07-04 from 9:00 a.m. to 10:30 a.m. and the car drove with a velocity of 30 $\frac{km}{h}$ always at the centerlines.

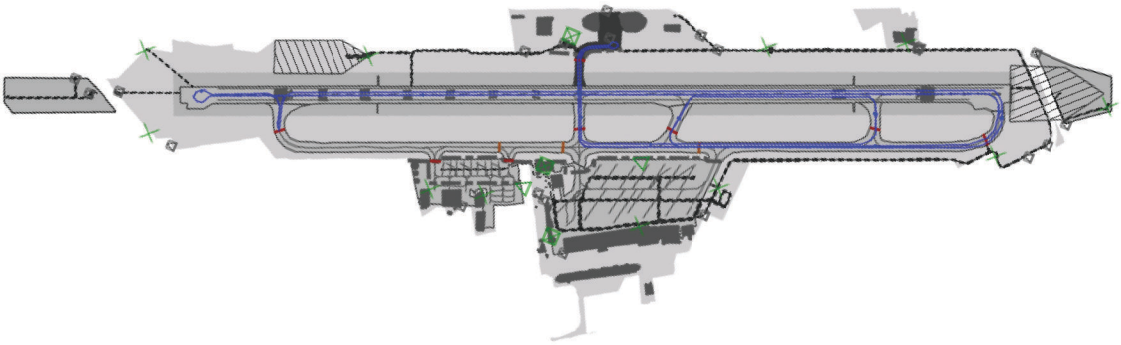

Figure 7.3: Test drive route part 1 [5]

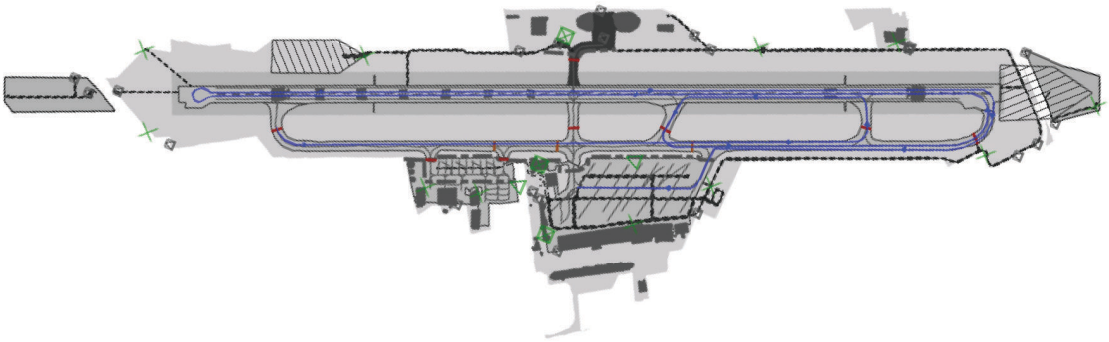

Figure 7.4: Test drive route part 2 [5]

7.2.3 Evaluation Sectors

The ED-117 performance evaluations are evaluated with a proprietary ADB Safegate surveillance analysis tool. It compares the measured DGPS reference points with the calculated positions from the recorded RX data and evaluates the performance parameters according to ED-117. For the performance evaluation the airport is split up into different sectors, runway, taxiway, aprons and stands, as defined in Table 7.1. The defined sectors (red polygons) are shown in Figure 7.5, 7.6, 7.7, 7.8 and 7.9.

Sector	Description
All_gnd	Includes all ground areas
Aprons	Includes main apron and general aviation center (GAC) apron
Man_area	Includes runway, taxiway and apron centerlines
Stands	Includes both aprons without taxiway

Table 7.1: Evaluation sectors [5]

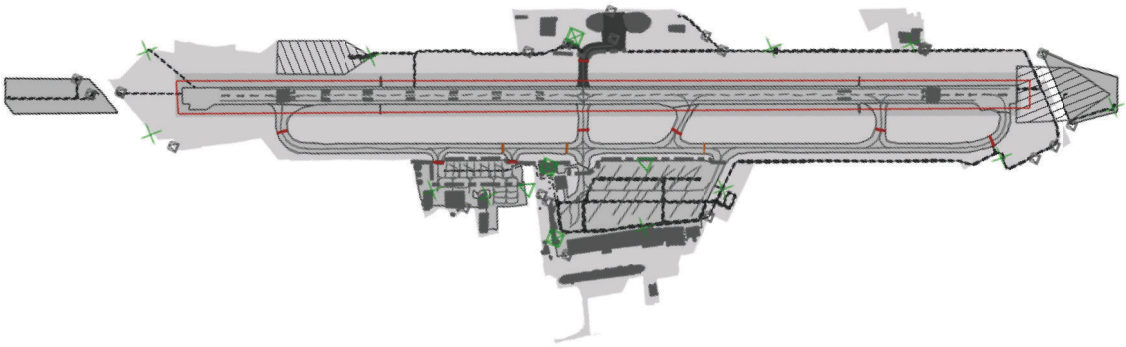

Figure 7.5: Evaluation sector runway [5]

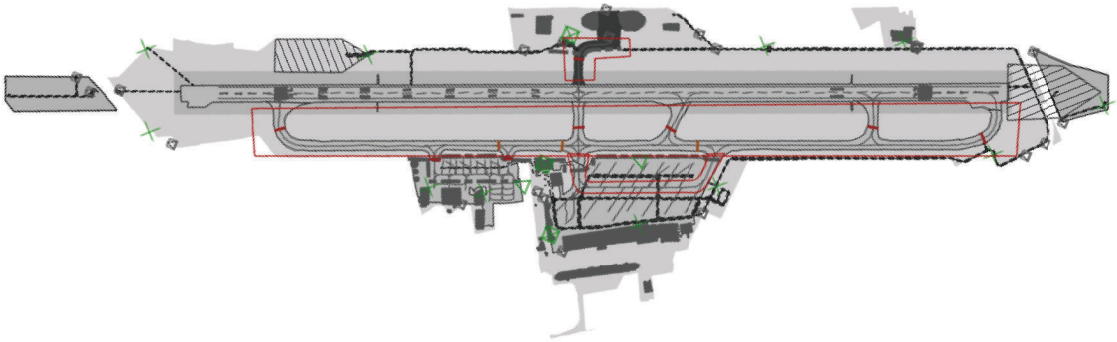

Figure 7.6: Evaluation sector taxiway and apron centerline [5]

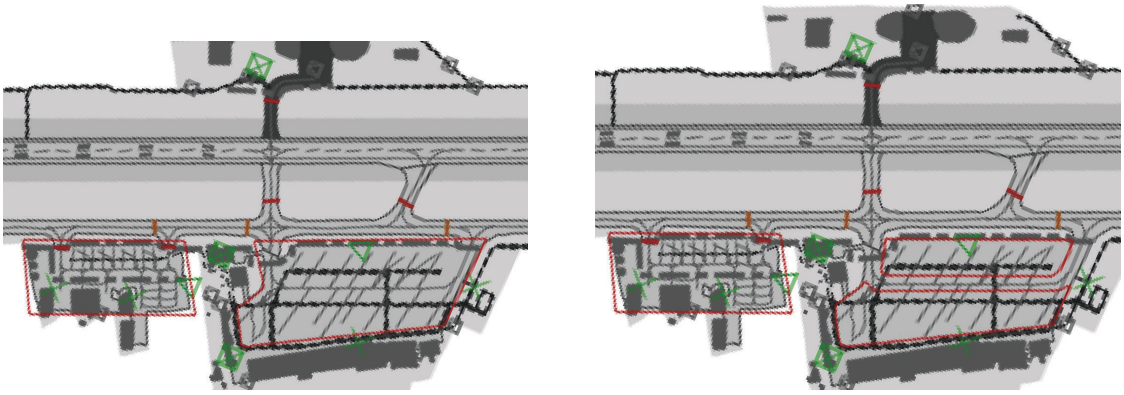

Figure 7.7: Evaluation sector aprons (left) and stands (right) [5]

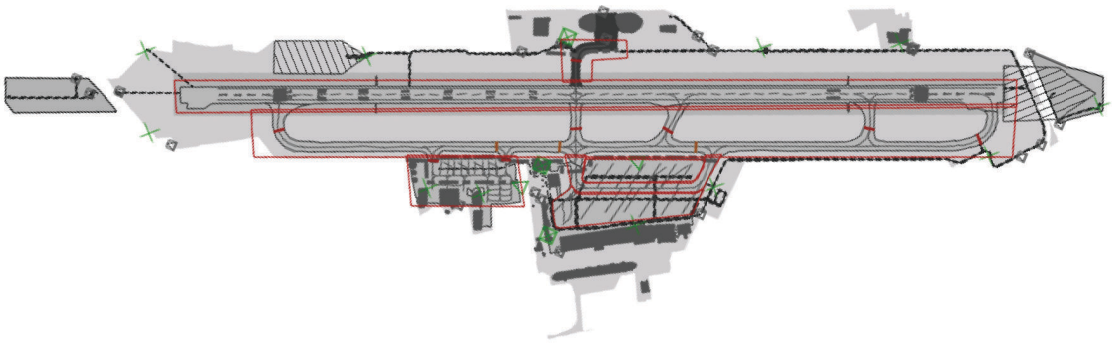

Figure 7.8: Evaluation sector all_gnd [5]

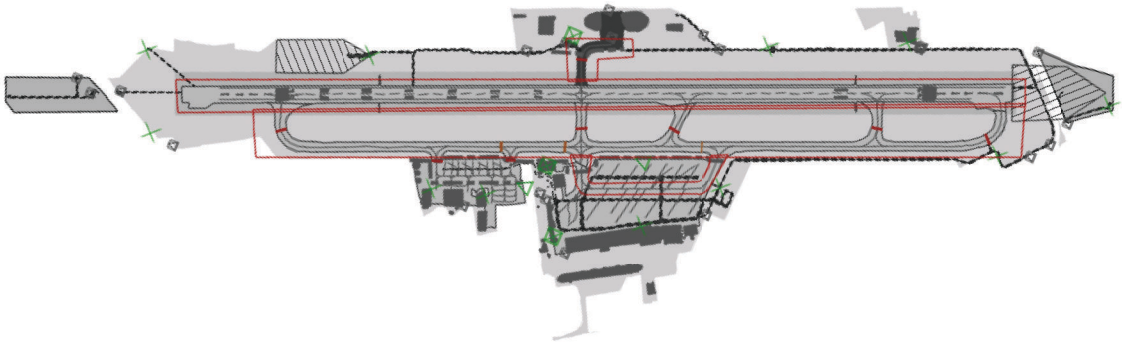

Figure 7.9: Evaluation sector man_area [5]

7.3 Evaluations

The evaluations contain the performance tables, the computation formulas, the evaluation details of the performance tables and the test drive tracks. The evaluation performance tables are separated for the position accuracy and the probability of (false) detection, (false) identification and update.

7.3.1 Position Accuracy

The position accuracy results of the REDTOE, threshold detection ToA estimation algorithm, the hybrid and MF with differentiator algorithm are evaluated with the test drive and results are shown in Table 7.3 using the abbreviations listed in Table 7.2. The best probability values of the columns are marked italic and bold in Table 7.3.

Abbreviation	Description
A.1	Algorithm REDTOE
A.2	Algorithm threshold detection ToA estimation algorithm
A.3	Algorithm matched filter with differentiator
A.4	Hybrid algorithm using algorithm A.1 with A.2 as fallback when A.1 is not available
PA	Position accuracy
RE	Requirement
Run	Runway
Taxi	Taxiway

Table 7.2: Abbreviations [5]

RE	Sector	A.1 (%)	A.2 (%)	A.3 (%)	A.4 (%)	ED-117 Condition
PA	Run	99.12	***99.41***	97.21	99.12	≥95% in 7.5 m
PA	Run	99.71	***100.00***	99.71	***100.00***	≥95% in 12 m
PA	Taxi	***100.00***	99.55	97.29	99.92	≥95% in 7.5 m
PA	Taxi	***100.00***	99.88	99.35	***100.00***	≥95% in 12 m
PA	Aprons	***99.70***	96.14	89.10	99.36	≥95% in 7.5 m
PA	Aprons	***99.95***	99.10	94.17	99.90	≥95% in 12 m
PA	Stands	***99.63***	95.21	86.62	99.21	≥95% in 7.5 m
PA	Stands	***99.94***	98.88	94.17	99.88	≥95% in 12 m
PA	Stands	***100.00***	***100.00***	98.92	***100.00***	under 20 m, averaged over 5 seconds
PA	All_gnd	***99.75***	98.04	93.68	99.56	≥95% in 7.5 m
PA	All_gnd	99.94	99.55	97.65	***99.96***	≥95% in 12 m
PA	Man_area	***99.81***	99.52	97.26	99.74	≥95% in 7.5 m
PA	Man_area	99.94	99.90	99.43	***100.00***	≥95% in 12 m

Table 7.3: Position Accuracy [5]

7.3.2 Probability of Detection, Identification and Update

The ED-117 [12] compliance includes not only PA evaluations of the test drive at the test airport. There is also the probability of detection, probability of false detection, probability of identification, probability of false identification and probability of update to consider. Abbreviations for the probabilities are listed in Table 7.4. The probability of detection and false detection is listed in Table 7.5 and the probability of identification, false identification and of update are listed in Table 7.6. The best probability values of the columns are marked italic and bold in Table 7.5 and 7.6.

Abbreviation	**Description**
PD	Probability of Detection
PFD	Probability of False Detection
PFID	Probability of False Identification
PID	Probability of Identification
PoU	Probability of Update

Table 7.4: Abbreviations [19]

RE	**Sector**	**A.1 (%)**	**A.2 (%)**	**A.3 (%)**	**A.4 (%)**	**ED-117 Condition**
PD	Run	***100.00***	***100.00***	***100.00***	***100.00***	≥99.9%
PD	Taxi	96.23	96.11	***97.21***	97.05	≥99.9%
PD	Aprons	99.28	***99.67***	99.17	97.52	≥99.9%
PD	Stands	99.23	***99.65***	99.12	97.41	≥99.9%
PD	All_gnd	98.59	***98.79***	98.76	97.54	≥99.9%
PD	Man_area	97.12	96.97	***97.90***	97.81	≥99.9%
PFD	All_gnd	***0.00***	***0.00***	0.0428	***0.00***	≤0.01%

Table 7.5: Probability of (False) Detection [19]

RE	**Sector**	**A.1 (%)**	**A.2 (%)**	**A.3 (%)**	**A.4 (%)**	**ED-117 Condition**
PID	All_gnd	***99.99***	***99.99***	***99.99***	99.97	≥99.9%
PFID	All_gnd	***0.00***	***0.00***	***0.00***	***0.00***	≤0.0001%
PoU	Aprons	98.96	***99.45***	98.84	96.10	≥95.0%
PoU	Stands	98.90	***99.42***	98.78	95.99	≥95.0%
PoU	Man_area	96.29	95.21	***97.46***	96.26	≥95.0%

Table 7.6: Probability of (False) Identification and of Update [19]

7.3.3 Computations

In this chapter, the computation formulas for the position accuracy, probability of detection, probability of false detection, probability of identification, probability of false identification and probability of update are listed [19].

7.3.3.1 Position Accuracy

The position accuracy evaluation details for the different sectors, as described in Section 7.3.4, list the average error, the update count and the in- and outside limit counts. The average error is the average of the position errors for all target positions in a track sector. The update count is almost equal for all the compared algorithms.
The DGPS position, $x_r[n]$ and $y_r[n]$, is the reference and recorded for the test drive. The Cartesian coordinates, $x_t[n]$ and $y_t[n]$ with n is element of 0 to N elements, are computed for each target report in each track segment with the recorded raw data of the RX stations. The reference position is calculated using linear interpolation to the same point in the time as the MLAT target report, the Euclidean distance $\delta[n]$ is computed, as shown in Equation 7.1. The Euclidean distance is used to compute the in- and outside limit counts for 7.5 m and 12 m. The inside limit count sums up all target reports, which are in the ED-117 boundaries of the evaluations, and the outside limit count those which are not [19].

$$\delta[n] = \sqrt{(x_t[n] - x_r[n])^2 + (y_t[n] - y_r[n])^2} \tag{7.1}$$

The average error distance δ_{avg} is calculated, as shown in Equation 7.2.

$$\delta_{avg} = \frac{\sum \delta[n]}{N} \tag{7.2}$$

7.3.3.2 Probability of Detection

For each target position report in each track segment, the time difference $\Delta t[n]$, as shown in Equation 7.3, to the last report is calculated:

$$\Delta t[n] = t[n] - t[n-1] \tag{7.3}$$

The miss per update interval counter $\#_{MUI}$, as shown in Equation 7.6, is incremented when the time difference, as shown in Equation 7.4, is larger than the update time interval t_{UI} of 2 seconds and the additional time epsilon t_ϵ of 0.05 seconds. An exception is when the time difference is larger than the outlier threshold t_{th} of 300 seconds, as shown in Equation 7.5. The outlier threshold is used to suppress the case when targets leave the coverage area [19].
It is a miss if:

$$\Delta t[n] > t_{UI} + t_\epsilon \tag{7.4}$$

$$\Delta t[n] > 2.05 \; seconds$$

The miss is suppressed if:

$$\Delta t[n] > t_{th} \tag{7.5}$$

$$\Delta t[n] > 300 \; seconds$$

$$\#_{MUI} = \sum \left\lfloor \frac{\Delta t[n]}{t_{UI}} \right\rfloor = \sum \left\lfloor \frac{\Delta t[n]}{2 \; seconds} \right\rfloor \tag{7.6}$$

The duration time t_{dur} is calculated for all elements of the track segment, as shown in Equation 7.7, by subtracting the last with the first time of elements [19].

$$t_{dur} = t[N-1] - t[0] \tag{7.7}$$

The expected update interval counter $\#_{EUI}$ is calculated for all elements of the track segment, as shown in Equation 7.8.

$$\#_{EUI} = \left\lfloor \frac{t_{dur}}{t_{UI}} \right\rfloor \tag{7.8}$$

The probability of detection PD is calculated for each track segment, as shown in Equation 7.9, and eventually summed up for the whole track [19]. The ED-117 specification for the probability of detection is $PD \geq 99.9\%$.

$$PD = 100 \left(1 - \frac{\#_{MUI}}{\#_{EUI}}\right) \% \tag{7.9}$$

7.3.3.3 Probability of False Detection

The false target detection counter $\#_{FD}$ is increased, if the reference distance $\delta[n]$ is larger than the maximum allowed distance δ_{max}, as shown in Equation 7.10. The target detection counter $\#_{CD}$ is increased, if the reference distance $\delta[n]$ is smaller or equal than the maximal allowed distance δ_{max} [19].

$$\delta_{max} = 50 \ m \tag{7.10}$$

$$\begin{gathered} \text{Count } \#_{FD} \text{ if } \delta[n] > \delta_{max} \\ \text{Count } \#_{CD} \text{ if } \delta[n] \leq \delta_{max} \end{gathered}$$

The probability of false detection PFD, as shown in Equation 7.11, is calculated by dividing the false detection counter with the sum count of all target reports $\#_{all}$. The ED-117 specification for the probability of false detection is $PFD \leq 0.01\%$.

$$PFD = 100 \frac{\#_{FD}}{N} \% \tag{7.11}$$

7.3.3.4 Probability of Identification

For each target report in each track segment it is checked if an identification exists. This means, that for each target report it is checked, if the identification check I_t results in the following types [19]:

- No secondary information in test data: I_{None}
- No secondary information in reference data: $I_{Unknown}$
- Correct secondary information: $I_{Correct}$
- Incorrect secondary information: $I_{Incorrect}$

For each defined category, counters are used to sum up the number of target reports $\#_{None}$, $\#_{Unknown}$, $\#_{Correct}$ and $\#_{Incorrect}$. Based on the identification check result, as described in Section 7.3.3.6, for each target report the corresponding counter is incremented. Test data with only primary information does not contribute to the calculation. The probability of identification PID, as shown in Equation 7.12, is calculated for each target report in each track segment. The ED-117 specification for the probability of identification is $PID \geq 99.9\%$.

$$PID = 100\frac{\#_{Correct} + \#_{Unknown}}{N}\% \tag{7.12}$$

7.3.3.5 Identification Period

The identification for Mode S is checked with the Mode A code and the Mode S address or the Mode S callsign. For each found identification both values are saved with start and end time. When there is a Mode S address found, only the address is saved, because it is unique. When getting a new Mode A code, the new time period with the identification value is saved. When no new Mode A code is received, the previous time period is extended with the new start and end time. Receiving different timing values for the same track results in an error [19].

7.3.3.6 Identification Check

If there exists a reference at the certain time, the identification check result is calculated based on the secondary information of the reference. When there is no reference the result is unknown ($I_{Unknown}$). When there is no reference, the secondary information is taken from the track itself. The following algorithm does for each identification value the identification check [19]:

- If there is no identification value: $I_t = I_{None}$
- If the time is outside of identification period, as described in Section 7.3.3.5: $I_t = I_{Unknown}$
- If the time is in the identification period and the identification value is not equal to the reference: $I_t = I_{Incorrect}$
- If the time is in the identification period and the identification value is equal to the reference: $I_t = I_{Correct}$

All existing identification information is validated, and the result is summarized. The identification check is very restrictive and requires that all existing identities must be correct, otherwise it results in an error.

7.3.3.7 Probability of False Identification

The probability of false identification $PFID$, as shown in Equation 7.13, is calculated for each target report in each track segment [19]. The calculation details of the fundamentals are the same as for the calculation of identification, as described in Section 7.3.3.4. The ED-117 specification for the probability of false identification is $PFID \leq 0.0001\%$.

$$PFID = 100\frac{\#_{Incorrect}}{N}\% \tag{7.13}$$

7.3.3.8 Probability of Update

The probability of update is computed in the same way and with the same formulas as the probability of detection, as described in Section 7.3.3.2. The difference is at the update time interval t_{UI}, which is 1 seconds and the ED-117 condition [19]. The ED-117 specification for the probability of update is $PoU \geq 95.0\%$.

7.3.4 Position Accuracy Details in Sectors

The position accuracy results of the evaluation are split up in the sectors runway, taxiway, aprons and stands, as defined in Table 7.1 are shown in Tables 7.7, 7.8, 7.9 and 7.10.

Name	**A.1**	**A.2**	**A.3**	**A.4**
Updates Count	2458	2457	2468	2461
Error Average [m]	1.56	1.92	2.88	1.87
Inside Limit Count for 7.5 m	2458	2446	2401	2459
Outside Limit Count for 7.5 m	0	11	67	2
Inside Limit Count for 12 m	2458	2454	2452	2461
Outside Limit Count for 12 m	0	3	16	0

Table 7.7: Sector Taxiways – Position Accuracy Details [5]

Name	**A.1**	**A.2**	**A.3**	**A.4**
Updates Count	680	681	680	681
Error Average [m]	2.00	2.15	2.96	2.12
Inside Limit Count for 7.5 m	674	677	661	675
Outside Limit Count for 7.5 m	6	4	19	6
Inside Limit Count for 12 m	678	681	678	681
Outside Limit Count for 12 m	2	0	2	0

Table 7.8: Sector Runway – Position Accuracy Details [5]

Name	**A.1**	**A.2**	**A.3**	**A.4**
Updates Count	2014	1996	1963	2023
Error Average [m]	1.71	2.54	4.11	1.93
Inside Limit Count for 7.5 m	2008	1919	1749	2010
Outside Limit Count for 7.5 m	6	77	214	13
Inside Limit Count for 12 m	2013	1978	1869	2021
Outside Limit Count for 12 m	1	18	94	2

Table 7.9: Sector Aprons – Position Accuracy Details [5]

Name	**A.1**	**A.2**	**A.3**	**A.4**
Updates Count	1630	1609	1577	1637
Error Average [m]	1.77	2.77	4.49	2.01
Inside Limit Count for 7.5 m	1624	1532	1366	1624
Outside Limit Count for 7.5 m	6	77	211	13
Inside Limit Count for 12 m	1629	1591	1485	1635
Outside Limit Count for 12 m	1	18	92	2
Inside Limit Count for 20 m averaged over 5 seconds	1630	1609	1560	1637
Outside Limit Count for 20 m averaged over 5 seconds	0	0	17	0

Table 7.10: Sector Stands – Position Accuracy Details [5]

7.3.5 Probability of Detection, Identification and Update Details in Sectors

Details of the evaluation results for the probability of (false) detection, (false) identification and update details in sectors are shown in Tables 7.11, 7.12, 7.13, 7.14, 7.15, 7.16, 7.17, 7.18, 7.19, 7.20 and 7.21.

Name	**A.1**	**A.2**	**A.3**	**A.4**
Updates Count $\#_{all}$	1360	1365	1362	2299
Counter of Missed Update Intervals $\#_{MUI}$	0	0	0	0
Expected Updates $\#_{EUI}$	668	671	671	1129
PD (%)	100.00	100.00	100.00	100.00
ED-117 Condition (%)	$\geq$99.90	$\geq$99.90	$\geq$99.90	$\geq$99.90
ED-117 Compliant	OK	OK	OK	OK

Table 7.11: Sector Runway – Probability of Detection Details [19]

Name	**A.1**	**A.2**	**A.3**	**A.4**
Updates Count $\#_{all}$	4333	4694	4150	6465
Counter of Missed Update Intervals $\#_{MUI}$	83	94	58	97
Expected Updates $\#_{EUI}$	2203	2417	2079	3291
PD (%)	96.23	96.11	97.21	97.05
ED-117 Condition (%)	≥99.90	≥99.90	≥99.90	≥99.90
ED-117 Compliant	NOK	NOK	NOK	NOK

Table 7.12: Sector Taxiways – Probability of Detection Details [19]

Name	**A.1**	**A.2**	**A.3**	**A.4**
Updates Count $\#_{all}$	13780	13846	13508	19264
Counter of Missed Update Intervals $\#_{MUI}$	50	23	56	244
Expected Updates $\#_{EUI}$	6930	6931	6786	9830
PD (%)	99.28	99.67	99.17	97.52
ED-117 Condition (%)	≥99.90	≥99.90	≥99.90	≥99.90
ED-117 Compliant	NOK	NOK	NOK	NOK

Table 7.13: Sector Aprons – Probability of Detection Details [19]

Name	**A.1**	**A.2**	**A.3**	**A.4**
Updates Count $\#_{all}$	13001	13072	12741	17973
Counter of Missed Update Intervals $\#_{MUI}$	50	23	56	237
Expected Updates $\#_{EUI}$	6511	6519	6377	9137
PD (%)	99.23	99.65	99.12	97.41
ED-117 Condition (%)	≥99.90	≥99.90	≥99.90	≥99.90
ED-117 Compliant	NOK	NOK	NOK	NOK

Table 7.14: Sector Stands – Probability of Detection Details [19]

Name	**A.1**	**A.2**	**A.3**	**A.4**
Updates Count $\#_{all}$	18601	19037	18148	26576
Counter of Missed Update Intervals $\#_{MUI}$	133	117	114	335
Expected Updates $\#_{EUI}$	9422	9642	9160	13597
PD (%)	98.59	98.79	98.76	97.54
ED-117 Condition (%)	≥99.90	≥99.90	≥99.90	≥99.90
ED-117 Compliant	NOK	NOK	NOK	NOK

Table 7.15: Sector All_gnd – Probability of Detection Details [19]

Name	**A.1**	**A.2**	**A.3**	**A.4**
Updates Count $\#_{all}$	5671	6038	5489	8720
Counter of Missed Update Intervals $\#_{MUI}$	83	94	58	97
Expected Updates $\#_{EUI}$	2884	3099	2760	4434
PD (%)	97.12	96.97	97.90	97.81
ED-117 Condition (%)	≥99.90	≥99.90	≥99.90	≥99.90
ED-117 Compliant	NOK	NOK	NOK	NOK

Table 7.16: Sector Man_area – Probability of Detection Details [19]

Name	**A.1**	**A.2**	**A.3**	**A.4**
Updates Count $\#_{all}$	4720	4704	4671	4729
False Position Counter $\#_{FD}$	0	0	0	0
Correct Position Counter $\#_{CD}$	4720	4707	4669	4729
PFD (%)	0	0	0.04	0
ED-117 Condition (%)	≤0.01	≤0.01	≤0.01	≤0.01
ED-117 Compliant	OK	OK	NOK	OK

Table 7.17: Sector All_gnd – Probability of False Detection Details [19]

Name	**A.1**	**A.2**	**A.3**	**A.4**
Updates Count $\#_{all}$	51732	52596	50773	71496
Identity None $\#_{None}$	7	7	3	18
Identity Unknown $\#_{Unknown}$	2	2	2	2
Identity Correct $\#_{Correct}$	51723	52587	50768	71476
Identity Incorrect $\#_{Incorrect}$	0	0	0	0
PID (%)	99.99	99.99	99.99	99.97
ED-117 Condition (%)	≥99.90	≥99.90	≥99.90	≥99.90
ED-117 Compliant	OK	OK	OK	OK
PFID (%)	0	0	0	0
ED-117 Condition (%)	≤0.0001	≤0.0001	≤0.0001	≤0.0001
ED-117 Compliant	OK	OK	OK	OK

Table 7.18: Sector All_gnd – Probability of (False) Identification Details [19]

Name	**A.1**	**A.2**	**A.3**	**A.4**
Updates Count $\#_{all}$	13780	13846	13508	19264
Counter of Missed Update Intervals $\#_{MUI}$	144	76	158	768
Expected Updates $\#_{EUI}$	13869	13875	13589	19709
PoU (%)	98.96	99.45	98.84	96.10
ED-117 Condition (%)	≥95.00	≥95.00	≥95.00	≥95.00
ED-117 Compliant	OK	OK	OK	OK

Table 7.19: Sector Aprons – Probability of Update Details [19]

Name	**A.1**	**A.2**	**A.3**	**A.4**
Updates Count $\#_{all}$	13001	13072	12741	17973
Counter of Missed Update Intervals $\#_{MUI}$	144	76	156	736
Expected Updates $\#_{EUI}$	13052	13061	12783	18351
PoU (%)	98.90	99.42	98.78	95.99
ED-117 Condition (%)	≥95.00	≥95.00	≥95.00	≥95.00
ED-117 Compliant	OK	OK	OK	OK

Table 7.20: Sector Stands – Probability of Update Details [19]

Name	**A.1**	**A.2**	**A.3**	**A.4**
Updates Count $\#_{all}$	5671	6038	5489	8720
Counter of Missed Update Intervals $\#_{MUI}$	215	298	141	333
Expected Updates $\#_{EUI}$	5793	6216	5546	8893
PoU (%)	96.29	95.21	97.46	96.26
ED-117 Condition (%)	≥95.00	≥95.00	≥95.00	≥95.00
ED-117 Compliant	OK	OK	OK	OK

Table 7.21: Sector Man_area – Probability of Update Details [19]

7.3.6 Test Drive Track

The test drive tracks of REDTOE algorithm (red track) is shown in Figure 7.10, of the threshold detection ToA estimation algorithm (green line) is shown in Figure 7.11 and of the MF with differentiator (blue line) is shown in Figure 7.12.

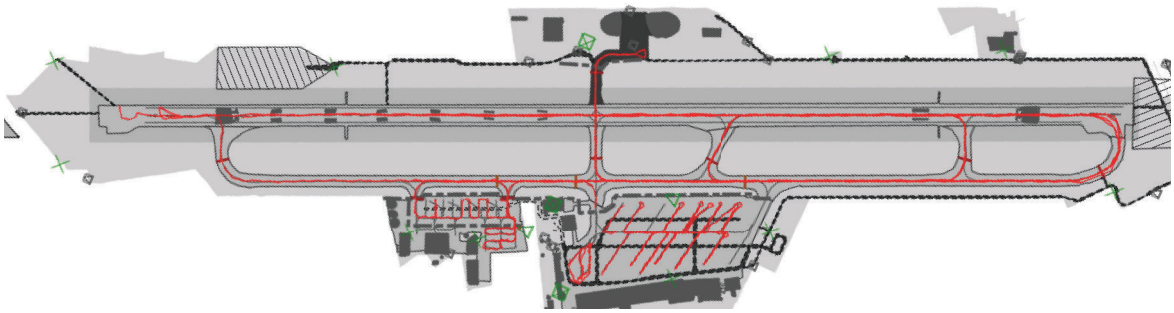

Figure 7.10: REDTOE test drive track [5]

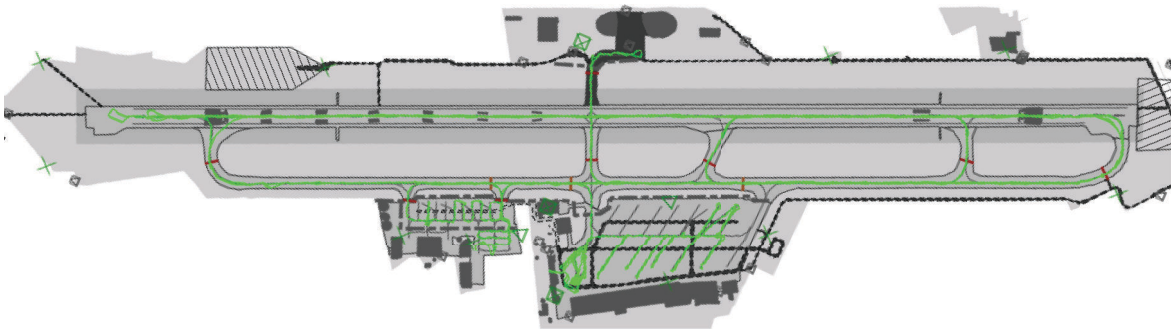

Figure 7.11: Threshold detection ToA estimation algorithm test drive track [5]

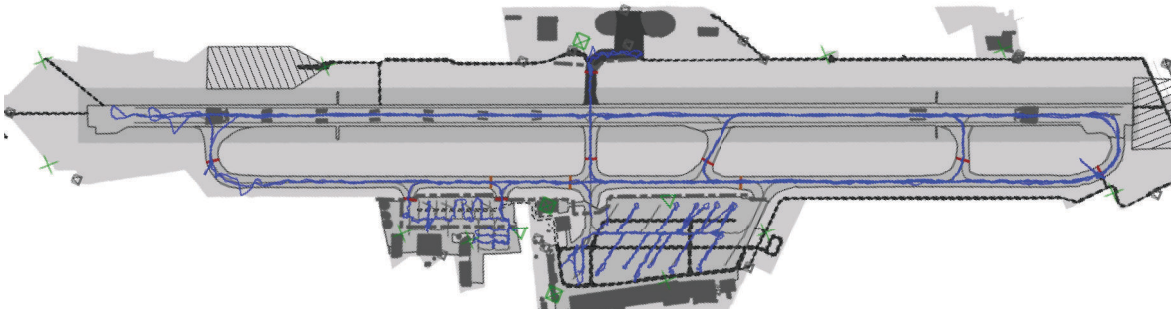

Figure 7.12: Matched filter with differentiator test drive track [5]

7.3.7 Results

The evaluation results are summarized for the most important ED-117 specifications of ToA estimation algorithms, the position accuracy and the probability of detection, identification and update.

7.3.7.1 Position Accuracy

The REDTOE algorithm (A.1) and the threshold detection ToA estimation algorithm (A.2) have mostly similar position accuracy results with slight differences in the per mill rate, except at the apron and stand sections. The REDTOE algorithm has an improvement of more than 3% for the 7.5 m condition in these sections, this is most probably the case due to the high number of multipath propagation from near buildings. The threshold detection ToA estimation algorithm has slightly better results at the runway section with an improvement of almost 0.3%.
The MF with differentiator (A.3) has mostly very close results to the threshold detection ToA estimation algorithm and the REDTOE, but in summary the performance in terms of accuracy is not that good. Taking a closer look to the implementation lead to the conclusion that the algorithm was not able to estimate the ToA in the given time window like the other algorithms, i.e. that unfortunately due to implementation issues this algorithm does not achieve very good results.
The 50% threshold detection ToA estimation and the MF with differentiator algorithms have their shortcomings in case of multipath overlapping. The threshold detection depends on the signal amplitude and the state-of-the-art algorithm on the falling edge of the first pulse. The REDTOE instead only depends on the rising edge, which leads typically due to the typical multipath overlapping occurrence as described in Section 5.3.1, to a higher position accuracy.
The evaluation results for the hybrid algorithm (A.4), using REDTOE and as fallback the threshold detection ToA estimation algorithm, show that the algorithm benefits from the higher position accuracy at apron and stand sections from the REDTOE and the higher accuracy at the runway from the fallback algorithm. The update count of the hybrid algorithm is higher than from others, resulting in a higher probability of detection, as shown in Tables 7.7, 7.9 and 7.10.
The comparison of the test tracks of the algorithms, as shown in Figures 7.10, 7.11 and 7.12, shows no big difference, except at areas like the apron, stands and at the northern end of the runway, where mostly multipath overlapping exists. The computed track points with high deviation, e.g. due to multipath propagation, are visible in the track as spikes.

7.3.7.2 Probability of Detection, Identification and Update

The threshold detection ToA estimation algorithm (A.2) has for most of the sectors the highest probability of detection and the lowest probability of false detection compared to other algorithms. Furthermore, it has also for most of the sectors the highest probability of identification, the lowest probability of false identification and the highest probability of update.

7.4 ToA Estimation Algorithms Evaluations at the Salzburg Airport Summary

In this chapter, the evaluations of the ToA estimation algorithms, the 50% threshold detection ToA estimation algorithm, as described in Section 5.1, the REDTOE, as described in Section 5.3, the MF with differentiator algorithm and the hybrid algorithm, which uses the REDTOE and as fallback the threshold detection ToA estimation algorithm, are presented. The algorithms are evaluated according European surveillance specifications EUROCAE ED-117 [12] at the Salzburg airport W. A. Mozart in Austria. The evaluations are done with the ADB Safegate MLAT test system using the implemented RX station, as described in Chapter 6. They have shown, that the REDTOE algorithm leads to the best results in terms of position accuracy, especially at aprons and stands where typically multipath overlapping deteriorates the signals. It also shows, that the threshold detection ToA estimation algorithm leads to the best probability of detection results for almost all areas. This leads to the conclusion to propose the hybrid algorithm, which combines both advantages and achieves best results to fulfill the given ED-117 specifications. The threshold detection ToA estimation algorithm has the best results in terms of probability of detection, identification and of update. The evaluations show that all presented algorithms fulfill the position accuracy specifications of ED-117.

8 Summary and Conclusions

In this chapter, the summary of the multipath overlapping analysis, as described in Chapter 3, the decoding algorithms, as described in Chapter 5, the ToA estimation algorithms and performance measurements at the Salzburg airport, as described in Chapter 5 and 7, and of the RX station, as described in Chapter 6 are presented.

8.1 Multipath Overlapping Analysis

The evaluations of the MATLAB simulations model for multipath overlapping of Mode S signals have shown that the CIC digital filtering for the decoding should done with 32 taps and for the ToA estimation algorithms with 2 taps, assuming to have 70 MHz IF. The simulation analysis of the multipath overlapping influence on the transponder replies, helped significantly to develop the REDTOE algorithm. Furthermore, is has been shown, that the pulse width and the ratio pulse power to pulse pause power could be used as multipath detector.

8.2 Decoding Algorithms

The evaluations of the real-world dataset from the Salzburg airport have shown that the multilevel threshold detection decoding algorithm with standard input has the lowest BER compared to the multilevel threshold detection decoding with mean input, the edge detection decoding and the Mode S secondary radar decoding technique [20]. All the decoding algorithms are low-cost and the implementation costs of the multilevel threshold detection decoding algorithm with standard input are 3,713 FPGA logic cells for Mode A/C and 4,957 cells for Mode S. The proposed algorithms show a high resistance against multipath overlapping.

8.3 ToA Estimation Algorithms and ED-117 Evaluations

The evaluations according ED-117 of the test drive at the Salzburg airport have shown that the REDTOE algorithm has the best results in terms of position accuracy and the threshold detection ToA estimation algorithm has the best probability of detection results for almost all areas. The hybrid algorithm combines both advantages and achieves even better results. All the ToA estimation algorithms are low-cost with implementation costs of the REDTOE algorithm of about 3,000 logic cells. The REDTOE algorithm leads to less ToA deviations in case of multipath overlapping with at least 50 nanoseconds time delay of the overlapped component.
Furthermore, the presented correlation ToA estimation algorithm can be used in case of multipath overlapping with high power. The algorithm can be used as fallback algorithm, steered by a multipath detector.

8.4 Receiving and ToA Estimation Station

The implementation of the RX station is presented and evaluated with real-world and the station fulfills the specifications defined in ICAO Annex X Volume IV [27], ED-117 [12], ED-117A [13], ED-129B [14] and ED-142 [15]. The implementation design of the RX station is installed with the ADB Safegate MLAT system at the Salzburg airport in Austria. The RX station has two linear receiving channels with 100 dB dynamic range and a high design flexibility in the FPGA implementation. The full FPGA implementation of the RX station is published for the first time in this work.

8.5 Outlook and Future Work

Although the implementations of the algorithms deliver acceptable performance, the low-cost design can be improved. Investigations on logic speed, chip area and power consumption can be subject of future work. Most of the algorithms contain static configured thresholds, i.e. noise floor threshold. These thresholds can also be computed dynamically. This can even improve the performance of the algorithms.
Although the noise suppression characteristic of the ToA estimation algorithms deliver acceptable performance for the ToA estimations, sufficient to outperform the prior-art solution, the performance limitations on ISI scenarios will be subject to future research. Investigations on equalizer algorithms and architectures known from wireless communications, including decision feedback equalizers and reduced state sequence estimation algorithms will be performed.
The transmitting part of the RX station is still missing and not published, it could be implemented for improving all ground station parts of a MLAT system. The TX station needs a control logic at the CPS and can be used for validation purposes and would complete the MLAT components.
Wide area applications are not addressed in the work. They would be the next step not only to provide wide area applications, but also local and wide area combined. From a technical point of view the RX station would have a different antenna and transmitter with more power to cover the wider area. The signal processing, decoding and ToA estimation algorithms of transponder replies could stay the same. Furthermore, the transmitting logic of the CPS would be different.

Notation and Acronyms

Symbols

A	Amplitude
$\delta[n]$	Euclidean position distance
δ_{avg}	Average position distance error
$\Delta t[n]$	Time difference
DF	Damping factor
f_C	Carrier frequency
$m(t)$	Mode S baseband signal
$n(t)$	White Gaussian noise
N_0	Noise power
ϕ_{MP}	Phase shift of the multipath component
$r(t)$	Received Mode S signal
τ	Time delay
t_{dur}	Time duration
t_{UI}	Time of update interval
$x[n]$	Input sample at element n
$x_t[n]$	Cartesian x-position of the target report
$x_r[n]$	Cartesian x-position of the DGPS reference position
$y(t)$	Modulated Mode S signal
$y[n]$	Output sample at element n
$y_t[n]$	Cartesian y-position of the target report
$y_r[n]$	Cartesian y-position of the DGPS reference position
$\#_{CD}$	Correct target detection counter
$\#_{EUI}$	Counter of expected update intervals
$\#_{FD}$	False target detection counter
$\#_{MUI}$	Counter of missed update interval

Operators

$\lvert \cdot \rvert$	Absolute value
$\lfloor \cdot \rfloor$	Floor value

Acronyms

ADC	Analog Digital Converter

ADS-B	Automatic Dependent Surveillance-Broadcast
AHB	AMBA High-performance Bus
AM	Amplitude Modulation
APOS	Austrian Positioning Service
ARM	Advanced Risc Machine
ASDS	Air Situation Display Systems
ASIC	Application Specific Integrated Circuit
A-SMGCS	Advanced-Surface Movement Guidance and Control System
ATM	Air Traffic Management
BER	Bit Error Rate
BITE	Build in Test-Equipment
BP	Bandpass filter
BRAM	Block RAM
CIC	Cascaded Integrated Comb
CLB	Configurable Logic Block
CMOS	Complementary Metal Oxide Semiconductor
CPS	Central Processing Station
CPU	Central Processing Unit
dB	deciBel
dBc	Power ratio in dB of a signal to a carrier signal
dBm	Power in dB relative to 1 milliwatt
DC	Direct Current
DCM	Digital Clock Manager
DDS	Direct Digital Synthesizer
DF	Downlink Format
DGPS	Differential GPS
DPSK	Differential Phase Shift Keying
DSP	Digital Signal Processor

EUROCAE	European Organisation for Civil Aviation Equipment
FAA	Federal Aviation Administration
FIR	Finite Impulse Response
FPGA	Field Programmable Gate Array
GAC	General Aviation Center
GPS	Global Positioning System
HRMS	Horizontal Root Mean Square
ICAO	International Civil Aviation Organization
IF	Intermediate Frequency
IFF	Identification Friend or Foe
IFR	Instrument Flight Rules
IP	Intellectual Property
ISI	Inter-Symbol Interference
LNA	Low Noise Amplifier
LO	Local Oscillator
LOS	Line-of-Sight
LP	Low Pass
LUT	Look-up Tables
MLAT	Multilateration
MSPS	Mega Samples per Seconds
NCO	Numerically Controlled Oscillator
NLOS	Non LOS
OCXO	Oven Controlled Crystal Oscillator
PLL	Phase Locked Loop
PPM	Pulse Position Modulated
PPS	Pulse per Second
PoI	Point of Interest
PSR	Primary Surveillance Radar

RAM	Random Access Memory
REDTOE	Rising Edge Detection Time of Arrival Estimation
RMS	Root Mean Square
RMSE	Root Mean Square Error
RF	Radio Frequency
RISC	Reduced Instruction Set Computer
RTK	Real Time Kinematic
RTL	Register Transfer Level
RX	Receiver
RXTX	Receiver and Transmitter
SAW	Surface Acoustic Wave
SESAR	Single European Sky ATM Research
SNMP	Simple Network Management Protocol
SNR	Signal-To-Noise Ratio
SOC	System On Chip
SPI	Special Purpose Identification
SSR	Secondary Surveillance Radar
SSR signal	Mode A/C or Mode S transponder reply
TCAS	Traffic Alert and Collision Avoidance System
TDOA	Time Differential of Arrival
TIS	Traffic Information Service
ToA	Time of Arrival
TX	Transmitter
TSOA	Time Sum of Arrival
UTC	Coordinated Universal Time
VAC	Voltage Alternating Current
VDC	Voltage Direct Current
VCO	Voltage Controlled Oscillator

VRMS	Vertical Root Mean Square
VFR	Visual Flight Rules
VHDL	Very High Speed Integrated Circuit Hardware Description Language
VRS	Virtual Reference Station
WAM	Wide Area Multilateration
WGS84	World Geodetic System 1984
2D	Two-Dimensional
3D	Three-Dimensional

Appendix

Multipath Overlapping MATLAB Simulation Model

```
function [signal t_bs] = createIFModeSSignal(cfg)

assert(length(cfg.mp_delays_s) == length(cfg.mp_reflection_dB));

cfg.mp_delays_s              = [0 cfg.mp_delays_s];
cfg.mp_reflection_dB         = [0 cfg.mp_reflection_dB];
cfg.mp_reflection_phase_rad = [0 cfg.mp_reflection_phase_rad];

Ts_bs = 1/cfg.fs_bs;

signal_length_s   = (length(cfg.payload) + 8) * 1e-6
                  * cfg.signal_stretching_factor
                  + max(cfg.mp_delays_s);
signal_start_time = -cfg.t_rise_s - cfg.pulse_width_s;
signal_end_time   = signal_length_s + cfg.t_fall_s
                  + cfg.pulse_width_s;

if(cfg.add_carrier_bump)
    signal_start_time = signal_start_time
                      - cfg.carrier_bump_length_before_signal_s;
end

t_bs = signal_start_time:Ts_bs:signal_end_time;

signal = t_bs*0;

for mp_nr = 1:length(cfg.mp_delays_s)
    % -- create baseband signal according to multipath timeshift
    signal_bs = createModeSSignal(t_bs, cfg.payload,
                cfg.pulse_width_s, cfg.t_rise_s, cfg.t_fall_s,
                cfg.mp_delays_s(mp_nr),
                cfg.signal_stretching_factor);

    if(cfg.add_carrier_bump)
        bump_start_i = find(t_bs >
                    -cfg.carrier_bump_length_before_signal_s,1);
```

```
37          length(t_bs);
38          bump = [zeros(1, bump_start_i)
39                          ones(1, length(t_bs) - bump_start_i)];
40          bump = bump * cfg.bump_amplitude/cfg.output_amplitude;
41          signal_bs = signal_bs + bump;
42          end
43
44      if(cfg.enable_baseband_filter)
45          if (cfg.baseband_filter_normalize)
46              signal_bs_pre_max = max(abs(signal_bs));
47          end
48          signal_bs = filter(cfg.baseband_filter_b,
49                      cfg.baseband_filter_a, signal_bs);
50          if (cfg.baseband_filter_normalize)
51              signal_bs_post_max = max(abs(signal_bs));
52              signal_bs = signal_bs / signal_bs_post_max
53                          * signal_bs_pre_max;
54          end
55      end
56
57      % ---------------- multipath damping ----------------------------
58      signal_bs = signal_bs * 10^(cfg.mp_reflection_dB(mp_nr)/20);
59      % ---------------- modulation -----------------------------------
60      phase_shift_hf = 2 * pi * cfg.f_hf * cfg.mp_delays_s(mp_nr);
61      carrier = cos(2*pi*cfg.f_if*t_bs + cfg.f_if_phase
62              - phase_shift_hf
63              + cfg.mp_reflection_phase_rad(mp_nr));
64
65      signal_modulated = carrier.*signal_bs.*cfg.output_amplitude;
66
67      signal_orig = signal;
68      signal = signal + signal_modulated;
69  end
70
71  % ------------------ noise ------------------------------------------
72  padding_length =  round(cfg.pulse_width_s/Ts_bs);
73  signal = [ zeros(1, padding_length) signal ];
74  ts_padding = t_bs(1)-padding_length*Ts_bs:Ts_bs:t_bs(1)-Ts_bs;
75  ts_bs = [ ts_padding t_bs ];
76
77  noise = randn(1, length(signal))*cfg.noise_amplitude_rms;
78  signal = signal + noise;
79  % ---------------- amplitude quantisation -------------------------
80  signal = ceil(signal);
81
```

```
82 if(any(signal > (2^14)/2))
83     error 'Amplitude is to high.'
84 end
```

Dipole Link Simulations

The simulations of a dipole link have the properties defined in Table C.1. The RX power diagram (Figure C.1), the free space loss of the link (Figure C.2) and the ground reflection phase and damping (Figure C.3) are shown.

Parameter	Value
TX antenna height	6 m
RX antenna height	6 m
TX power	1 W
Ground type	typical ground (not wet, rocky, dry)
RX to TX distance	0 - 500 m

Table C.1: Link Power Properties

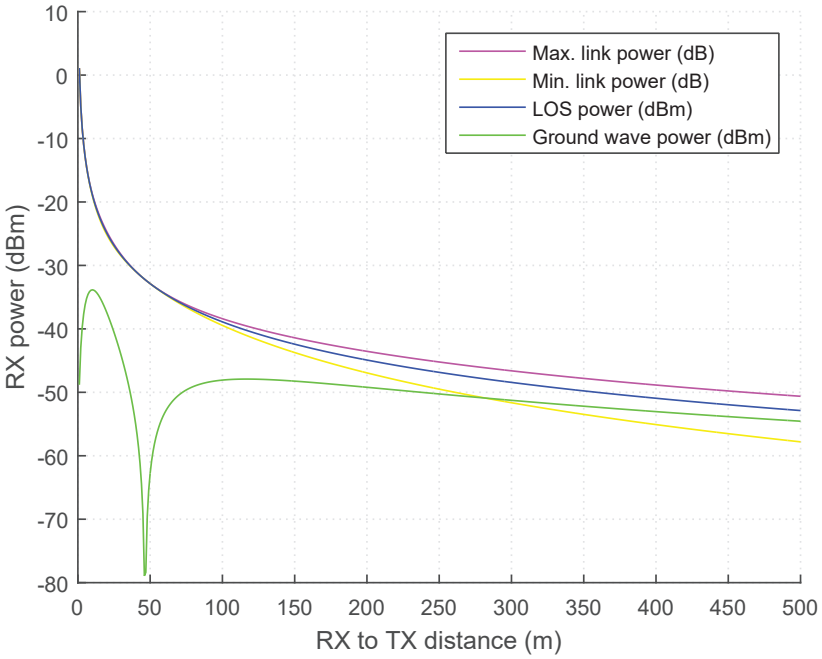

Figure C.1: Dipole link - RX power simulation

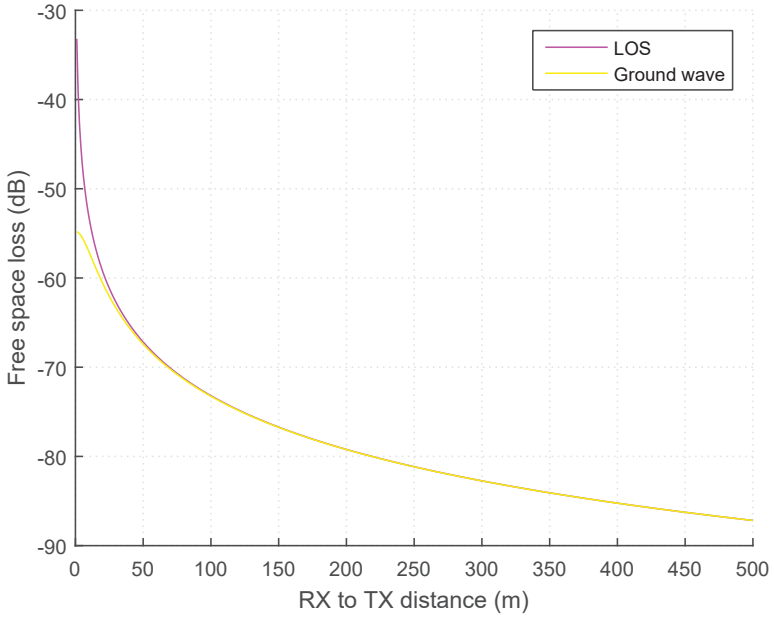

Figure C.2: Dipole link - free space loss simulation

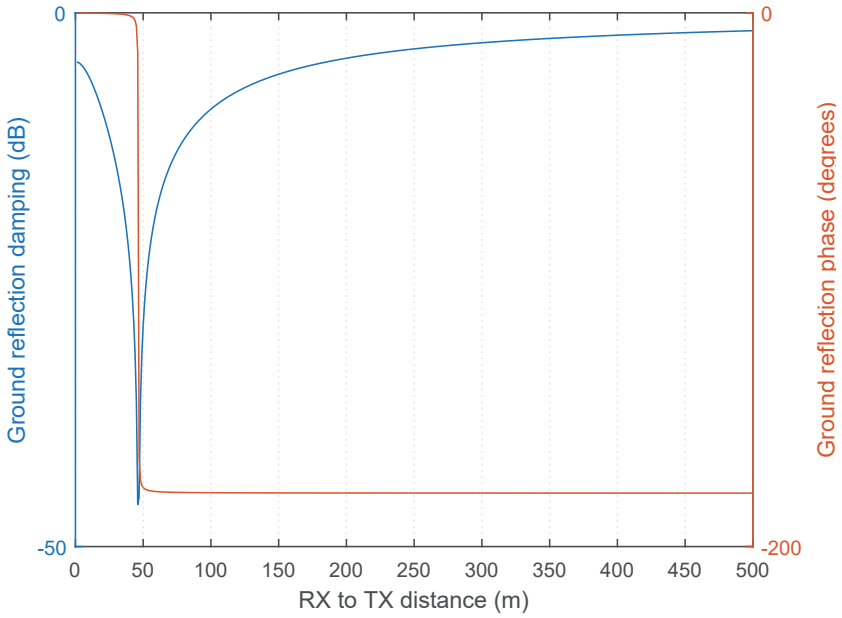

Figure C.3: Dipole link - ground reflection phase and damping

Mode S Preamble Examples

The Mode S preamble examples are recorded at the Salzburg airport, as described in Section 4.5.1. The distortion in the Mode S preambles, as shown in Figure C.4, is multipath overlapping.

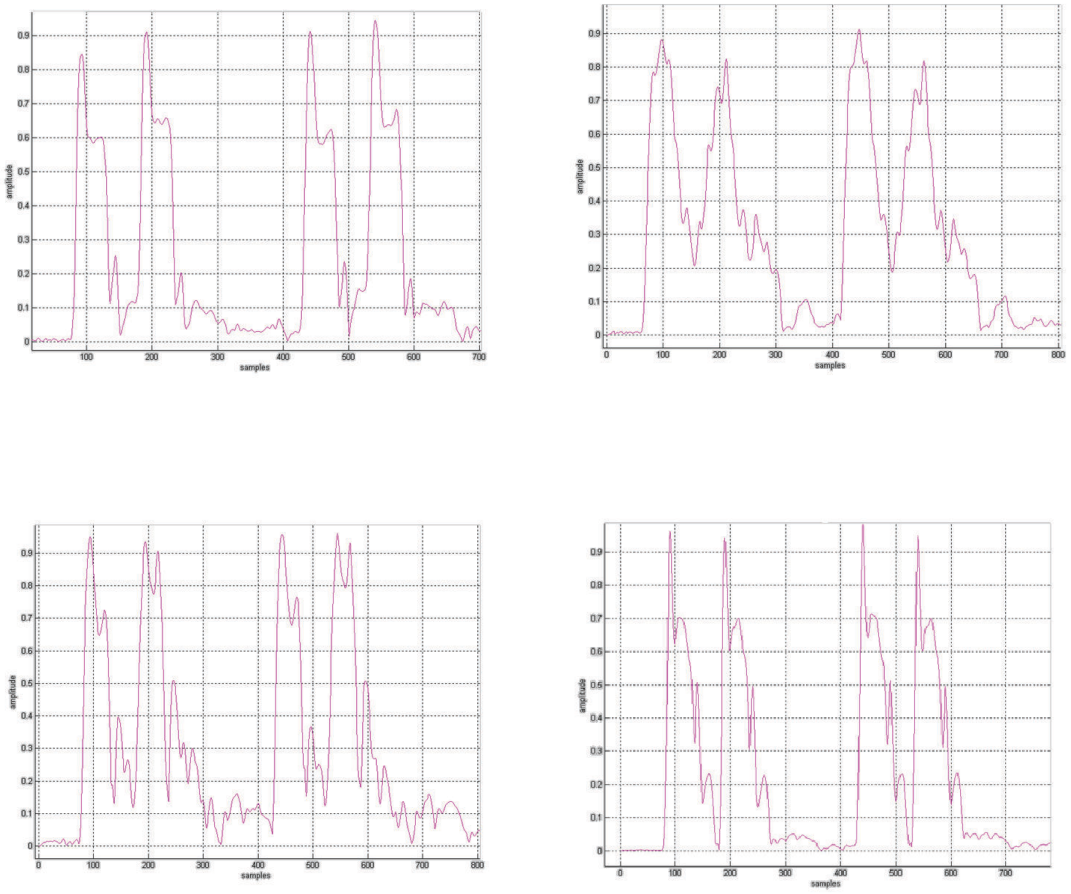

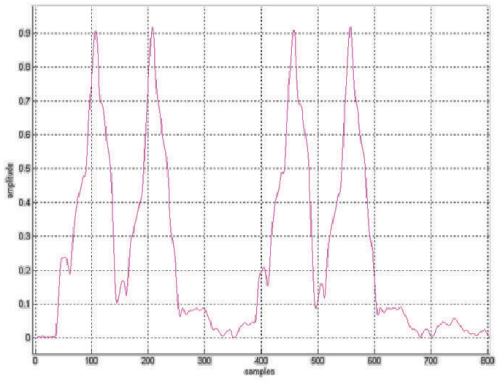
amplitude
samples

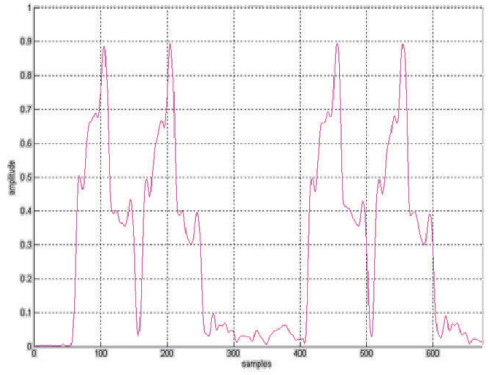
amplitude
samples

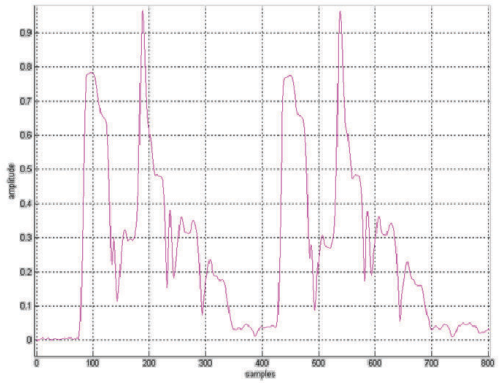
amplitude
samples

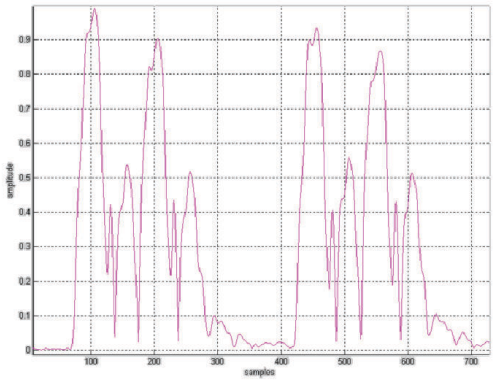
amplitude
samples

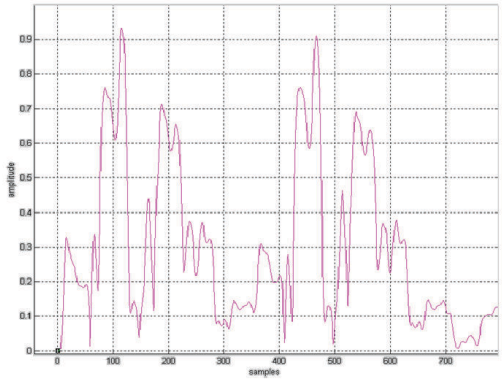
amplitude
samples

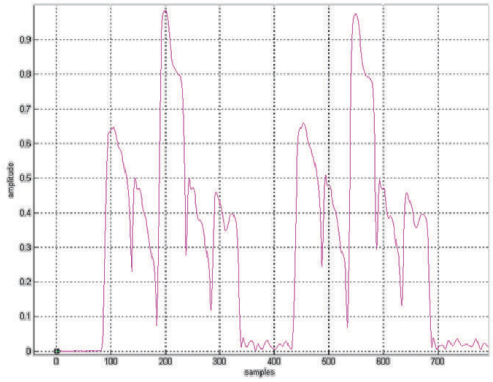
amplitude
samples

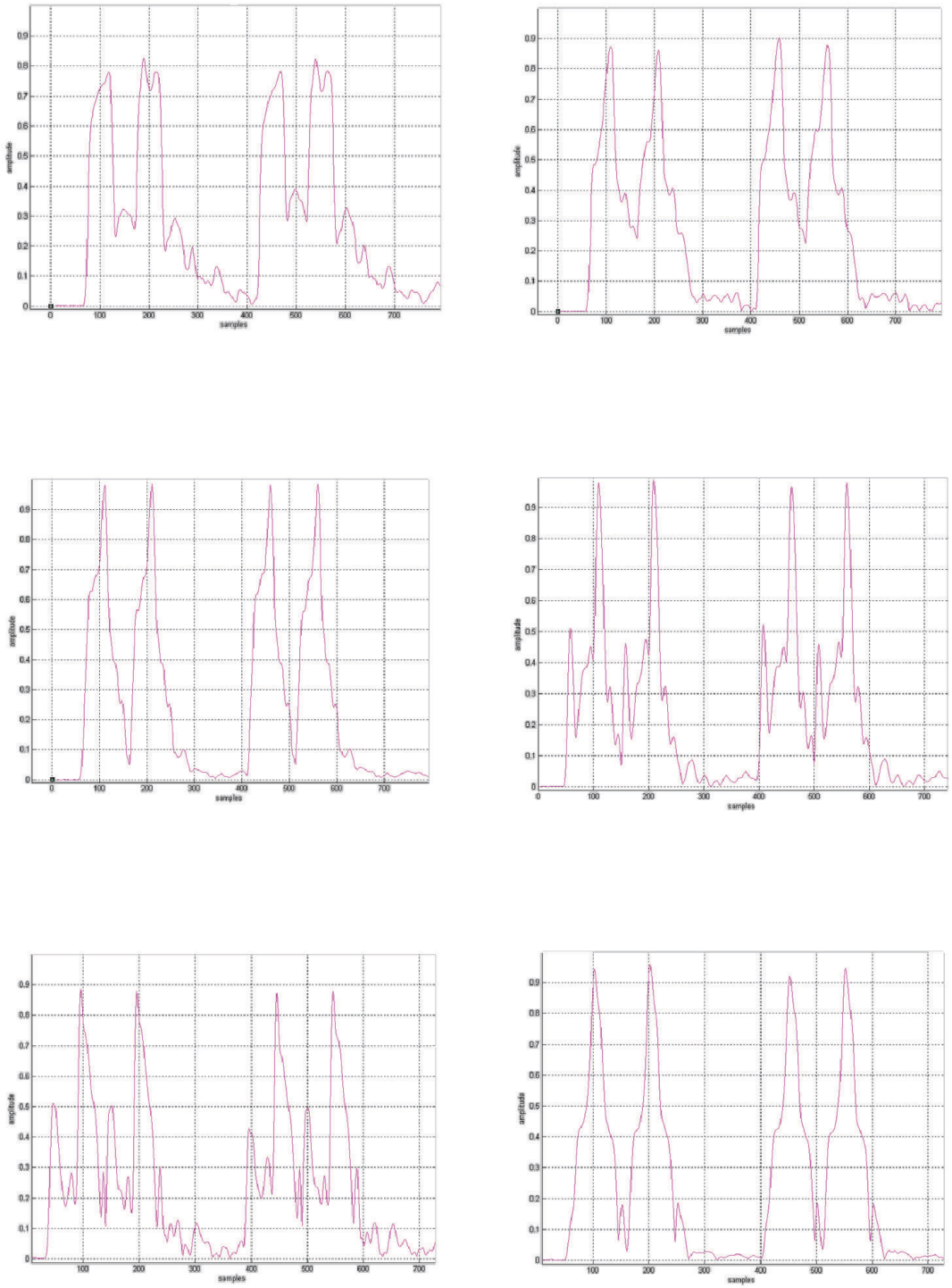

Figure C.4: Mode S preamble examples

Receiver Station Specifications

Specification	Value	Remarks
Power Supply	230 VAC/50 Hz	Optional: 110-130 VAC or 24 VDC
Weight	Approx. 34 kg	Depends on installed options.
Power Consumption	Max. 65 W	
Input Sensitivity	-89 dBm	
Input Bandwidth	Less than -60 dBc @ $<$ 1,030 MHz & $>$ 1,150 MHz. Less than -85 dB @ $<$ 960 MHz.	
Dynamic Range	Min. 100 dB	
Output Power Transmitter	200 W @ 1,090 MHz and 1,030 MHz	Configurable
Size	600 x 600 x 400 mm	Outdoor box
Connectivity	Ethernet 100 $\frac{Mbit}{second}$	Optional modems, media converters, etc.
MTBF	136,000 h	

Table C.2: RX General Specifications

Specification	Value	Remarks
ToA Estimation Resolution	39 ps	
ToA Estimation Accuracy	$<$ 300 ps	In conducted test environment.
Mode S Decoding Rate	6,500 $\frac{signals}{second}$	Long Mode S.
Channels	Dual decoder with quadruple ToA estimation circuitry.	

Table C.3: RX Decoder Specifications

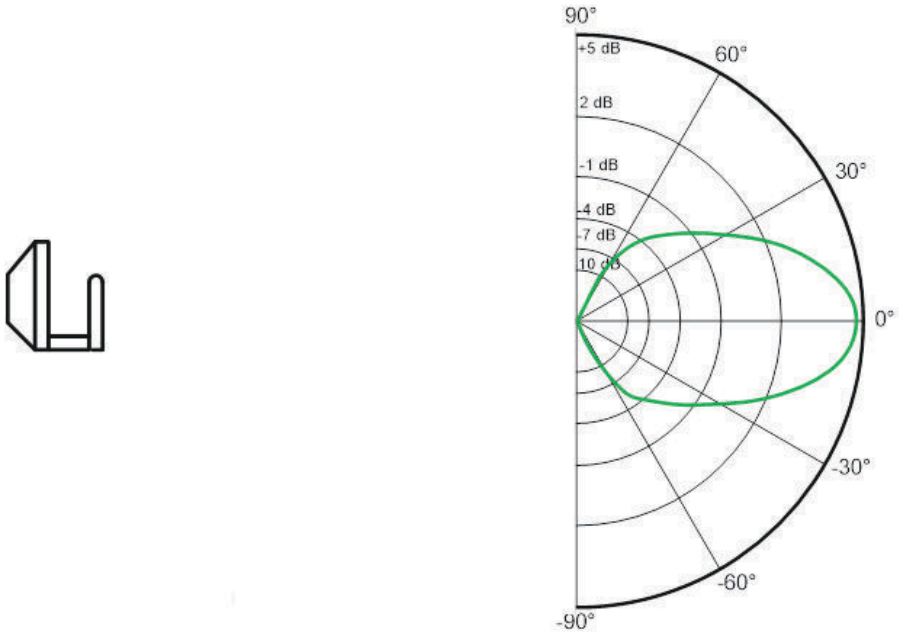

Figure C.5: Antenna with reflector position (left) vertical dipole azimuth (right) gain pattern

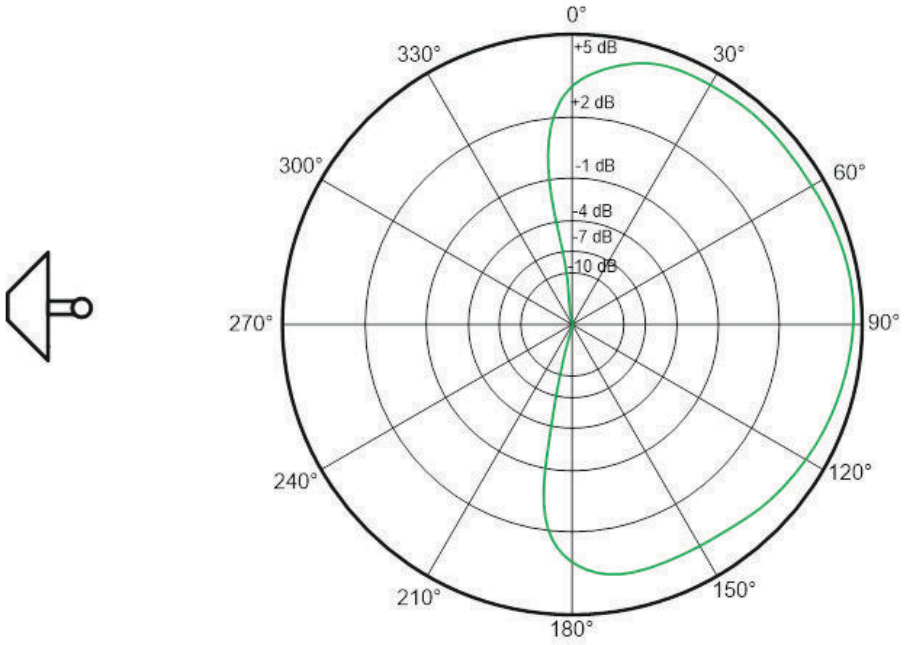

Figure C.6: Antenna with reflector position (left) vertical dipole elevation (right) gain pattern

ToA Estimation Algorithms Evaluations at the Salzburg Airport

Some further evaluated specifications are listed in Table C.4. Abbreviations for the probabilities are listed in Table 7.4. The PA5s is the position accuracy averaged over 5 seconds.

RE	**Sector**	**A.1 (%)**	**A.2 (%)**	**A.3 (%)**	**A.4 (%)**	**ED-117 Condition**
PA5s	Stands	***100.00***	***100.00***	98.92	***100.00***	≥100.0% in 20 m
PA5s	Aprons	***100.00***	***100.00***	98.98	***100.00***	≥100.0% in 20 m
PID	Run	***100.00***	***100.00***	***100.00***	***100.00***	≥99.9%
PID	Taxi	***100.00***	***100.00***	***100.00***	***100.00***	≥99.9%
PID	Aprons	99.98	99.98	***99.99***	99.97	≥99.9%
PID	Stands	99.98	99.98	***99.99***	99.96	≥99.9%
PoU	Run	99.85	99.85	***99.93***	99.91	≥95.0%
PoU	Taxi	95.20	93.20	***96.66***	95.00	≥95.0%

Table C.4: ED-117 Evaluations [19]

Position accuracy averaged over 5 seconds details of the evaluation results are shown in Tables C.5 and C.6.

Name	**A.1**	**A.2**	**A.3**	**A.4**
Updates Count	1630	1609	1577	1637
Error Average [m]	1.98	2.67	3.89	2.13
Inside Limit Count for 20 m	1630	1609	1560	1637
Outside Limit Count for 20 m	0	0	17	0

Table C.5: Sector Stands – Position Accuracy averaged over 5 Seconds [19]

Name	**A.1**	**A.2**	**A.3**	**A.4**
Updates Count	2014	1996	1963	2023
Error Average [m]	1.92	2.45	3.56	2.08
Inside Limit Count for 20 m	2014	1996	1963	2023
Outside Limit Count for 20 m	0	0	20	0

Table C.6: Sector Aprons – Position Accuracy averaged over 5 Seconds [19]

Probability of identification details of the evaluation results are shown in Tables C.7, C.8, C.9 and C.10.

Name	**A.1**	**A.2**	**A.3**	**A.4**
Updates Count $\#_{all}$	3400	3411	3404	6214
Identity None $\#_{None}$	0	0	0	0
Identity Unknown $\#_{Unknown}$	0	0	0	0
Identity Correct $\#_{Correct}$	3400	3411	3404	6214
Identity Incorrect $\#_{Incorrect}$	0	0	0	0
PID (%)	100.00	100.00	100.00	100.00
ED-117 Condition (%)	≥99.90	≥99.90	≥99.90	≥99.90
ED-117 Compliant	OK	OK	OK	OK

Table C.7: Sector Runway – Probability of Identification Details [19]

Name	**A.1**	**A.2**	**A.3**	**A.4**
Updates Count $\#_{all}$	11124	11845	10768	16771
Identity None $\#_{None}$	0	0	0	0
Identity Unknown $\#_{Unknown}$	0	0	0	0
Identity Correct $\#_{Correct}$	11124	11845	10768	16771
Identity Incorrect $\#_{Incorrect}$	0	0	0	0
PID (%)	100.00	100.00	100.00	100.00
ED-117 Condition (%)	≥99.90	≥99.90	≥99.90	≥99.90
ED-117 Compliant	OK	OK	OK	OK

Table C.8: Sector Taxiways – Probability of Identification Details [19]

Name	**A.1**	**A.2**	**A.3**	**A.4**
Updates Count $\#_{all}$	39384	39506	38785	52048
Identity None $\#_{None}$	7	7	3	18
Identity Unknown $\#_{Unknown}$	2	2	2	2
Identity Correct $\#_{Correct}$	39375	39497	38780	52028
Identity Incorrect $\#_{Incorrect}$	0	0	0	0
PID (%)	99.98	99.98	99.99	99.97
ED-117 Condition (%)	≥99.90	≥99.90	≥99.90	≥99.90
ED-117 Compliant	OK	OK	OK	OK

Table C.9: Sector Aprons – Probability of Identification Details [19]

Name	**A.1**	**A.2**	**A.3**	**A.4**
Updates Count $\#_{all}$	37442	37571	36865	48911
Identity None $\#_{None}$	7	7	3	18
Identity Unknown $\#_{Unknown}$	2	2	2	2
Identity Correct $\#_{Correct}$	37433	37562	36860	48891
Identity Incorrect $\#_{Incorrect}$	0	0	0	0
PID (%)	99.98	99.98	99.99	99.96
ED-117 Condition (%)	≥99.90	≥99.90	≥99.90	≥99.90
ED-117 Compliant	OK	OK	OK	OK

Table C.10: Sector Stands – Probability of Identification Details [19]

Probability of update details of the evaluation results are shown in Tables C.11 and C.12.

Name	**A.1**	**A.2**	**A.3**	**A.4**
Updates Count $\#_{all}$	1360	1365	1362	2299
Counter of Missed Update Intervals $\#_{MUI}$	2	2	1	2
Expected Updates $\#_{EUI}$	1346	1349	1349	2272
PoU (%)	99.85	99.85	99.93	99.91
ED-117 Condition (%)	≥95.00	≥95.00	≥95.00	≥95.00
ED-117 Compliant	OK	OK	OK	OK

Table C.11: Sector Runway – Probability of Update Details [19]

Name	**A.1**	**A.2**	**A.3**	**A.4**
Updates Count $\#_{all}$	4333	4694	4150	6465
Counter of Missed Update Intervals $\#_{MUI}$	213	296	140	331
Expected Updates $\#_{EUI}$	4441	4856	4190	6621
PoU (%)	95.20	93.90	96.66	95.00
ED-117 Condition (%)	≥95.00	≥95.00	≥95.00	≥95.00
ED-117 Compliant	OK	NOK	OK	OK

Table C.12: Sector Taxiways – Probability of Update Details [19]

Bibliography

[1] Ahlin L., Zander J. and Slimane B. *Principles of Wireless Communications*. Studentlitteratur AB, ISBN 9789144030807, August 2006, pp. 143-148.

[2] Ashenden P. J. *The Designer's Guide to VHDL*. Morgan Kaufmann, third edition, ISBN 9780120887859, May 2008, pp. 1-936.

[3] Bernhart S. *Design und Implementierung eines FPGA-basierenden SSR Message Decoders*. Master thesis, Graz University of Technology, February 2008, pp. 1-136.

[4] Bernhart S. and Leitgeb E. *Evaluations of Low-Cost Decoding Methods for 1090 MHz SSR Signals*. International Conference on Broadband Communications (CoBCom), Graz, July 2018, pp. 1-5.

[5] Bernhart S., Hofbauer A. G., Feichter U. and Leitgeb E. *TOA Estimation Algorithms evaluated according ED-117 Minimum Operational Performance Specifications for Mode S Multilateration Systems*. 12$^{\text{th}}$ European Conference on Antennas and Propagation (EUCAP), London, April 2018, pp. 1-5.

[6] Bernhart S., Hofbauer A. G., Feichter U. and Leitgeb E. *FPGA Implementation of a 1,090 MHz Receiving Station and precision ToA estimation station*. 13$^{\text{th}}$ International Conference on Telecommunications (ConTEL), Graz, July 2015, pp. 1-5.

[7] Bernhart S., Hofbauer A. G., Feichter U. and Leitgeb E. *Rising Edge Detection used as TOA estimator for Mode S Signals with Multipath Propagation*. 25$^{\text{th}}$ International Conference on Software, Telecommunications and Computer Networks (SoftCOM), Split, September 2017, pp. 1-6.

[8] Callan J. *Multilateration: Radar's replacement*. Avionics, [Online]. Available: `http://www.aviationtoday.com/2007/04/01/multilateration-radars-replacement/`, April 2007.

[9] Collin R. E. *Antennas and Radiowave propagation*. McGraw-Hill Higher Education, ISBN 9780070118089, February 1985, pp. 1-508.

[10] Cover T. M. and Thomas J. A. *Elements of Information Theory*. Wiley-Interscience a john wiley & sons, inc., publication, second edition, ISBN 9780471241959, 2006, pp. 1-774.

[11] Dillinger T. *VLSI Engineering*. Prentice Hall, first edition, ISBN 9780139427312, October 1987, pp. 1-832.

[12] EUROCAE ED-117. *Minimum Operational Performance Specification for Mode S Multilateration Systems for use in Advanced Surface Movement Guidance and Control Systems (A-SMGCS).* European Organization for Civil Aviation Equipment (EUROCAE), September 2003, pp. 1-54.

[13] EUROCAE ED-117A. *Minimum Operational Performance Specification for Mode S Multilateration Systems for use in Advanced Surface Movement Guidance and Control Systems (A-SMGCS).* European Organization for Civil Aviation Equipment (EUROCAE), Revision A, September 2016, pp. 1–83.

[14] EUROCAE ED-129B. *Technical Specification for a 1090 MHz Extended Squitter ADS-B Ground System.* European Organization for Civil Aviation Equipment (EUROCAE), Revision B, March 2016, pp. 1–351.

[15] EUROCAE ED-142. *Technical Specification for Wide Area Multilateration (WAM) Systems.* European Organization for Civil Aviation Equipment (EUROCAE), 2010 Edition, September 2010, pp. 1–80.

[16] EUROCONTROL. *Multi-Static Primary Surveillance Radar – An examination of Alternative Frequency Bands.* EUROCONTROL, Report No: 72/07/R/376/U Issue 1.2, July 2008, pp. 1-186.

[17] European Organisation for the Safety of Air Navigation. *Single European Sky ATM Research.* [Online]. Available: `http://www.eurocontrol.int/sesar-research`, July 2018.

[18] Feichter U. *Elaboration of Methods and Algorithms for Passive Aircraft and Vehicle Detection over Time of Signal Arrival Differences.* Master thesis, Graz University of Technology, Institute of Broadband Communications, February 2010, pp. 32-33.

[19] Feichter U. and Puhr H. *Airport Salzburg - Performance Evaluation Report.* Unpublished, August 2017.

[20] Galati G., Bartolini S. and Menē L. *Analysis of SSR Signals by Super Resolution Algorithms.* Proceedings of the Fourth IEEE International Symposium on Signal Processing and Information Technology, 2004, pp. 166-170.

[21] Galati G., Gasbarra M. and Leonardi M. *Multilateration Algorithms for Time of Arrival Estimation and Target Localization in Airports.* European Radar Conference (EuRAD), Amsterdam, February 2004, pp. 1-4.

[22] Galati G., Gasbarra M. and Piracci E. *Decoding techniques for SSR Mode S signals in high traffic environment.* European Radar Conference (EURAD), Paris, October 2005, pp. 383-386.

[23] Galati G., Leonardi M., Piracci E. G., Petrochilos N. and Samanta S. *The transponder data recorder: First implementation and applications.* Tyrrhenian International Workshop on Digital Communications - Enhanced Surveillance of Aircraft and Vehicles, Capri, 2011, pp. 147-151.

[24] GPS.GOV. *"Global positioning system standard positioning service performance standard.* [Online]. Available: `https://www.gps.gov/`, 2008.

[25] Haralick R. *Digital Step Edges from Zero Crossing of Second Directional Derivatives.* IEEE Trans. on Pattern Analysis and Machine Intelligence, vol. PAMI-6, no. 1, January 1984, pp. 56-68.

[26] Haykin S., Litva J. and Shepherd T. J. *Radar Array Processing.* Springer-Verlag Berlin Heidelberg, ISBN 9783642773495, 1993, pp. 1-317.

[27] ICAO. *Annex 10 to the Convention on International Civil Aviation, Aeronautical Telecommunications, Volume IV.* International Civil Aviation Organization (ICAO) Doc. 7300, July 2014.

[28] ICAO. *Multilateration (MLAT), Concept of use.* International Civil Aviation Organization (ICAO), edition 1.0, September 2007, pp. 1-19.

[29] ICAO. *ADS-B Implementation and Operations Guidance Document.* International Civil Aviation Organization (ICAO), edition 7.0, [Online]. Available: `https://www.icao.int/APAC/Documents/edocs/cns/ADSB_AIGD7.pdf`, September 2014, pp. 1-85.

[30] Kay S. M. *Fundamentals of Statistical Signal Processing, Estimation Theory.* Prentice Hall, first edition, ISBN 9780133457117, April 1993, pp. 1-625.

[31] Kingsley S. and Quegan S. *Understanding Radar Systems.* SciTech Publishing, ISBN 9781891121050, 1992, pp. 1-375.

[32] Mantilla-G I. A., Balbastre-T J. V., de los Reyes E., Leonardi M. and Galati G. *Strategies to design and deploy Mode-S multilateration systems.* Tyrrhenian International Workshop on Digital Communications - Enhanced Surveillance of Aircraft and Vehicles, Capri, 2011, pp. 167-172.

[33] Mantilla-Gaviria I. A., Leonardi M., Galati G. and Balbastre-Tejedor J. V. *Time-difference-of-arrival regularised location estimator for multilateration systems.* IET Radar, Sonar & Navigation, vol. 8, no. 5, June 2014, pp. 479-489.

[34] Oppenheim A.V. and Schafer R. W. *Digital Signal Processing.* Englewood Cliffs, NJ: Prentice-Hall, Inc., first edition, ISBN 9780132162920, 1989, pp. 1-879.

[35] Oppenheim A.V. and Schafer R. W. *Discrete-Time Signal Processing.* Prentice-Hall Signal Processing Series, 3rd edition, ISBN 0131988425, August 2009, pp. 1-1144.

[36] Rabaey J. M., Chandrakasan A. and Nikolic B. *Digital Integrated Circuits.* Pearson, second edition, ISBN 9780130909961, January 2003, pp. 1-761.

[37] Radio Technical Commission for Aeronautics. *Minimum Aviation System Performance Standards for Automatic Dependent Surveillance Broadcast (ADS B).* Radio Technical Commission for Aeronautics (RTCA), RTCA Inc., standard DO-242, December 2006, pp. 1-12.

[38] Rappaport T. S. *Wireless Communications Principles and Practice*. Prentice Hall, second edition, ISBN 9780130422323, January 2002, pp. 1-736.

[39] Stevens M. C. *Secondary Surveillance Radar*. Artech House Radar Library, Norwood MA, ISBN 9780890062920, March 1988, pp. 179-211.

[40] Tietze U., Schenk Ch. and Gamm E. *Electronic Circuits: Handbook for Design and Application*. Springer, second edition, 2008 edition, ISBN 9783540004295, January 2008, pp. 1-1543.

[41] Wai-Kai C. *The VLSI Handbook*. CRC Press, second edition, ISBN 9780849341991, December 2006, pp. 1560.

[42] Weste N. and Eshraghian K. *Principles of CMOS VLSI Design: A Systems Perspective*. Addison Wesley Longman Publishing Co, ISBN 9780201082227, July 1985, pp. 1-534.

[43] Xilinx. *Spartan-6 Family Overview*. Xilinx inc., product specification, DS160 v2.0, [Online]. Available: `https://www.xilinx.com/support/documentation/data_sheets/ds160.pdf`, October 2011, pp. 2-3.

[44] Zarchan P. and Musoff, H. *Fundamentals of Kalman Filtering: A Practical Approach*. American Institute of Aeronautics and Astronautics 2015, Incorporated, fourth edition, ISBN 9781624102769, August 2015, pp. 1-877.

Publications

Throughout the thesis the following scientific contributions as first author were accepted and published:

1. **Bernhart S.**, Hofbauer A. G., Feichter U. and Leitgeb E. *FPGA Implementation of a 1,090 MHz Receiving Station and precision ToA estimation station*, 13$^{\text{th}}$ International Conference on Telecommunications (ConTEL), Graz, July 2015, pp. 1-5.

2. **Bernhart S.**, Hofbauer A. G., Feichter U. and Leitgeb E. *Rising Edge Detection used as ToA estimator for Mode S Signals with Multipath Propagation*, 25$^{\text{th}}$ International Conference on Software, Telecommunications and Computer Networks (SoftCOM), Split, September 2017, pp. 1-6.

3. **Bernhart S.**, Hofbauer A. G., Feichter U. and Leitgeb E. *ToA Estimation Algorithms evaluated according ED-117 Minimum Operational Performance Specifications for Mode S Multilateration Systems*, 12$^{\text{th}}$ European Conference on Antennas and Propagation (EUCAP), London, April 2018, pp. 1-5.

4. **Bernhart S.** and Leitgeb E. *Evaluations of Low-Cost Decoding Methods for 1090 MHz SSR Signals*, International Conference on Broadband Communications (CoBCom), Graz, July 2018, pp. 1-5.

Furthermore, the following scientific contributions as first author were submitted and are under review:

5. **Bernhart S.** and Leitgeb E. *Evaluations of Decoding and ToA Estimation Methods for 1090 MHz SSR Signals*, Radioengineering Journal, vol. 28, no. 2, 2019.

6. **Bernhart S.** and Leitgeb E. *Multipath Overlapping Analysis of 1090 MHz SSR Signals*, 1$^{\text{st}}$ European Microwave Conference in Central Europe (EUMCE), Prague, May 2019, pp. 1-4.